Paramagnetic Meissner effect of small topological superconductors

Shu-Ichiro Suzuki

February 10, 2017

Paramagnetic Meissner effect of small topological superconductors

Shu-Ichiro Suzuki

Abstract

The perfect diamagnetism is the most fundamental property of all superconductors. In the presence of an external magnetic field, the coherent motion of Cooper pairs generates the electric current along a surface of a superconductor and screens the magnetic field. Consequently, the superconducting condensate deep inside the superconductor can keep its phase coherence and minimize the free energy. Every standard textbook explains this phenomenon is called the Meissner effect. Several experiments, however, have reported the paramagnetic response of small superconductors and mesoscopic proximity structures. At present, the mechanism of the paramagnetic property is an open question in physics of superconductivity.

Recent theoretical investigations have suggested the existence of novel types of Cooper pairs called odd-frequency pairs in a spatially inhomogeneous superconductor. In the mean-field theory of superconductivity, an odd-frequency pair appears as the local pairing correlation induced by the spatial variation of the pair potential. For instance, an odd-frequency Cooper pair exists at surfaces of a superconductor, in vortex cores, at interfaces between a superconductor and another material. Surprisingly, to our knowledge, an odd-frequency pair would exhibit the paramagnetic response to an external magnetic field. Such paramagnetic pairs are thermodynamically unstable because they attract a magnetic field. Unfortunately, only a few experimental studies have caught the signs of an odd-frequency pair.

In this thesis, on the contrary to the description in standard textbooks, we theoretically demonstrate that a small unconventional superconductor can be paramagnetic at low temperature. On the basis of the quasiclassical Green function formalism, we calculate magnetic susceptibility of a small superconductor which belongs to unconventional pairing symmetry classes such as spin-singlet d-wave and spin-triplet p-wave. The magnetic response at low temperature is dominated by odd-frequency Cooper pairs appearing at a surface of the superconductor. Our numerical results show that a small superconductor changes its magnetic response from the usual diamagnetic response at high temperatures near the transition temperature to the unusual paramagnetic one at low temperature. In addition, we discuss the effects of surface roughness on the paramagnetic Meissner effect and the stability of the paramagnetic phase. We also discuss a role of an odd-frequency pair in the topological edge current in chiral superconductors.

Supervisor: Yasuhiro Asano
Title: Associate Professor of Applied Physics

Acknowledgements

First of all, I would like to express my sincere gratitude to my supervisor Associate Prof. Yasuhiro Asano for the continuous support of my Ph.D study, for his motivation, immense knowledge, and patience. His guidance helped me in all the time. He is a mentor in my life and a person who I respect the most. I would like to thank Prof. Kousuke Yakubo, who always give me useful advices on my research and my presentations. I am grateful to Dr. Hideaki Obuse, who taught me about recent issues on topological insulators.

I am grateful to Yukio Tanaka, Alexander A. Golubov, Seiji Higashitani, and Yakov V. Fominov for useful discussions on odd-frequency Cooper pairs. I would like to thank to Yoshiteru Maeno, Satoshi Kashiwaya, Sergey V. Bakurskiy, and Mikhail Yu. Kupriyanov for fruitful discussions on chiral superconductors.

Lastly, I would like to express my appreciation for Ryusuke and Toshiko Suzuki who are my parents. They gave me essential advices on life. Although their words ware sometimes harsh, I felt their warmness and kindness behind such words. Without their cooperations, I could not finish this research and could not take my PhD degree. I hope they live a long and healthy life.

Contents

Chapter 1

General introduction

The perfect diamagnetism is a fundamental property of all superconductors [1–5]. When a superconductor is located in a weak magnetic field, the coherent motion of Cooper pairs generates an electric current along a surface and screens the external field. This phenomenon is called the Meissner effect. In the presence of weak electron-electron attractive interactions, two electrons near the Fermi level try to form a Cooper pair to decrease their energy. Quantum mechanically, electron number in Cooper pairing condensate must be unfixed. As a consequence, the superconducting ground state gain the condensation energy and the phase coherence. The phase coherence is of the essence in the superconducting phenomena. Generally speaking, a weak external magnetic field disturbs the phase coherence through the vector potential. The superconducting state, however, keeps its phase coherence because the energy of a phase-fluctuating state is higher than the energy of the phase-coherent ground state. Therefore a magnetic field cannot penetrate deeply into a superconductor, which is observed as a perfect diamagnetism of the superconductor. The superconducting state is stable as far as the superconductor is diamagnetic as explained in every standard textbook on superconductivity.

Several experiments, however, have reported the paramagnetic response of small superconductors and mesoscopic proximity structures. H. Walter *et al.* investigated experimentally the magnetic response of thin films of a high-T_c superconductor [6, 7]. They fabricated two types of samples. One is a wide thin film, the other is a large thin film cut into narrow bars by heavy-ion irradiations. The London penetration depths of the thin films were measured in the experiment. They found at very low temperature that the penetration depth of the narrow bars increases slightly with decreasing temperature. The increasing of the penetration depth means the decreasing of the Meissner diamagnetic current [8]. Namely the diamagnetic response becomes weaker by reducing their sizes. Such anomalous magnetic response has been confirmed also in a superconducting nanowire covered by a normal metal [9–12], mesoscopic superconducting disks with giant

vortices [13,14], granular high-T_c superconductors [15–18], and Au/Ho/Nb junctions [19]. At present, the mechanisms of the paramagnetic property have been an open question in physics of superconductivity [20–30].

Recent several theories have suggested the existence of novel types of Cooper pairs called odd-frequency pairs [31–35] in spatially inhomogeneous superconductors [36–57]. So far, properties of odd-frequency Cooper pairs have been partially clarified. Unfortunately, the superconductivity by the odd-frequency pairing order have never been confirmed in any experiments. Basically, odd-frequency Cooper pairs are absent when an even-frequency superconductor is spatially uniform [A]. However, odd-frequency Cooper pairs appear in usual even-frequency superconductors such as spin-singlet even-parity superconductors and spin-triplet odd-parity superconductors. The spatial inhomogeneity (e.g., surfaces, junction interfaces, and vertex cores) induces odd-frequency Cooper pairs as a local pairing correlation. In a realistic finite-size superconducting sample, there must be boundaries such as surfaces and interfaces. In the vicinity of such boundaries, odd-frequency Cooper pairs should exist.

The most significant difference between even- and odd-frequency Cooper pairs is their response to an electromagnetic field [48–51,53–58]. Y. Asano *et al.* have theoretically studied the response of Cooper pairs to a low-frequency electromagnetic wave in the diffusive-normal-metal/superconductor junctions in terms of the surface impedance [48, 49]. They have discussed an anomalous behavior of the surface impedance in the presence of odd-frequency Cooper pairs. It was concluded that the anomalous magnetic response would be a direct experimental evidence of the emergence of odd-frequency Cooper pairs. In addition, they also discussed the origin of the anomalous magnetic response of odd-frequency Cooper pairs. The linear response kernel to electromagnetic filed is called "pair density" because it is proportional to the density of Cooper pairs in a homogeneous superconductor. Surprisingly, odd-frequency Cooper pairs have "negative pair densities" according to their discussion. When Cooper pair has such a negative density, the supercurrent flows in the opposite direction the conventional Meissner screening current. Namely, odd-frequency Cooper pairs would be rather paramagnetic than diamagnetic. When the amplitude of odd-frequency Cooper pairs becomes comparable to that of even-frequency Cooper pairs in a superconductor, the superconductor could indicate anomalous paramagnetic response. Since a paramagnetic superconductor attracts magnetic field, it is unclear whether the paramagnetic superconducting state is thermodynamically stable or not.

In this thesis, on the contrary to the description in standard textbooks, we theoretically demonstrate that small unconventional superconductors can be paramagnetic at low

[A] In this thesis, we do not discuss the odd-frequency Cooper pairs in multiband superconductors as discussed in Refs. [59–61].

temperature. On the basis of the quasiclassical Green function formalism, we calculate the magnetic susceptibility of a small superconductor with unconventional pairing symmetry such as spin-singlet d-wave and spin-triplet p-wave. Our numerical results show that a small superconductor changes its magnetic response from the usual diamagnetic response at rather-high temperatures near the transition temperature to the unusual paramagnetic one at low temperature. We also show that odd- frequency Cooper pairs are responsible for the paramagnetic response. In these small superconductors, the magnetic response at low temperature is dominated by odd-frequency Cooper pairs appearing at their surfaces. In addition, we discuss the effects of surface roughness on the paramagnetic Meissner effect and the stability of the paramagnetic phase. We also discuss an important role of an odd-frequency pair in the topological edge current in chiral superconductors.

This thesis is organised as follows. In chapter 2, we explain the symmetry classification of Cooper pairs and define the odd-frequency symmetry. In addition, we discuss unusual properties of odd-frequency pairs and how to detect them experimentally. In chapter 3, we demonstrate that a small superconductor with an unconventional pairing symmetry can be paramagnetic because of the paramagnetic current carried by odd-frequency Cooper pairs. In chapter 4, we discuss the stability of the paramagnetic superconducting state. In chapter 5, we study the effects of surface roughness on the paramagnetic Meissner effect. In chapter 6, we expand our knowledge on odd-frequency Cooper pairs to the issue on spontaneous edge currents in a small chiral superconductor.

Chapter 2

Odd-frequency Cooper pairs

In this chapter, we introduce odd-frequency Cooper pairs and their properties. We first explain the symmetry classification of Cooper pairs, and introduce odd-frequency Cooper pairs. Such odd-frequency pairings do not appear in the conventional classification based on the equal-time pairing. The odd-frequency Cooper pairs appear only in inhomogeneous systems, and show anomalous magnetic response due to their "negative pair density".

2.1 Classification of Cooper pairs

The presence of Cooper pairs are described by the so-called anomalous Green's function in the Bogoliubov mean-field theory [62]. We refer to the anomalous Green's function as the pair function. The pair function is defined in terms of the product of two annihilation operators of electron as

$$F_{\sigma_1\sigma_2}(\boldsymbol{r}_1, \boldsymbol{r}_2) = -\Big\langle \Psi_{\sigma_1}(\boldsymbol{r}_1)\Psi_{\sigma_2}(\boldsymbol{r}_2) \Big\rangle \tag{2.1}$$

because a Cooper pair consists of tow electrons, where the operator $\Psi_\sigma(\boldsymbol{r})$ annihilate the electron at $\boldsymbol{r}$ with a spin σ. The angle brackets $\langle \cdots \rangle$ means the quantum and statistical average value. The field operator Ψ satisfies the anticommutation relation

$$\Big\{ \ \Psi_{\sigma_1}(\boldsymbol{r_1}), \ \Psi_{\sigma_2}(\boldsymbol{r_2}) \ \Big\}_+ = 0 \tag{2.2}$$

because the electron is a fermionic particle. Substituting Eq. (2.2) into Eq. (2.1), we obtain the relation

$$F_{\sigma_1\sigma_2}(\boldsymbol{r}_1, \boldsymbol{r}_2) = -F_{\sigma_2\sigma_1}(\boldsymbol{r}_2, \boldsymbol{r}_1). \tag{2.3}$$

This relation means that the pair function must be antisymmetric under the exchange of the two electrons [i.e., $(\boldsymbol{r}_1, \sigma_1) \leftrightarrow (\boldsymbol{r}_2, \sigma_2)$]. Here the electrons have two degrees of freedom; coordinate and spin. Thus the Cooper pairs are classified into the two symmetry classes. One is the spin-singlet even-parity symmetry class as

$$\begin{cases} F_{\sigma_1\sigma_2}(\boldsymbol{r}_1, \boldsymbol{r}_2) = -F_{\sigma_2\sigma_1}(\boldsymbol{r}_1, \boldsymbol{r}_2) \\ F_{\sigma_1\sigma_2}(\boldsymbol{r}_1, \boldsymbol{r}_2) = +F_{\sigma_1\sigma_2}(\boldsymbol{r}_2, \boldsymbol{r}_1) \end{cases}, \tag{2.4}$$

the other is the spin-triplet odd-parity symmetry class as

$$\begin{cases} F_{\sigma_1\sigma_2}(\boldsymbol{r}_1, \boldsymbol{r}_2) = +F_{\sigma_2\sigma_1}(\boldsymbol{r}_1, \boldsymbol{r}_2) \\ F_{\sigma_1\sigma_2}(\boldsymbol{r}_1, \boldsymbol{r}_2) = -F_{\sigma_1\sigma_2}(\boldsymbol{r}_2, \boldsymbol{r}_1) \end{cases}. \tag{2.5}$$

Superconductors discovered so far always belong to these two symmetry classes. For instance, the Cooper pairs causing the conventional superconductors such as aluminum and niobium belong to the spin-singlet s-wave pairing symmetry. The pairs in the cuprate superconductors (i.e., compounds of copper and oxygen) is the spin-singlet d-wave pairing symmetry. The strontium ruthenate Sr_2RuO_4 has been widely believed to be realized by the spin-triplet chiral-p-wave pairings [89–91]. In the heavy-fermion compounds such as UPt_3 is realised by the spin-triplet p- or f-wave pairings [103–106].

The classification above is true only when a system is completely homogeneous. Spatial inhomogeneity such as the presences of surfaces and junction interfaces induces the Cooper pairs with novel symmetry classes [36–57]. To describe these novel pairs, We first expand the pair function into the general expression as

$$F_{\sigma_1\sigma_2}(\boldsymbol{r}_1\, t_1, \boldsymbol{r}_2\, t_2) = -\left\langle \mathrm{T}_\tau\, \Psi_{\sigma_1}(\boldsymbol{r}_1\, \tau_1)\Psi_{\sigma_2}(\boldsymbol{r}_2\, \tau_2)\right\rangle, \tag{2.6}$$

where we explicitly introduce the imaginary time of the electron τ. The operator T_τ is the time-ordering operator which act upon the operators including imaginary time τ as

$$\begin{aligned} \mathrm{T}_\tau\, \Psi_{\sigma_1}(\boldsymbol{r}_1\, \tau_1)\Psi_{\sigma_2}(\boldsymbol{r}_2\, \tau_2) =& \Theta(\tau_1 - \tau_2)\Psi_{\sigma_1}(\boldsymbol{r}_1\, \tau_1)\Psi_{\sigma_2}(\boldsymbol{r}_2\, \tau_2) \\ & - \Theta(\tau_2 - \tau_1)\Psi_{\sigma_2}(\boldsymbol{r}_2\, \tau_2)\Psi_{\sigma_1}(\boldsymbol{r}_1\, \tau_1), \end{aligned} \tag{2.7}$$

where the negative sign in front of the second term in the right-hand side comes from the anticommutation relation of the fermionic particles. In other words, the operator T_τ re-orders operators with respect to imaginary times. We can find that the pair function must satisfy the following relation under the exchange of the two electrons [i.e., $(\sigma_1, \boldsymbol{r}_1, \tau_1) \leftrightarrow$

Table 2.1: Expanded symmetry classification of Cooper pairs. In this classification, the relative imaginary time of the two electrons consisting a Cooper pair is took into account. Thus the pair function has three degrees of freedom: spin, orbital, and Matsubara frequency. The four symmetry classes below can satisfy the antisymmetricity relation in Eq. 2.9.

Conventional classification

	Frequency	Spin	Parity
ESE class	Even-ω	Singlet	Even parity
ETO class	Even-ω	Triplet	Odd parity
OSO class	Odd-ω	Singlet	Odd parity
OTE class	Odd-ω	Triplet	Even parity

$(\sigma_2, \boldsymbol{r}_2, \tau_2)]$ as

$$F_{\sigma_1\sigma_2}(\boldsymbol{r}_1, \boldsymbol{r}_2, \tau_1, \tau_2) = -F_{\sigma_2\sigma_1}(\boldsymbol{r}_2, \boldsymbol{r}_1, \tau_2, \tau_1). \tag{2.8}$$

Exactly speaking, the anticommutation relation including the time degree of freedom has not been defined in quantum mechanics. However, in the Green function method, we can consider the antisymmetric property of pair functions through the time-ordering. The symmetry of Cooper pairs is usually discussed in terms of the Matsubara frequency ω_n with n being integers, which is conjugate of relative imaginary time $\tau_1 - \tau_2$. Thus we adopt the frequency representation. In this case, the pair function satisfies

$$F_{\sigma_1\sigma_2}(\boldsymbol{r}_1, \boldsymbol{r}_2, \omega_n) = -F_{\sigma_2\sigma_1}(\boldsymbol{r}_2, \boldsymbol{r}_1, -\omega_n) \tag{2.9}$$

Here a Cooper pair has the three degrees of freedom; coordinates, spins, and Matsubara frequencies. The rule restricting the combination of these degrees of freedom is only the antisymmetric relation in Eq. (2.9). Therefore, as summarized in Table (2.1), the pair functions are classified into the four symmetry classes[A]: (i) even-frequency spin-singlet even-parity, (ii) even-frequency spin-triplet odd-parity, (iii) odd-frequency spin-singlet odd-parity, and (iv) odd-frequency spin-triplet even-parity symmetry classes. In Table 2.1, the red-colored components account for antisymmetricity under the exchange

[A] Recently, several theoretical groups expanded the classification of Cooper pairs to multiband superconductors [59–61]. They confirmed the emergence of odd-band odd-frequency spin-singlet s-wave Cooper pairs in the presence of band hybridizations. However we focus only on single-band superconductors for simplicity.

of the two electrons sharing a Cooper pair. In the conventional classification, there are only two symmetry classed, whereas there are four classes in the generalized classification. The symmetry classes in the third and fourth lines from the top of Table 2.1 have the odd-frequency symmetry. Such Cooper pairs are so-called odd-frequency Cooper pairs.

2.2 Emergence of odd-frequency Cooper pairs

2.2.1 Superconductor/diffusive-normal-metal junction

We first consider superconductor/diffusive-normal-metal junctions as shown in Fig. (2.1). When a non-superconducting material is attached to a superconductor, the Cooper pairs causing the superconductivity penetrate into the attached material. As a result, the attached material also shows the qualitatively-similar properties to the superconductor (e.g., diamagnetic response and resistivity decreasing). These phenomena are called the superconducting proximity effects. The proximity effects have been so far observed in various types of superconducting junctions [See, for example, A. A. Golubov *et al.*, Phys. Rev. B **51**, 1073 (1995)]. The Cooper pairs appearing in a non-superconducting material could have different pairing symmetry from that of the Cooper pairs staying in the superconductor. We first assume the superconductor consisting the junction is a d-wave superconductor, which is realized in cuprate superconductors such as YBCO. In this case, Cooper pairs are induce in the diffusive normal metal attached to the superconductor by the proximity effect. However the orbital symmetry of such Cooper pairs is restricted to be the s-wave. In the disordered system as $\ell/\xi_0 \ll 1$, the phenomena occurring there are basically isotropic because the isotropic impurity scatterings prohibit anisotropy. In terms of Cooper pairs, only the s-wave pairing correlation can survive under such a strong disorder. Thus, even if the attached superconductor is realized by anisotropic Cooper pairs, pairing symmetry induced in the diffusive normal metal is always the s-wave. In the diffusive metal attached to the d-wave superconductor, we can find the spin-singlet s-wave Cooper pairs because the superconductor is the spin-singlet one and we do not consider spin-dependent potentials here. According Table. (2.1), the induced Cooper pairs belong to the ESE class. Namely they are the conventional even-frequency Cooper pairs.

When one employs a spin-triplet superconductor instead of the spin-singlet one, the story above is changed. Here we assume the superconductor is a spin-triplet chiral-p-wave one as realized in strontium ruthenate Sr_2RuO_4 [89–91]. In this junction, the spin-triplet s-wave Cooper pairs nucleate in the diffusive normal metal as shown in Fig. (2.2). However both of the orbital and the spin parts of their pair function are symmetric under the exchange of two electrons. Although such a pairing seems to violate the Pauli rule in

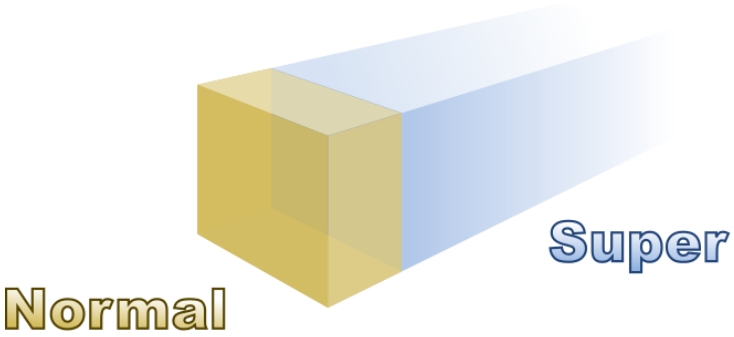

Figure 2.1: Schematic of the superconductor/diffusive-normal-metal junction. When a diffusive normal metal is attached to a superconductor, the Cooper pairs penetrate into the normal metal from the superconductor (the superconducting proximity effect). In the diffusive normal metal, Cooper pairs with a different symmetry class from those in the superconductor can be induced due to the impurity scattering.

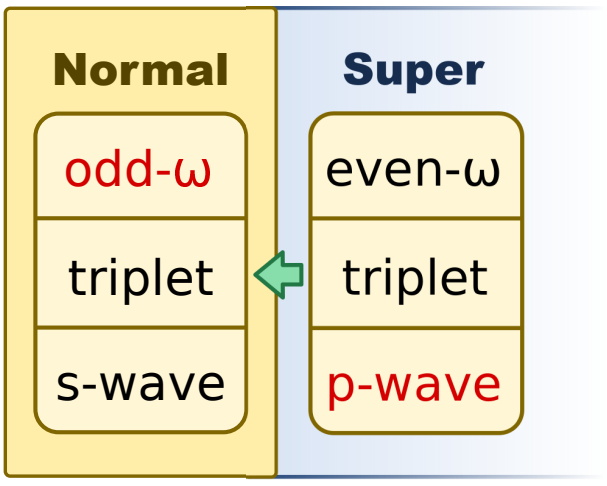

Figure 2.2: Pairing symmetries of the Cooper pairs in the superconductor/diffusive-normal-metal junction. Only the s-wave Cooper pairs can survive in the diffusive normal metal. When a spin-triplet superconductor such as Sr_2RuO_4 is employed in a junction, odd-frequency Cooper pairs are induced in the attached normal metal.

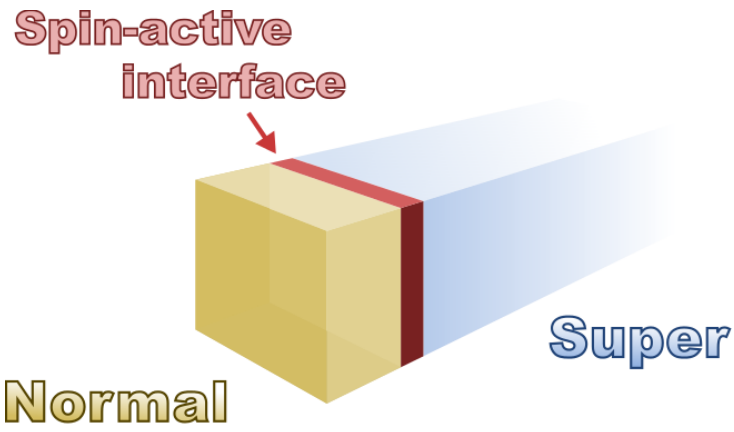

Figure 2.3: Schematic of a superconductor/diffusive-normal-metal junction with a spin-active interface. The superconductor is limited to be the conventional s-wave superconductor. The Cooper pairs appear in the diffusive normal metal because of the proximity effect. The spin-active interface affects on the symmetry of the Cooper pairs induced there through the spin-dependent scattering at the surface.

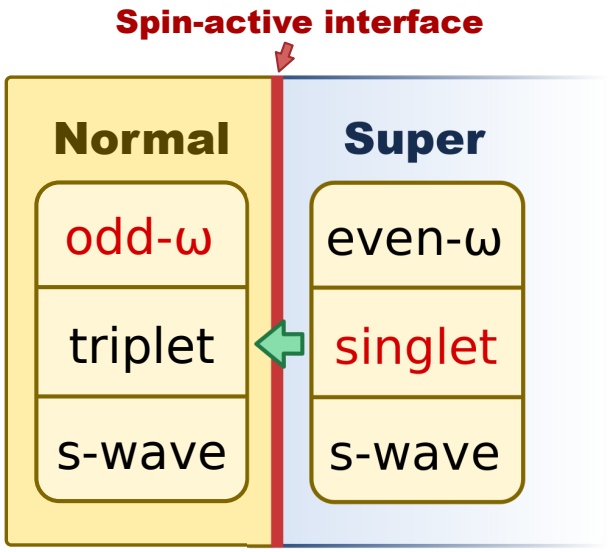

Figure 2.4: Pairing symmetry of the Cooper pairs in the junction. When there is a spin-active interface, both of the spin-singlet and spin-triplet Cooper pairs are induced in the diffusive normal metal due to the spin-dependent scattering at the interface. The spin-triplet component has the odd-frequency s-wave pairing symmetry.

Eq. (2.9), they can avoid such violation by changing their frequency symmetry. Namely, we always obtain the odd-frequency spin-triplet s-wave Cooper pairs (OTE class) in the diffusive normal metal.

2.2.2 Superconductor/diffusive-normal-metal junction with a spin-active interface

Spin-rotational symmetry breaking can locally induce odd-frequency Cooper pairs [36,37, 40,41,43,44,46,47] as well as the translational symmetry breakdown discussed above. Here we discuss a diffusive-normal-metal/superconductor junction with an spin-active interface as shown in Fig. 2.3, where we assume the superconductor belongs to the conventional spin-singlet s-wave symmetry class. The proximity effect generates Cooper pairs in the diffusive normal metal as discussed above. If there is no spin-dependent potential, all of the Cooper pairs in the system should have spin-singlet pairing symmetry because the superconductivity is realized by the spin-singlet pairs. However, in this junction, the spin mixing is occurred in the vicinity of the spin-active interface [46, 47]. The spin mixing gives rise to spin-triplet components in the diffusive normal metal. The symmetry of induced Cooper pairs are the spin-triplet s-wave class because only the s-wave pairing is allowed in diffusive materials. Namely the Cooper pairs in the diffusive normal metal should have the odd-frequency pairing symmetry to satisfy the Fermi-Dirac statistics.

2.2.3 Surface of a superconductor

When additional symmetry breaking is occurred, odd-frequency Cooper pairs appear in systems. This symmetry breaking induces additional Cooper pairs with different symmetry from that deep inside of a superconductor. In what follows, we discuss the pairing symmetry of Cooper pairs near the surface of a Cooper pairs. We here consider the surface of a d-wave superconductor. The superconductivity is realized by the even-frequency spin-singlet d-wave Cooper pairs in this case. We find only the d-wave Cooper pairs in a spatially-homogeneous system. Near a surface, however, the parity mixing occurs in the vicinity of a surface due to the inversion-symmetry breaking. In other words, the pairing function of the Fourier components with different orbital symmetry from the d-wave have finite amplitudes there. Here we focus on the odd-parity components. These induced components can not satisfy the Fermi-Dirac statistics Eq. (2.9). Thus they must have odd-frequency symmetry. The inversion-symmetry breaking due to the presence of a surface induces odd-frequency Cooper pairs.

However we do not have always sufficiently-large pair amplitude of odd-frequency

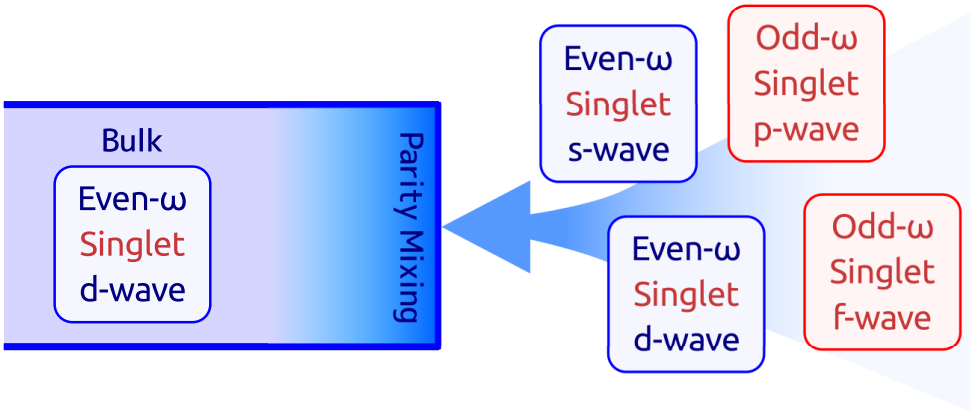

Figure 2.5: Pairing symmetries at the surface of a semi-infinite d-wave superconductor. In the vicinity of the surface, the pair functions with the different orbital symmetry from those in the bulk region such as s-, p-, f-wave pairings have finite amplitudes due to the local inversion-symmetry breaking. The odd-parity pairs must be the odd-frequency Cooper pairs to satisfy the Fermi-Dirac statistics.

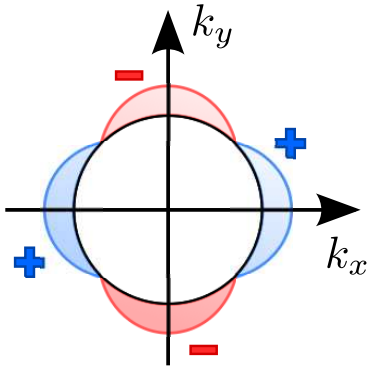

Figure 2.6: Pair potential in momentum space for $d_{x^2-y^2}$-wave superconductors. The white circle represents the Fermi surface in two dimensions. The superconducting gap is opened at the Fermi level as indicated the red or blue parts. The signs (+ and −) indicate the internal phase of the pair potential because of the d-wave nature.

Cooper pairs at surfaces. At the surface of a conventional (s-wave) superconductor, their amplitudes are usually much smaller compared to those of even-frequency pairings. In these cases, the presence of odd-frequency Cooper pairs does not affect on the phenomena which is occurred in a superconductor. Namely the presence of odd-frequency Cooper pairs is negligible. At surfaces of unconventional (topological) superconductors, on the other hand, we can obtain sufficiently-large amplitude of odd-frequency Cooper pairs. One of the most remarkable characters of unconventional superconductors is that their pair potentials changes their signs on the Fermi surface as shown in Fig. 2.6. It is well known these sign changes result in the emergence of the Andreev bound states [63–65, 68, 69] (ABSs) at their surfaces.

The Andreev bound states are quasiparticle bound states which appear at surfaces and junction interfaces. Here we focus on the ABSs appearing at the surface of a topological superconductor such as d-wave and chiral-p-wave one. The ABSs and odd-frequency Cooper pairs are deeply related to each other. When the ABSs emerge at a surface of a superconductor, the pair potential is strongly suppressed close to the surface. In other words, the spatial gradient of the pair potential $\nabla_{\boldsymbol{r}}\Delta(\boldsymbol{r})$ becomes non-zero there. This spatial variation gives rise to odd-frequency Cooper pairs as subdominant pairing components [58]. Namely condition for the emergence of the ABSs is completely equivalent to the condition for the emergence of odd frequency Cooper pairs.

The surface ABSs are the results of quasiparticle interference near the surface, and are deeply related to the reflection of a quasiparticle at a surface. Here we consider the quasiparticle reflection at a surface of a topological d-wave superconductor in two dimensions as shown in Fig. 2.7. One of the most representative properties of topological superconductors is the sign change of pair potentials on the Fermi surface. This sign changes are play important roles for forming ABSs. In a superconducting state, quasiparticles propagate under the pair potential depending on their momentum $\Delta(k_x, k_y)$. When a quasiparticle is reflected by a surface, the pair potential for this quasiparticle suddenly changes from $\Delta(k_x, k_y)$ to $\Delta(-k_x, k_y)$ because the momentum is changed by the surface reflection. If the sign of the pair potential changes while the quasiparticle is reflected, the surface ABS always appears. In the case of a $d_{x^2-y^2}$-wave superconductor, even though the pair potential is anisotropic and its sign changes on the Fermi surface, the sign of Δ is not changed while the quasiparticle reflection as shown in Fig. 2.7(a). On the other hand, in the case of a d_{xy}-wave superconductor as shown in Fig. 2.7(b), the sign of the pair potential changes from minus to plus. In this case, the surface ABSs appear at the surface as indicated red region.

2.3 Magnetic response of odd-frequency Cooper pairs

2.3.1 Anomalous surface impedance and negative pair density

Odd-frequency Cooper pairs induced in inhomogeneous systems shows qualitatively-different properties from those of conventional even-frequency pairs. In 2012, Y. Asano *et al.* studied theoretically the response of a semi-infinite superconductor covered by a thin diffusive normal metal to an electromagnetic wave in terms of the surface impedance $Z = R - iX$. The surface resistance R represents the electric resistance due to the electrons. The surface reactance X represents the power loss due to the Cooper pairs. The surface impedance is calculated from the complex conductivity within the linear response theory.

The typical behavior of the surface impedance can be obtained when a semi-infinite conventional s-wave superconductor (e.g., Nb and Al) is employed in a junction, and is shown in Fig. 2.8(a), where the energy of the electromagnetic wave is set to $\hbar\omega = 0.01\Delta_0$ with Δ_0 being the amplitude of the pair potential. Throughout this chapter, Z is normalized to $Z_0 = 2\pi\Delta_0/\sigma_N\hbar c^2$ with σ_N and c being the Drude conductivity and the speed of light. When the superconducting transition is occurred, both of the surface resistance and the reactance decrease suddenly. At low temperature, the surface resistance and reactance converge at certain values, respectively. Most importantly, in whole of the temperature range below T_c, the relation $R < X$ is always satisfied. It is well known that this relation is satisfied in most superconducting systems.

The surface impedance of the bilayer with spin-singlet $d_{x^2-y^2}$-wave superconductor is shown in Fig. 2.9(a). In this junction, the even-frequency s-wave Cooper pairs are induced in the diffusive normal metal. The results are not qualitatively-different from the result in an s-wave superconducting junction as shown in Fig. 2.8(b) because the induced Cooper pairs have the same frequency symmetry as those stay in the superconductor. In this spin-singlet junction, the typical behavior $R < X$ is always satisfied below the critical temperature.

In the spin-triplet junction, on the other hand, the surface impedance breaks this relation. The temperature dependence of the surface impedance of the spin-triplet junction is shown in Fig. 2.9(b), where the authors employed a chiral p-wave superconductor as a spin-triplet superconductor. The surface impedance satisfies the typical relation $R < X$ almost all temperature regime $0.3T_c < T < T_c$. However a peak appears in the surface resistance R at $T \sim 0.2T_c$ and the surface reactance X changes its sign at that temperature. The typical relation $R < X$ is partially broken around $T \sim 0.2T_c$. When a triplet superconductor is employed as a superconductor and the proximity effect is occurred, the typical relation $R < X$ is broken at a certain temperature regime. In this junction,

the Cooper pairs in the superconductor have the even-frequency spin-triplet chiral-p-wave symmetry, whereas those in the diffusive normal metal have the odd-frequency spin-singlet s-wave symmetry as discussed above.

The authors attempted to understand the anomalous surface impedance by analyzing the contribution from the diffusive normal metal Z_N to the total surface impedance of the junction Z_{NS}. The result of Z_N in the spin-singlet junctions are shown in Fig. 2.10(a). In the results, the typical relation $R < X$ is satisfied. Thus the total surface impedance of the spin-singlet junctions also satisfies the typical relation. The contributions from the diffusive normal metal in a spin-triplet junction are shown in Fig. 2.10(b). The surface resistance R is larger than the surface reactance X for the spin-triplet chiral-p-wave case. The difference between the spin-singlet and spin-triplet junctions is only the frequency symmetry of Cooper pairs induced in the diffusive normal metal because spin-dependent potentials are not take into account in their theory. Thus they concluded that the anomalous surface impedance a direct evidence of the emergence of the odd-frequency Cooper pairs in the diffusive normal metal.

The authors further considered the origin of the anomalous surface impedance. They focused on the quantity $K_s(\varepsilon)$ which is called the spectral pair density. It is connected to the pair density through the relation as

$$n_s \sim \int_{-\infty}^{\infty} d\varepsilon K_s(\varepsilon) \tanh(\varepsilon/2T) \tag{2.10}$$

$$= \int_{0}^{\infty} d\varepsilon K_s(\varepsilon) \tanh(\varepsilon/2T), \tag{2.11}$$

where the relation $K_s(\varepsilon) = -K_s(-\varepsilon)$ is used. The spectral pair densities calculated at the diffusive normal metals attached to spin-singlet s-wave and spin-triplet chiral-p-wave superconductors are shown in Figs. 2.11(a) and 2.11(b), respectively. In the spin-singlet s-wave junction, $K_s(\varepsilon)$ is positive for almost all temperatures and there is a positive peak around $T = 0.3T_c$. The pair density obtained from the integration in Eq. (2.11) is clearly positive for the s-wave case. In the spin-triplet chiral-p-wave junction, on the other hand, there is a large negative peak at $\varepsilon = 0$. The authors have concluded the anomalous response to electromagnetic fields stems from their negative pair density.

2.3.2 Phenomenological theory for odd-frequency Cooper pairs

According to basic textbooks on superconductivity [1–4], all superconductors should be diamagnetic. Superconductivity is caused by the electrons condensation into Cooper pairs. In the superconducting states the electron wave functions can be described by only

one macroscopic wave function because the superconductivity is a result of a coherent motions of condensed electrons. When a superconductor is located in a weak magnetic field, the Cooper pairs screen the external magnetic field by driving diamagnetic supercurrents to preserve the phase coherence of the superconducting condensate. Therefore the diamagnetic property is an essential property of all superconductors.

The diamagnetism of superconductors can easily be shown by using the London equation [1–3]. The diamagnetic supercurrent is phenomenologically described by this London equation as

$$\boldsymbol{j}_s(\boldsymbol{r}) = -\frac{n_s e^2}{mc}\boldsymbol{A}(\boldsymbol{r}), \tag{2.12}$$

where n_s is the superfluid density, e and m is the charge and the mass of an electron respectively, c is the speed of light. Here let us consider a semi-infinite s-wave superconductor occupying the region $x > 0$. Its surface is located at $x = 0$. An external magnetic field is applied in the z-direction $\boldsymbol{H}(x) = H_z(x)\hat{\boldsymbol{z}}$. The magnetic field is obtained from the vector potential as $\partial_x A_y(x) = H_z(x)$, where we employ the gauge $\boldsymbol{A}(x) = A_y(x)\hat{\boldsymbol{y}}$. In this situation, the supercurrent flows only in the y-direction $\boldsymbol{j}(x) = j_y(x)\hat{\boldsymbol{y}}$. The magnetic field is connected to the Meissner screening current through the Maxwell equation as

$$-\partial_x H(x) = \frac{4\pi}{c} j_y(x). \tag{2.13}$$

Combining the London and Maxwell equations, we can obtain the differential equation

$$\left[\partial_x^2 - \frac{1}{\lambda_L^2}\right] H_z = 0, \tag{2.14}$$

where $\lambda_L = \sqrt{mc^2/4\pi n_s e^2}$ is the London depth. The spatial profile of the magnetic field can be obtained by solving this equation under the two conditions: $H(x)|_{x=0} = H^{\rm ext}$ and $H(x)|_{x\to\infty} = 0$. In a superconductor, the magnetic field decays exponentially with increasing the distance from the surface as

$$H(x) = H^{\rm ext}\exp(-x/\lambda_L). \tag{2.15}$$

The equation above means that the external magnetic field can penetrate only into the region near the surface characterized by the magnetic penetration depth λ_L. Thus superconductors are regarded as perfectly-diamagnetic materials. The conventional even-frequency Cooper pairs generate a magnetic field in the opposite direction of the external field as shown in Fig. 2.12(a).

Odd-frequency Cooper pairs, on the other hand, show qualitatively-different magnetic response. As discussed in the previous section, odd-frequency Cooper pairs have the negative pair density. This sign change results in a significant difference of magnetic response. We hare discuss the magnetic response of odd-frequency Cooper pairs just by introducing the negative pair density $n_s' = -|n_s|$. Substituting the negative pair density into Eq. (2.12), we can obtain the "London equation" for odd-frequency Cooper pairs as

$$\boldsymbol{j}_s(\boldsymbol{r}) = +\frac{n_s' e^2}{mc}\boldsymbol{A}(\boldsymbol{r}). \tag{2.16}$$

The equation above means that the odd-frequency Cooper pairs carry the magnetic current in the opposite direction compared with the case for conventional even-frequency Cooper pairs. The supercurrents carried by the odd-frequency pairs would enhance the magnetic field in a superconductor because they flow in the opposite direction of the diamagnetic current as illustrated schematically in Fig. 2.12(b). In fact, by combining the "London equation" Eq. (2.16) and the Maxwell equation, we can find that the magnetic field in a superconductor is not screened, and can penetrate deep inside a superconductor with an oscillating behavior. Since odd-frequency Cooper pairs appear at surfaces, sufficiently-small superconductor, in which odd-frequency Cooper pairs would dominate its magnetic response, would show the paramagnetic response. As discussed above, on the basis of the phenomenological theory, we can find that odd-frequency Cooper pairs do not show the diamagnetic Meissner response. However, within the phenomenological theory, we can not conclude whether the odd-frequency Cooper pairs alter the magnetic response of a small superconductor from the usual diamagnetic to unusual paramagnetic response.

2.4 Experiments on the magnetic response of small superconductors

The sings of anomalous magnetic response of odd-frequency Cooper pairs have already been observed in several experiments [6–19]. H. Walter *et al.* studied experimentally the magnetic response of narrow thin d-wave superconductors [6, 7]. They first fabricated thin films of $YBa_2Cu_3O_7$ (YBCO) superconductors (i.e., unconventional superconductors) [Fig. 2.13(a)], and irradiated an heavy-ion beam to the films with a sufficiently-low incident angle about 15° as shown in Fig. 2.14(a). As a results, long but narrow elliptic holes are created on the films [Fig. 2.13(b)] whose length and width are about 2 μm and about 20 nm, respectively. In other words, the wide superconducting films are cut

into fractions of superconductors. The superconducting film with the long holes can be regarded as a collection of narrow superconductors [Fig. 2.13(c)]. They measured the temperature dependence of the screening factor $S^{-1}(T)$ obtained from the inductance of superconducting film. The screening factor corresponds directly to the magnetic penetration depth $\lambda_L(T)$. The experiments are carried out with several choices of the angle between the long holes and the a-axis of the crystal of YBCO high-T_c superconductors [Fig 2.14(b)]. The results are shown in Fig. 2.15, where the screening factors are normalized to their values at 18K. The typical temperature dependence of the penetration depth is monotonic decreasing with decreasing temperature. In their experiments, the screening factors decrease monotonically above 10K as the typical behavior. However they increase slightly at low temperature. The increasing of the screening factors depend on the angle between the major axis of holes and the a axis. When the angle is 45° the increasing of the screening factor is maximized. The increasing of the screening factors imply that the diamagnetic response of the superconductors becomes weaker at low temperature.

The anomalous magnetic response has been confirmed also in the superconducting nanowire covered by gold [9–12], mesoscopic superconducting disks with giant vortices [13, 14], and granular high-T_c superconductors [15–18], in the Au/Ho/Nb junction [19]. At present, the mechanism of the paramagnetic property is an open question in physics of superconductivity [20–30].

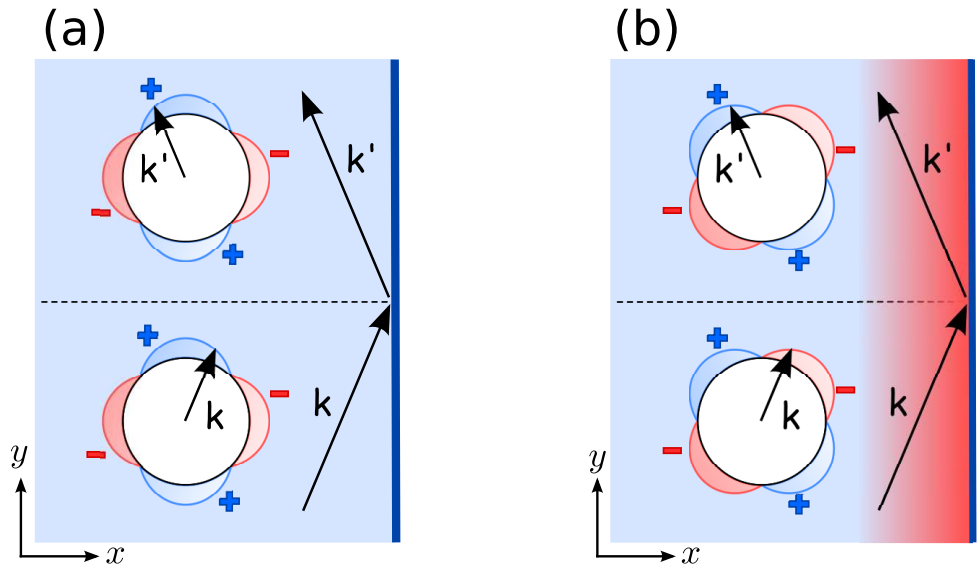

Figure 2.7: Schematics of quasiparticle reflections at surface of (a) $d_{x^2-y^2}$- and (b) d_{xy}-wave superconductors. While a quasiparticle is reflected by a surface, its momentum changes discontinuously from $\boldsymbol{k} = (k_x, k_y)$ to $\boldsymbol{k}' = (-k_x, k_y)$. Simultaneously, the momentum-dependent pair potential for the quasiparticle is also changes suddenly. If the signs of the pair potential is changed by a reflection at a surface, the surface Andreev bound states appear as shown in the panel (b).

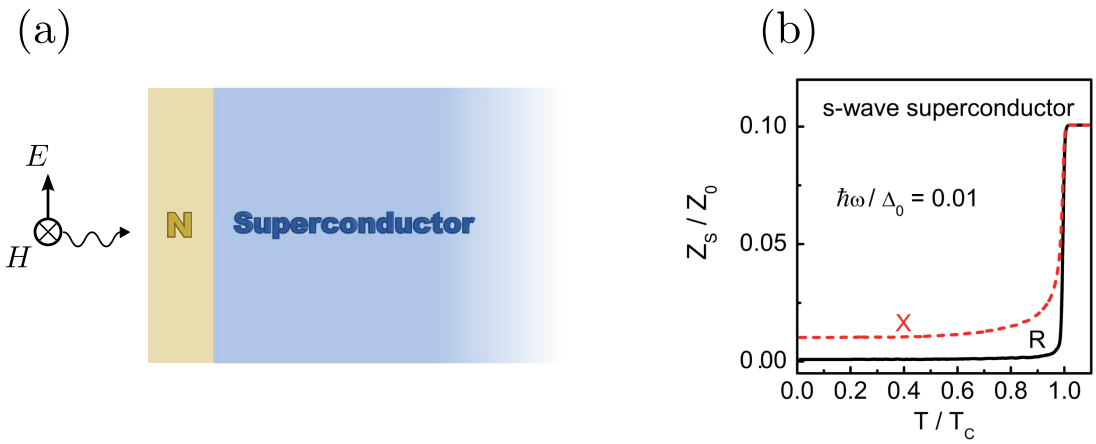

Figure 2.8: (a) Schematic of the system considered by Y. Asano *et al.* [48]. A sufficiently weak electromagnetic wave $\hbar\omega = 0.01\Delta_0$ is irradiated to a semi-infinite superconductor covered by a thin diffusive normal metal, where ω and Δ_0 are the frequency of the electromagnetic wave and the amplitude of the pair potential. The thickness of a diffusive normal metal is the order of the coherence length at the zero temperature. (b) Typical temperature dependence of the surface impedance $Z = R - iX$. The surfaced impedance Z is normalized to $Z_0 = 2\pi\Delta_0/\sigma_N\hbar c^2$ with σ_N and c being the Drude conductivity and the speed of light. The robust relation $R < X$ is always satisfied below the superconducting transition temperature.

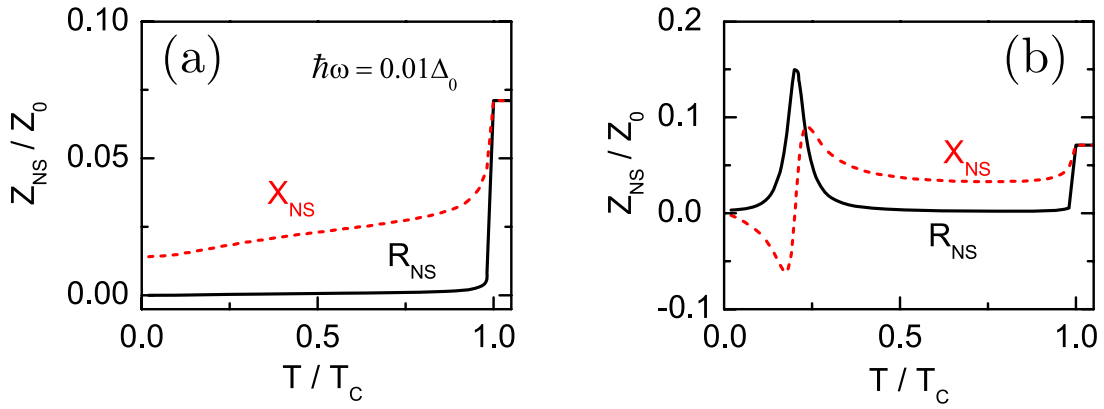

Figure 2.9: Surface impedance of the superconductor/diffusive-normal-metal junction $Z_{\rm NS}$ [48]. The results for the spin-singlet s-wave and the spin-triplet chiral-p-wave junctions are shown in the panel (a) and (b), respectively. In the former case, the Cooper pairs in the diffusive normal metal have the even-frequency symmetry, whereas those have the odd-frequency symmetry in the latter case. In case that the even-frequency Cooper pairs, the typical relation $R_{\rm NS} < X_{\rm NS}$ is always satisfied below T_c. On the other hand, in case that the odd-frequency Cooper pairs appear in the normal metal, a peak appears in the surface resistance $R_{\rm NS}$ at $T \sim 0.2T_c$ and the surface reactance $X_{\rm NS}$ changes its sign at that temperature. In addition, the typical relation $R_{\rm NS} > X_{\rm NS}$ is broken at certain temperature regions.

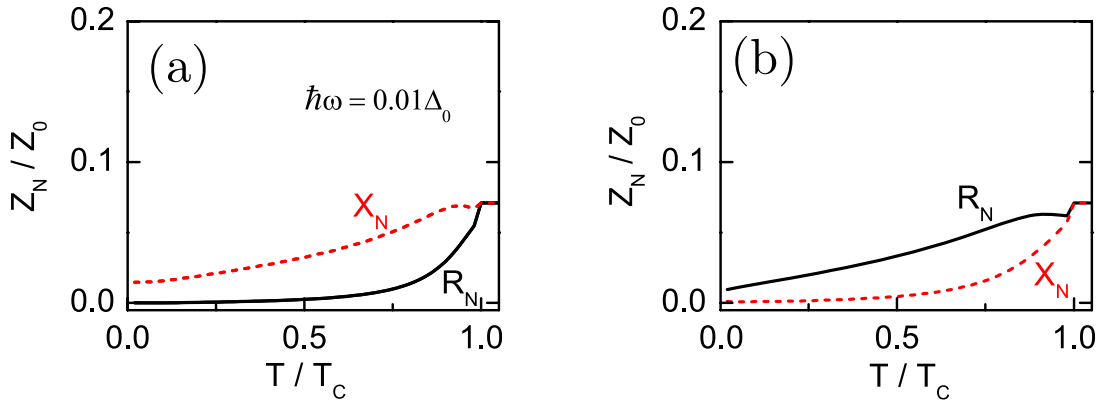

Figure 2.10: Contributions from the diffusive normal metal to the total surface impedance $Z_{\rm N}$ in each junction [48]. The results for the spin-singlet s-wave and the spin-triplet chiral-p-wave junctions are shown in the panel (a) and (b), respectively. When the Cooper pairs in the normal metal have the even-frequency symmetry, the typical relation $R_{\rm N} < X_{\rm N}$ is alway satisfied. On the other hand, when the odd-frequency Cooper pairs appear in the normal metal, the surface impedance shows the anomalous behavior as $R_{\rm N} > X_{\rm N}$.

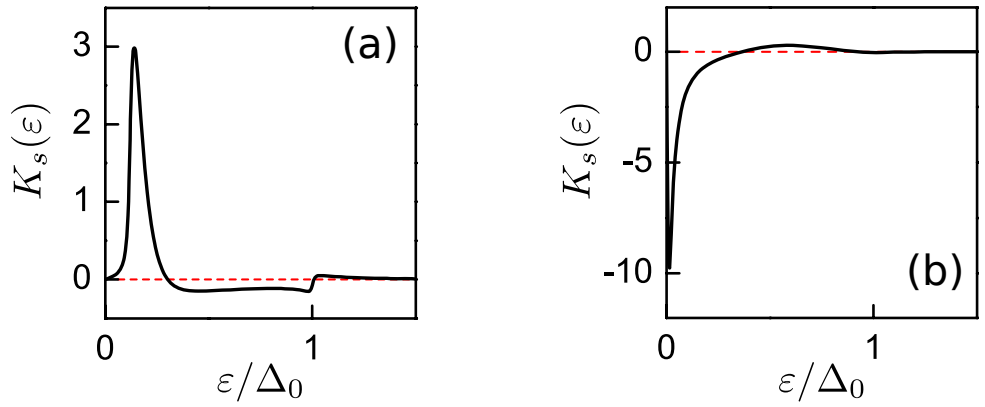

Figure 2.11: Spectral pair densities at the surface of the junction. The results with s-wave and chiral-p-wave superconducting junction are shown in the panels (a) and (b), respectively. In the result with a s-wave superconductor, there is a positive peak at about $T = 0.2T_c$. The resultant pair density n_s obtained by Eq. (2.11) should be positive. On the other hand, in the junction with a chiral p-wave superconductor, there is a negative peak at low-energy regime. The resultant pair density for odd-frequency Cooper pairs should be negative.

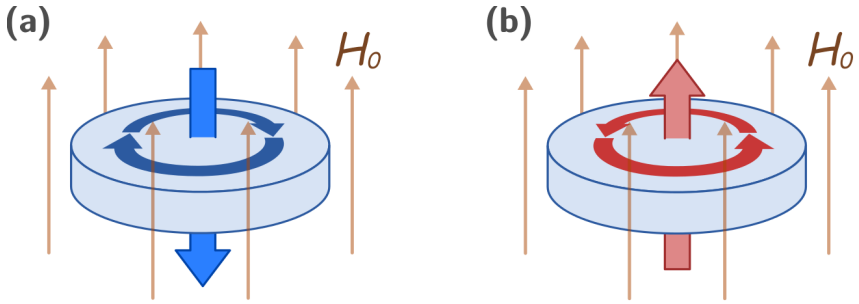

Figure 2.12: Direction of the supercurrent carried by (a) even-frequency and (b) odd-frequency Cooper pairs. The supercurrent by even-frequency Cooper pairs generates a magnetic field which cancels the external field. In the case odd-frequency Cooper pairs, the supercurrent flows in the opposite direction and the magnetic field enhances the external field.

Figure 2.13: Schematic figures of thin films of a high-T_c superconductor as studied in Ref. [6]. They first fabricated thin films of a cuprate superconductor YBCO (a). After that, they irradiate heavy-ion beam on the films and create long but narrow holes (b). These samples can be regarded the collection of narrow superconductors (c).

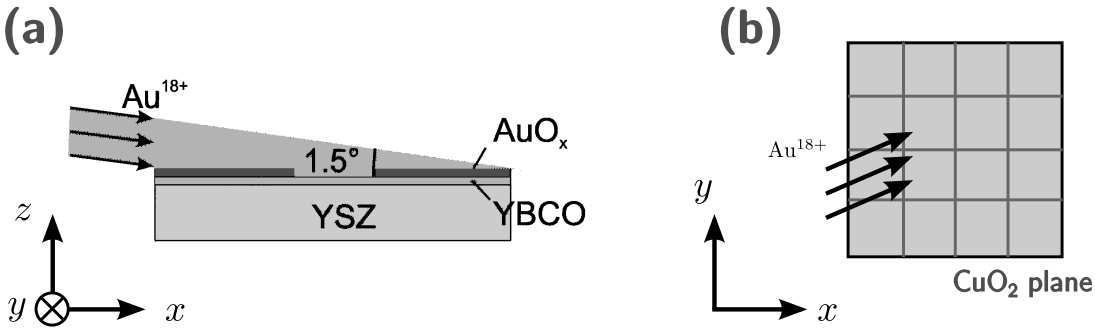

Figure 2.14: Irradiation angles of heavy-ion beams. In their experiments, the angle between the direction of a beam and the surface of the samples are set to 15° as shown in (a). (b) Top view of the sample. In cuprate superconductor, the quasi-two-dimensional superconductivity is realized the CuO_2 plain whose crystal structure is a square lattice. The authors tuned the angle between the direction of the irradiation in the xy plain and the a axis of the samples.

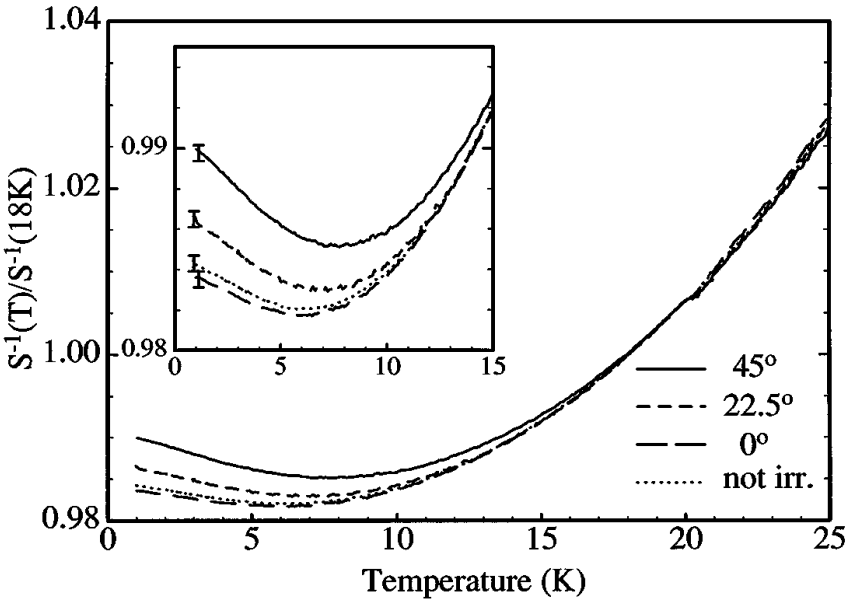

Figure 2.15: Temperature dependences of the screening factors $S^{-1}(T)$ which correspond to the magnetic penetration depth $\lambda_L(T)$. The screening factors are normalized to their values at 18K. The results ware measured in the samples which are irradiated ion beams from different angles in xy plain. The typical behaviour of the penetration depth is monotonic decreasing with decreasing temperature. However $S^{-1}(T)$ increase slightly at low temperature.

Chapter 3

Paramagnetic response of small topological superconductors

3.1 Abstract

The diamagnetism is an essential property of all superconductors. However, we will show that small topological (or unconventional) superconductors can be intrinsically paramagnetic by solving the quasiclassical Eilenberger equation and the Maxwell equation self-consistently on two-dimensional superconducting disks in weak magnetic fields. Because of the topologically nontrivial character of the wave function, the unconventional superconductors host the zero-energy surface Andreev bound states, which always accompany so-called odd-frequency Cooper pairs. The paramagnetic property of the odd-frequency pairs explains the paramagnetic response of the disks at low temperature.

3.2 Introduction

The Meissner effect is a fundamental property of superconductors as shown in standard textbooks [1]. The response of superconductors is usually diamagnetic because a superconductor excludes weak enough magnetic fields from its interior. The anomalous paramagnetic response, however, has been observed in small disks of metallic superconductor [13,14], small high-T_c compounds [15–18], and mesoscopic proximity structures [9–12]. The spatial inhomogeneity of the magnetic property is a key feature to realize the paramagnetic phase. In metallic superconductors, the inhomogeneous distribution of magnetic fields [20] and the formation of giant vortex are responsible for the paramagnetic Meissner effect (PME) [21]. The presence of the π junctions is also pointed out as an origin of

PME in a network of Josephson junction [22]. In unconventional superconductors (USs), on the other hand, an experiment [6, 7] has shown the decrease of the pair density with decreasing temperature, which suggests a peculiar mechanism of the PME unique to the USs. As a result of the topological nature in the wave function, the USs have the topologically protected surface Andreev bound states (ABSs) at the zero-energy [63–65, 68, 69]. So far theoretical studies have shown that the magnetic response at the (110) surface of high-T_c superconductor is nonlinear [25, 30] and paramagnetic [26–29] due to the ABSs. The paramagnetic response has been mainly explained in terms of the energetics of the ABSs. Weak magnetic fields shift the energy of the surface ABSs away from the Fermi level and decrease the total energy of superconductor, which leads to the paramagnetic response or the paramagnetic instability. However, there is an important open question: what carries the large paramagnetic supercurrent? By addressing this issue, we will conclude that the magnetic properties of USs are intrinsically inhomogeneous and that small USs can be paramagnetic at low temperature.

The electric current in equilibrium has two contributions, (i.e., $\boldsymbol{j} = \boldsymbol{j}_{\rm pq} + \boldsymbol{j}_{\rm A}$). The quasiparticle current $\boldsymbol{j}_{\rm pq}$ due to the spatial phase gradient of the wave function is paramagnetic, whereas $\boldsymbol{j}_{\rm A} = -ne^2\boldsymbol{A}/mc$ is diamagnetic. In a normal metal, $\boldsymbol{j}_{\rm pq}$ cancels $\boldsymbol{j}_{\rm A}$ because the phase of an electron is not rigid at all [4]. In a superconductor, on the other hand, the phase rigidity of superconductivity drastically suppress the spatial gradient of phase, which leads to $\boldsymbol{j}_{\rm qp} = 0$. As a result, a superconductor shows the perfect diamagnetism. In contrast to excited quasiparticles *above* the superconducting gap, the quasiparticles *below* the gap have the phase rigidity because they are the shadow of Cooper pairs. In fact, a normal metal attaching to a metallic superconductor shows the diamagnetic Meissner effect [23]. This phenomenon is explained by two different but equivalent pictures: the penetration of a Cooper pair into the normal metal (proximity effect) and the Andreev reflection of a quasiparticle *below* the gap. The appearance of the surface ABSs is a direct result of the coherent Andreev reflections of a quasiparticle at the Fermi level [69]. Therefore such phase-rigid quasiparticles at the ABS cannot carry the large paramagnetic current.

In this paper, we theoretically study the spatial distribution of magnetic fields and that of electric currents on small two-dimensional superconducting disks with unconventional pairing symmetry such as spin-singlet d wave and spin-triplet p wave. There are several d-wave superconductors in organic compounds and heavy fermionic materials in addition to high-T_c cuprates. Recently, the effective Hamiltonian for superconducting states in nanowires [70, 71] has shown to be unitary equivalent to that for p_x wave superconducting states [52]. The simulation at least two-dimensional system is necessary to evaluate the magnetic susceptibility quantitatively because the d and p wave pair poten-

tials are anisotropic in real space. We solve the Eilenberger equation for the quasiclassical Green function and the Maxwell equation for magnetic fields self-consistently. The self-consistency of pair potential and magnetic field is necessary to regularize the nonlinear property in the magnetic response [25, 30]. The solution of the Green function near the disk edge shows the presence of the odd-frequency Cooper pairs. The odd-frequency pairs have paramagnetic property [48, 50, 51] because of their *negative pair density*. The calculated results of the magnetic susceptibility suggest the PME in small USs. We conclude that the odd-frequency Cooper pairs carry the large paramagnetic current and causes the paramagnetic response of small superconducting disks.

3.3 Formulation

Let us consider a superconducting disk in two-dimension as shown in Fig. 3.1, where R is the radius of the disk. We assume that the disk is in the clean limit and its surface is specular enough. To analyze the superconducting states in equilibrium, we solve the Eilenberger equation [72],

$$i\hbar v_F \hat{\boldsymbol{k}} \cdot \boldsymbol{\nabla}_{\boldsymbol{r}} \check{g} + \left[\check{H}, \check{g}\right] = 0, \tag{3.1}$$

$$\check{H}(\boldsymbol{r}, \boldsymbol{k}, i\omega_n) = \begin{bmatrix} \hat{\xi}(\boldsymbol{r}, \boldsymbol{k}, i\omega_n) & \hat{\Delta}(\boldsymbol{r}, \boldsymbol{k}) \\ \underset{\sim}{\hat{\Delta}}(\boldsymbol{r}, \boldsymbol{k}) & \underset{\sim}{\hat{\xi}}(\boldsymbol{r}, \boldsymbol{k}, i\omega_n) \end{bmatrix}, \tag{3.2}$$

$$\check{g}(\boldsymbol{r}, \boldsymbol{k}, i\omega_n) = \begin{bmatrix} \hat{g}(\boldsymbol{r}, \boldsymbol{k}, i\omega_n) & \hat{f}(\boldsymbol{r}, \boldsymbol{k}, i\omega_n) \\ -\underset{\sim}{\hat{f}}(\boldsymbol{r}, \boldsymbol{k}, i\omega_n) & -\underset{\sim}{\hat{g}}(\boldsymbol{r}, \boldsymbol{k}, i\omega_n) \end{bmatrix}, \tag{3.3}$$

$$\hat{\xi}(\boldsymbol{r}, \boldsymbol{k}, i\omega_n) = i\omega_n + (ev_F/c)\boldsymbol{k} \cdot \boldsymbol{A}(\boldsymbol{r}), \tag{3.4}$$

where $\boldsymbol{k}$ is the unit vector on the Fermi surface, v_F is the Fermi velocity, $\omega_n = (2n+1)\pi T$ is the Matsubara frequency, n is an integer number, and T is a temperature. In this paper,

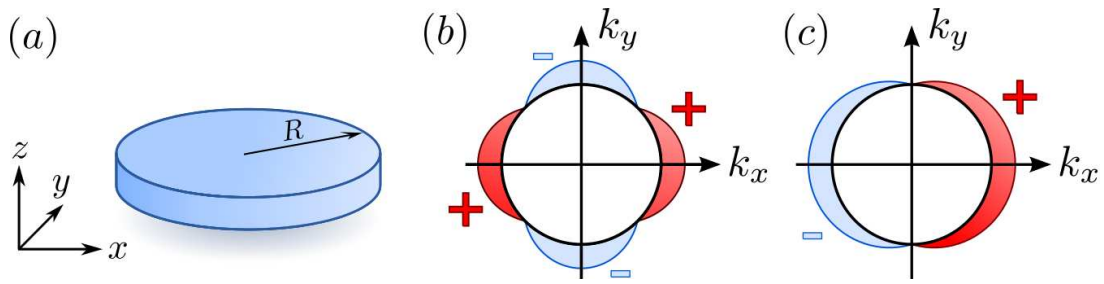

Figure 3.1: (a) Schematic figure of a superconducting disk. The pair potentials in momentum space are illustrated for the d wave symmetry in (b) and for the p wave symmetry in (c).

the symbol $\cdot\hat{\cdot}\cdot$ represents 2×2 matrix structure in spin space and $\hat{\sigma}_j$ for $j=$ 1-3 are the Pauli matrices. The vector potential is denoted by $\boldsymbol{A}$ and the magnetic field $\boldsymbol{H}=\nabla\times\boldsymbol{A}$ is in the z direction. We introduced a definition $\underset{\sim}{X}(\boldsymbol{r},\boldsymbol{k},i\omega_n)\equiv X^*(\boldsymbol{r},-\boldsymbol{k},i\omega_n)$ for all functions X. The electric current is given by

$$\boldsymbol{j}(\boldsymbol{r})=\frac{\pi e v_F N_0}{2i}T\sum_{\omega_n}\int\frac{d\boldsymbol{k}}{2\pi}\mathrm{Tr}\left[\check{T}_3\ \boldsymbol{k}\ \check{g}(\boldsymbol{r},\boldsymbol{k},\omega_n)\right], \tag{3.5}$$

with $\check{T}_3=\mathrm{diag}[\hat{\sigma}_0,-\hat{\sigma}_0]$, where $\hat{\sigma}_0$ is the identity matrix in spin space and N_0 is the density of state per spin at the Fermi level. We mainly consider the two equal-time pairing order parameters in two dimension: spin-singlet d-wave symmetry $\hat{\Delta}(\boldsymbol{r},\theta)=\Delta(\boldsymbol{r})\cos(2\theta)i\hat{\sigma}_2$ and spin-triplet p-wave symmetry $\hat{\Delta}(\boldsymbol{r},\theta)=\Delta(\boldsymbol{r})\cos(\theta)\hat{\sigma}_1$, where θ is a directional angle with $k_x=\cos\theta$ and $k_y=\sin\theta$. The pair potentials are determined self-consistently from the gap equation

$$\Delta(\boldsymbol{r})i\hat{\sigma}_\nu\hat{\sigma}_2=\pi N_0 gT\sum_{\omega_n}\int_0^{2\pi}\frac{d\theta}{2\pi}\hat{f}(\boldsymbol{r},\theta,i\omega_n)V_x(\theta), \tag{3.6}$$

where $x=s,p$ and d indicate the pairing symmetry, $\nu=0$ and 3 for the spin-singlet and the spin-triplet order parameters, respectively. The coupling constant g satisfies $\{N_0 g\}^{-1}=\ln(T/T_c)+\sum_{0\le n<\omega_c/2\pi T}(n+1/2)^{-1}$ with T_c and ω_c being the transition temperature and the cut-off energy, respectively. The attractive potentials depends on the pairing symmetry $V_x(\theta)=s_x\phi_x(\theta)$ with $s_s=1$ and $\phi_s(\theta)=1$ for s wave symmetry, $s_p=2$ and $\phi_p(\theta)=\cos\theta$ for p wave symmetry, and $s_d=2$ and $\phi_d(\theta)=\cos(2\theta)$ for d wave symmetry. The local magnetic susceptibility is defined by

$$\chi_m(\boldsymbol{r})=\left(H(\boldsymbol{r})-H^{\mathrm{ext}}\right)/(4\pi H^{\mathrm{ext}}), \tag{3.7}$$

where H^{ext} is the uniform external magnetic field in the z direction. The susceptibility of the whole disk is calculated to be $\chi=\int d\boldsymbol{r}\chi_m(\boldsymbol{r})/(\pi R^2)$. In the absence of spin-dependent potential, the spin structure of $\hat{\Delta}$ and that of $\hat{f}$ are always the same with each other. We use the standard Riccati parametrization [74–76] to solve the Eilenberger equation Eq. (3.1). To obtain numerical solutions of the Riccati type differential equation in closed disks, we apply a method discussed in Ref. [77]. An initial value at a certain place in the closed system is necessary to solve the Riccati equation. The obtained solution usually depends on the initial condition. However, when we solve the equation along the long enough classical trajectory, the effects of the initial condition is eliminated. In numerical simulation, we increase the length of the trajectory until solutions do not depend on the

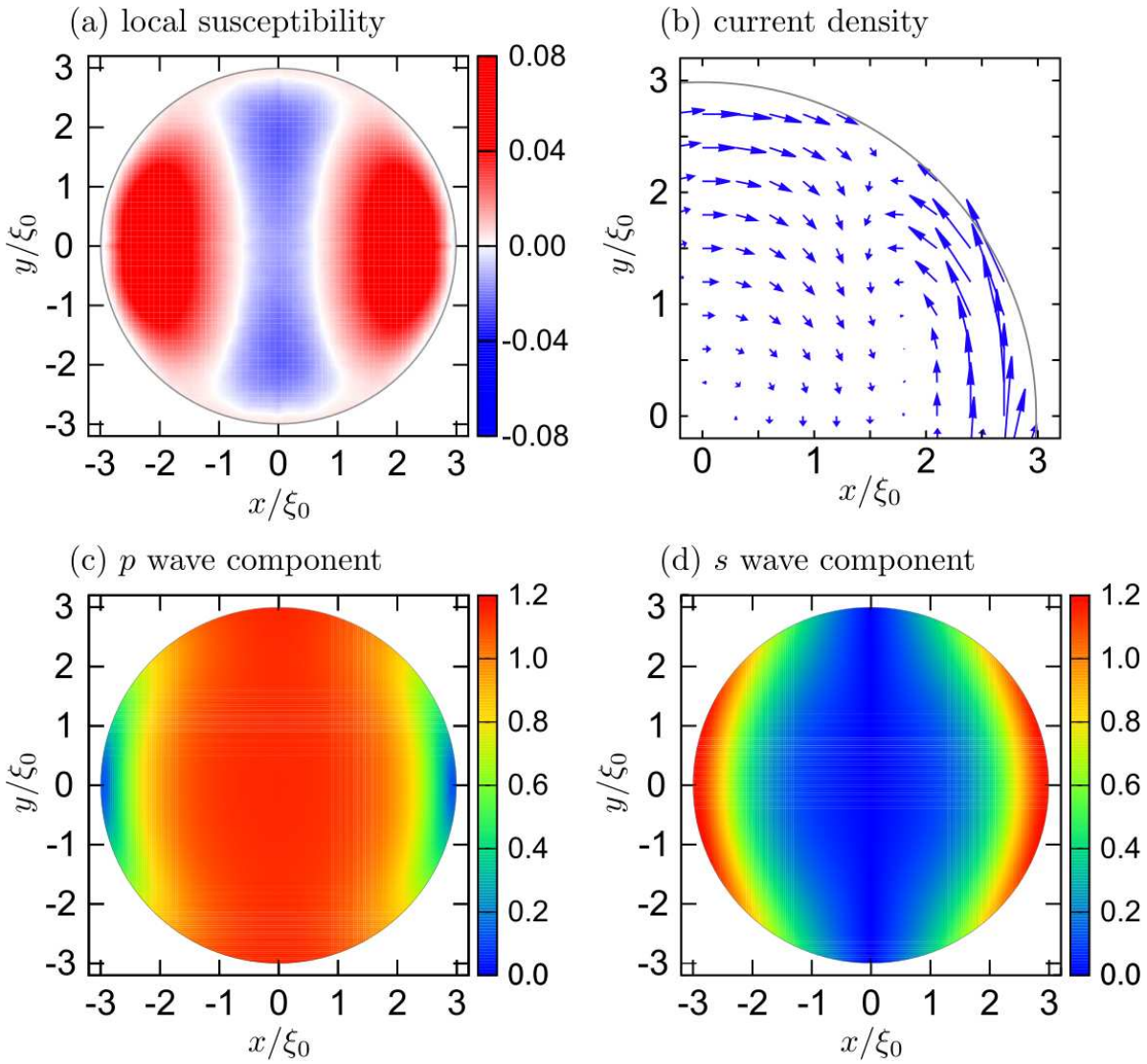

Figure 3.2: (a) The local susceptibility and (b) the current density of the d-wave superconductor, where $R = 3\,\xi_0$, $\lambda_L = 3\,\xi_0$, $\omega_c = 10\,\Delta_0$, and $H^{\rm ext} = 0.001 H_{c1}$. (c) The d-wave and (d) the p-wave components of the anomalous Green function.

initial conditions. The vector potential $\boldsymbol{A}$ is obtained by solving the Maxwell equation $\nabla \times \boldsymbol{H} = (4\pi/c)\boldsymbol{j}$ with Eq. (3.5). We calculate self-consistent solutions of the vector potential and pair potential by solving the Maxwell equation and the Eilenberger equation simultaneously. The anomalous Green function $\hat{f}(\boldsymbol{r}, \theta, i\omega_n)$ is originally defined by the two annihilation operators of two electrons consisting of a Cooper pair. Therefore $\hat{f}(\boldsymbol{r}, \theta, i\omega_n)$ must be antisymmetric under the interchange of the two electrons, which stems from the Fermi-Dirac statistics of electrons. Such fundamental relation is represented by

$$\hat{f}(\boldsymbol{r}, \theta, i\omega_n) = -[\hat{f}(\boldsymbol{r}, \theta + \pi, -i\omega_n)]^{\mathrm{T}}, \tag{3.8}$$

where T represents the transpose of matrices.

3.4 Results

The external magnetic field and the cut-off energy are fixed at $H^{\mathrm{ext}} = 0.001 H_{c_1}$ and $\omega_c = 10\Delta_0$, respectively. Here $H_{c_1} = \hbar c/|e|\xi_0^2$ is the first critical magnetic field. The length is measured in units of $\xi_0 = \hbar v_F/\Delta_0$ with Δ_0 being the amplitude of the pair potential at $T = 0$. The current density is normalized to $J_0 = \hbar c/|e|\xi_0^3$. The characteristic length scale of the Maxwell equation is $\lambda_L = (4\pi n e^2/mc^2)^{-1/2}$ and is a parameter in the numerical simulation. Throughout this paper, we use a unit of $k_B = 1$.

In Fig. 3.2, we first show the calculated results of the local susceptibility (a) and the current density (b) for the d-wave superconducting disk, where we fix the parameters as $R = 3\,\xi_0$, $\lambda_L = 3\,\xi_0$, and $T = 0.3\,T_c$. We set $+x$ and $+y$ axes to be identical to (100) and (010) directions of the high-T_c crystal. The central region of the disk is diamagnetic as usual, whereas the surfaces in the (110) and $(1\bar{1}0)$ directions are paramagnetic as shown in (a). The current density has the complex structure near the surface as shown in (b), where the arrow indicates the direction of current and its length represents the amplitude of current. Here we present the picture only for $x > 0$ and $y > 0$ in (b) because the results are fourfold symmetric due to the d-wave character of order parameter. The diamagnetic current flows at the edges in the (100) and (010) directions, whereas the paramagnetic current flows at the edges in the (110) direction. The vortex-like current profile can be seen near the surfaces because the two currents flow the opposite directions to each other. At the central region, on the other hand, only the diamagnetic current flows. Such magnetic properties are unique to unconventional superconductors. In s-wave case, the susceptibility is diamagnetic everywhere in the disk as show in the Appendix A.

The anomalous paramagnetic response is well explained by appearing the odd-frequency Cooper pairs. The anomalous Green function can be decomposed into s-, p-, and d-wave

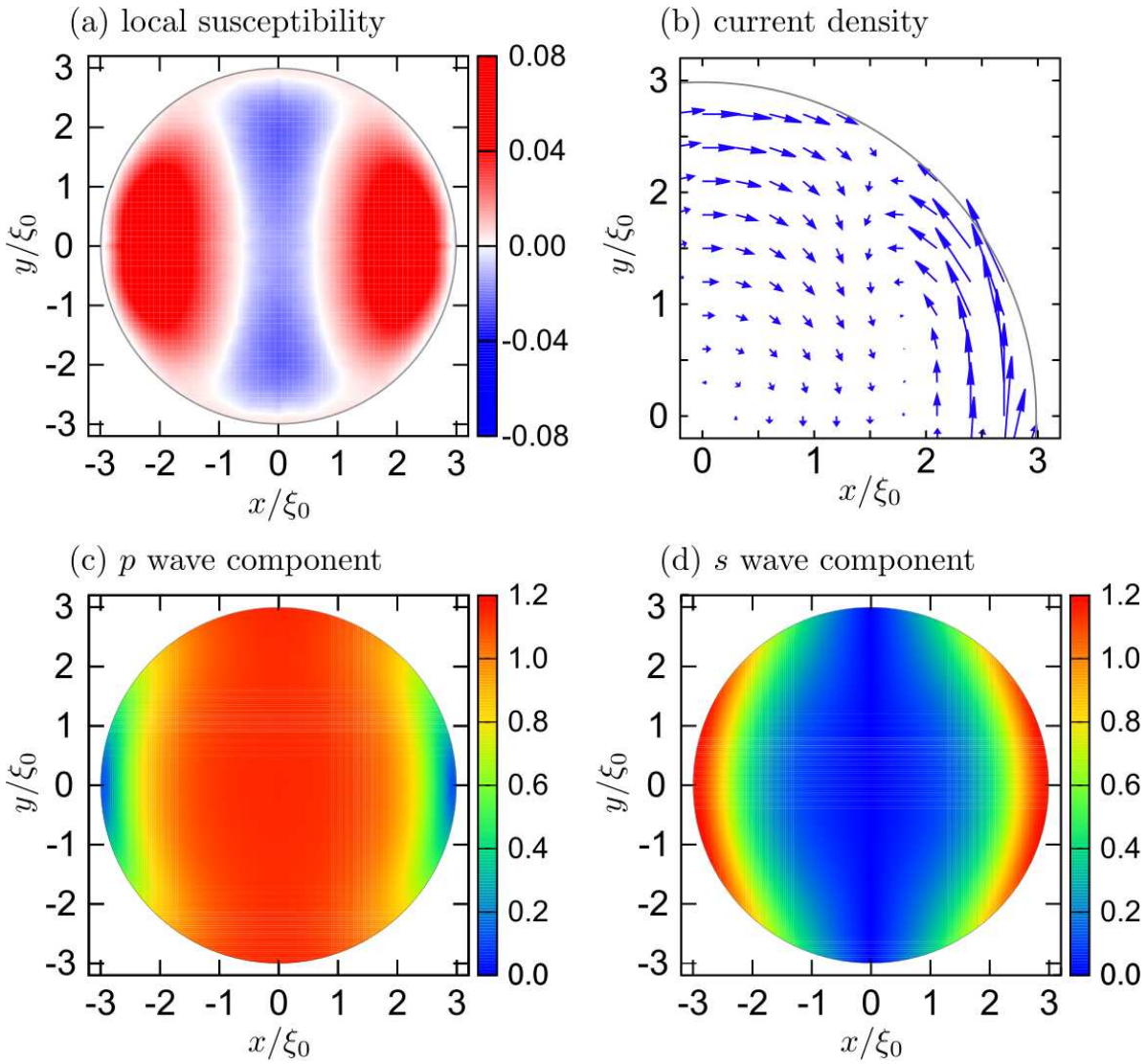

Figure 3.3: (a) The local susceptibility and (b) the current density of the p-wave superconductor, where $R = 3\,\xi_0$, $\lambda_L = 3\,\xi_0$. (c) The p-wave and (d) the s-wave component of the anomalous Green function.

components by

$$f_x(\boldsymbol{r}, i\omega_n) i\hat{\sigma}_\nu \hat{\sigma}_2 = \int_0^{2\pi} \frac{d\theta}{2\pi} V_x(\theta) \hat{f}(\boldsymbol{r}, \theta, i\omega_n), \tag{3.9}$$

for $x = s, p$, and d. Figure 3.2(c) shows the amplitude of the d-wave component at $\omega_0 = \pi T$. The spatial profile of the order parameter is almost similar to that of (c). The d-wave component drastically suppresses in (110) and $(1\bar{1}0)$ directions, which has been well known as a result of appearing of topologically protected Andreev surface bound states at the zero-energy [65, 66]. At the same time, the p-wave component of the anomalous Green function grows at the corresponding edges as shown in (d). The spin-singlet p-wave Cooper pairs must have the odd-frequency symmetry to satisfy Eq. (3.8). The breakdown of the translational symmetry at the surface mixes the even- and odd-parity components. The appearance of the Andreev surface bound states and that of the odd-frequency pairs are the two different faces of the same phenomenon. To have the zero-energy peak in the density of states, the frequency symmetry of Cooper pair must be odd [36,38,48]. The odd-frequency pairs have so called *negative pair density* [48], which leads to the paramagnetic instability as shown in Appendix B. Therefore we conclude that the paramagnetic current is carried by the induced odd-frequency Cooper pairs. Comparing the Figs. 2(b) with 2(d), the paramagnetic current flows at the regions where the odd-frequency Cooper pairs stay.

We have also obtained qualitatively the same results for a spin-triplet p-wave superconducting disk at $T = 0.2T_c$ as shown in Fig. 3.3, where the local magnetic susceptibility (a), the current density (b), the p-wave component of $\hat{f}$ (c), and s-wave component of $\hat{f}$ (d) are presented in the same manner as Fig. 2. The results in Fig. 3.3 show the twofold symmetry reflecting the p-wave order parameter. The surface bound states are appear at the (100) surfaces at which the p-wave component of the anomalous Green function is suppressed. Correspondingly, the s-wave component becomes large at the surfaces of (100) directions. The spin-triplet s-wave component belongs to the odd-frequency symmetry class according to Eq. (3.8). The main difference between Figs. 2 and 3 is the property of the surface ABS at the zero-energy. In the spin-triplet p-wave disk, Majorana fermions appear at the surface [52]. From Figs. 2 and 3, we conclude that the magnetic property of unconventional superconductors are intrinsically inhomogeneous and can be paramagnetic because of the odd-frequency Cooper pairs at the surface.

The magnetic properties of superconductors strongly depends on the disk size because the odd-frequency pairs spatially localize near the surface limited by ξ_0 from the edge. Next, therefore, we discuss the relation between the magnetic property and the disk size. Figure 3.4 is the paramagnetic-diamagnetic phase diagram of the d- and p-wave superconducting disks, where the vertical axis is the paramagnetic-diamagnetic crossover

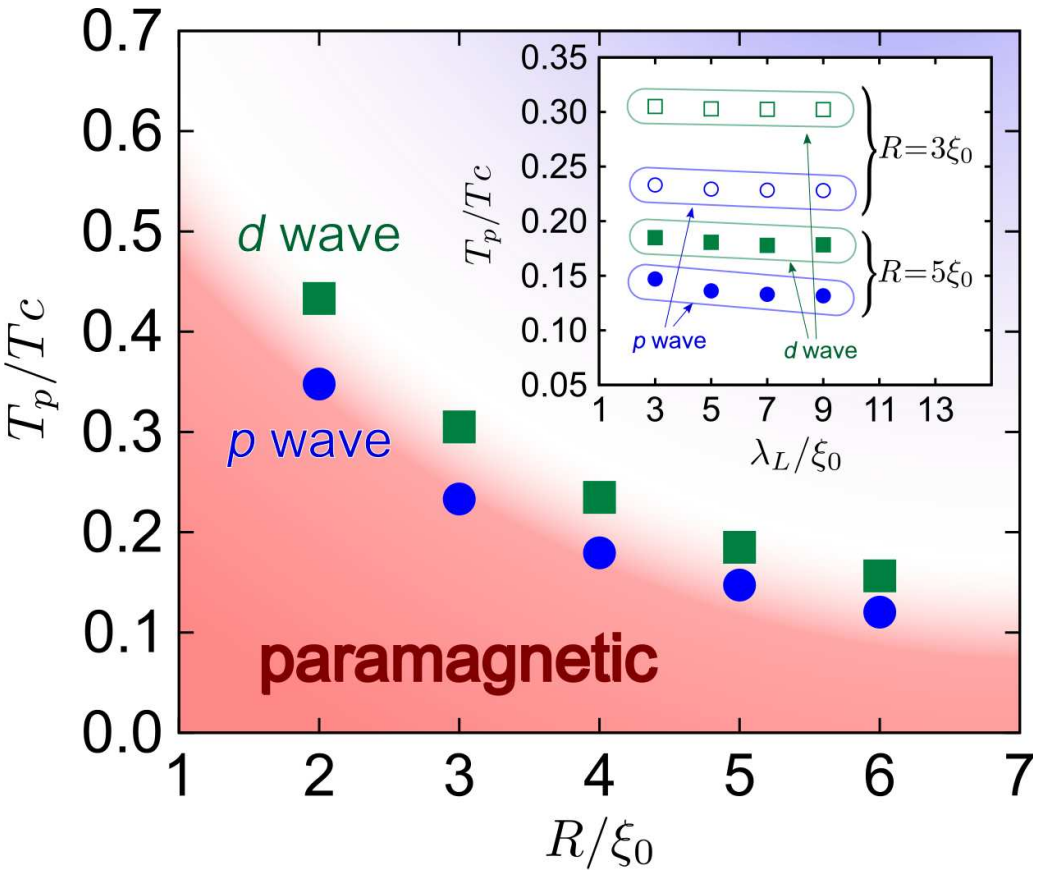

Figure 3.4: (a) The diamagnetic-paramagnetic phase diagram of superconducting disks for the d-wave (square) and p-wave (circle) pairing symmetry, where $\lambda_L = 3\,\xi_0$, $\omega_c = 10\Delta_0$. (b) The penetration length dependencies of the paramagnetic-diamagnetic crossover temperatures, where the square and circle symbols are the results for the d-wave and p-wave pairings, and the open and closed symbols are the results for the $R = 3\,\xi_0$ and $R = 5\,\xi_0$ superconducting disks, respectively.

temperature T_p and the horizontal one is the radius of superconducting disk R. The disk is paramagnetic $\chi > 0$ at the temperatures below T_p. The results show that T_p decrease with increasing the radius of the superconductor. As shown in Figs. 2 and 3, the paramagnetic area is limited to ξ_0 from the surface because odd-frequency pairs are confined there. On the other hand, the bulk area are diamagnetic because even-frequency pairs stay there. Roughly speaking, the relative area of staying the odd-frequency pairs to the whole area of disk qualitatively determines the magnetic response of the disk. Thus the paramagnetic phase disappears in large disks with $R \gg \xi_0$ because the contribution from the surface is negligible in large enough disks. This argument is supported by the λ_L dependence of T_p shown in the inset of Fig. 4, where open (filled) symbols represent the results for $R/\xi_0 = 3$ (5) and the circles (squares) are the results for p (d) wave disks. The crossover temperature is totally insensitive to λ_L. To be paramagnetic, the larger disks require the stronger contribution from the odd-frequency Cooper pairs. The odd-frequency Cooper pairs energetically localize around the zero-energy [48]. The temperature smears effects of them on the magnetic response. Therefore T_p decreases with increasing the disk size as shown in Fig. 4.

Finally, we discuss the susceptibility of whole superconducting disk as a function of temperature as shown in Fig. 5, where we fix the penetration depth at $\lambda_L = 3\,\xi_0$. The results for d- and p- wave symmetries are presented in (a) and (b), respectively. The magnetic susceptibility just below T_c is negative as usual. With decreasing temperature, the paramagnetic current due to the odd-frequency Cooper pairs increases. As a consequence, the susceptibility upturns at low temperature, which is qualitatively different from the susceptibility in the s wave case as shown in Appendix A. Below T_p, the paramagnetic odd-frequency Cooper pairs dominate the magnetic response of the superconductor. Therefore the dependence of the susceptibility on temperature shows the reentrant behavior as demonstrated in Fig. 5. In experiments, it is possible to measure the susceptibility as a function of temperature.

3.5 Discussion

Our theoretical results may correlate to the measurement of the pair density at low temperature [6,7]. They measured the penetration depth $\lambda_L = (4\pi n_s e^2/mc^2)^{-1/2}$ of a YBCO film on which (110) oriented internal surfaces are introduced by heavy-ion bombardment. They found that λ first decreases with decreasing temperature from T_c then increases at very low temperature. This results can be interpreted as a result of decreasing the pair density n_s at low temperature. The odd-frequency pairs have the negative pair density. Thus the decrease of n_s may suggest the increase of odd-frequency pair fraction.

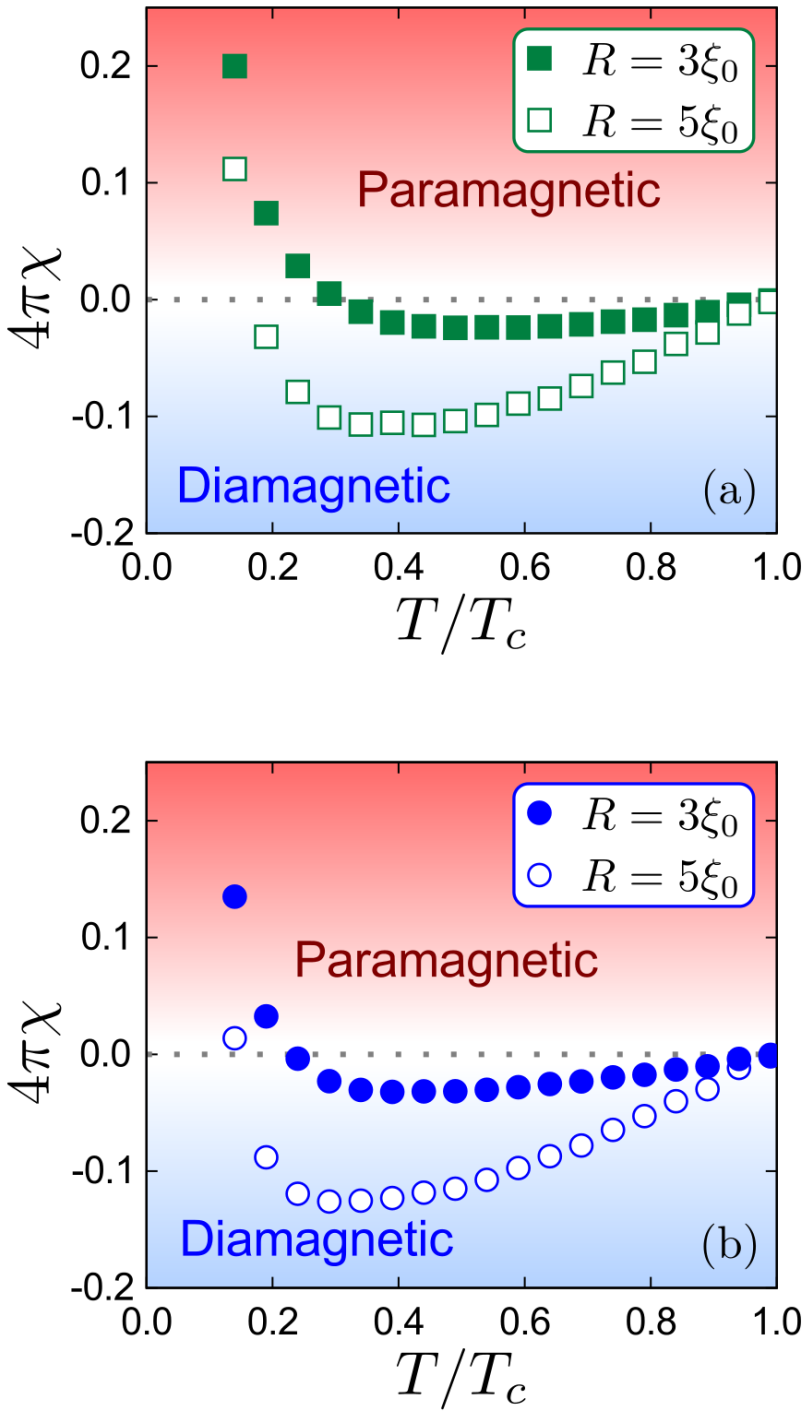

Figure 3.5: Temperature dependencies of the magnetic susceptibility for the (a) spin-singlet d-wave and (b) spin-triplet p-wave superconducting disks. The open and closed symbols indicate the results for the larger disk ($R = 5\xi_0$) and for the smaller disk ($R = 3\xi_0$).

The experimental results on a high-T_c superconductor are consistent with our theoretical results.

In real materials, the inelastic scatterings dephase the Cooper pairs and broaden the energy profile of the pairing functions. The inelastic mean free path also limits the size of disks in the phase diagram shown in Fig. 4. In d-wave superconductors, it has been shown that the surface roughness also broadens the zero-energy peak at the surface. In such situation, we infer that the roughness would suppress the paramagnetic effect. On the other hand in p-wave superconductors, the surface zero-energy peak is robust under the disordered potential. Therefore effects of surface roughness on the paramagnetic effect would be different in the two pairing symmetries. This is an important future issue.

The diamagnetism of superconductor is a result of gaining the condensation energy below the transition temperature. Therefore the paramagnetic superconducting states may be impossible in uniform thermodynamic limit. The paramagnetic phase in Fig. 4 can be considered as an unstable state and should disappear for large R/ξ_0. As shown in Fig. 2. and 3, the magnetic inhomogeneity is an intrinsic feature of unconventional superconductors. Such inhomogeneous property assists the appearance of the paramagnetic phase in small disks. Indeed we confirm that the paramagnetic phase appears in two cooling processes: field cool and zero-field cool.

The spontaneously time-reversal symmetry (TRS) breaking states has been discussed in high-T_c grains [82]. The subdominant component of order parameter near the surface breaks TRS. The results in Fig. 2 also indicates the TRS breaking superconducting state even when we simply assume the pure d wave order parameter. We are thinking that the symmetry crossover from d wave to TRS breaking $d + is$ might be possible in small samples. To prove this, however, we need to compare the free-energy among possible symmetry states. This issue goes beyond the scope of this paper.

Odd-frequency pairs appear also in superconductor/ferromagnet proximity structures [36]. When odd-frequency pairs are dominant in the ferromagnet [40, 41, 44], the paramagnetic instability may lead to spontaneous current there [51].

3.6 Conclusion

In conclusion, we have theoretically studied the magnetic response of small unconventional superconducting disks by using the quasiclassical Green function method. We conclude that small unconventional superconductors can be paramagnetic at low temperature due to the appearance of odd-frequency Cooper pairs at their surface. The magnetic properties of unconventional superconductors are intrinsically inhomogeneous as a result of their topologically nontrivial nature. Our results show up such universal property of

unconventional superconductivity.

Chapter 4

Stability of Paramagnetic Superconducting States

Generally speaking, a superconducting phase is more stable than a normal one as far as a superconductor is diamagnetic and homogeneous [1]. Therefore a homogeneous paramagnetic superconducting phase is usually unstable. The calculated results in Sec. III, however, show that the paramagnetic phase on a small superconducting disk is spatially inhomogeneous. In such situation, it would be worthy to check if the paramagnetic phase is a stable state at a free-energy minimum or a metastable state corresponding to a free-energy local minimum. In this section, we discuss the stability of paramagnetic phase in small unconventional superconductors by calculating the free-energy in clean superconducting disks.

The free-energy is calculated from the quasiclassical Green functions [73],

$$F_S - F_N = \int d\boldsymbol{r}\, \mathcal{F}(\boldsymbol{r}), \tag{4.1}$$

$$\mathcal{F}(\boldsymbol{r}) = \mathcal{F}_\Delta(\boldsymbol{r}) + \mathcal{F}_H(\boldsymbol{r}), \tag{4.2}$$

$$\mathcal{F}_H(\boldsymbol{r}) = \frac{\left\{H(\boldsymbol{r}) - H^{\rm ext}\right\}^2}{8\pi}, \tag{4.3}$$

$$\mathcal{F}_\Delta(\boldsymbol{r}) = \mathcal{F}_f(\boldsymbol{r}) + \mathcal{F}_g(\boldsymbol{r}), \tag{4.4}$$

$$\mathcal{F}_f(\boldsymbol{r}) = \pi N_0 \int \frac{d\theta}{2\pi}\, T \sum_{\omega_n} \Delta^*(\boldsymbol{r},\theta) f(\boldsymbol{r},\theta,i\omega_n), \tag{4.5}$$

$$\mathcal{F}_g(\boldsymbol{r}) = 4\pi N_0 \int \frac{d\theta}{2\pi}\, T \sum_{\omega_n>0}^{\omega_c} \times \int_{\omega_n}^{\omega_{c_2}} d\omega\ {\rm Re}\left\{g(\boldsymbol{r},\theta,i\omega) - 1\right\}, \tag{4.6}$$

where $\mathcal{F}_\Delta(\boldsymbol{r})$ is the condensation energy density of electron system and $\mathcal{F}_H(\boldsymbol{r})$ is the energy density of a magnetic field. We introduce an additional energy cut-off ω_{c_2} to evaluate the integration in Eq. (4.6). In this paper, we set $\omega_{c_2} = 400\Delta_0$ so that $\int d\boldsymbol{r}\mathcal{F}(\boldsymbol{r})$ reaches to a converged value. The free-energy densities normalized to $\mathcal{F}_0 = N_0|\Delta_0|^2/2$ which is the condensation energy density in a homogeneous s-wave superconductor. A temperature is set to be sufficiently low at $T = 0.1T_c$ so that a superconductor is in the paramagnetic phase.

The calculated results of the free-energy density for a d-wave disk and those for a p-wave one are shown in Fig. 4.1(a) and (b), respectively. The free-energy density is calculated along a trajectory ρ_α oriented by an angle α which is measured from the x axis as shown in Fig. 4.1. In a d-wave disk, the results in Fig. 4.1(a) show that $\mathcal{F}(\boldsymbol{r})$ is negative around the disk center. However it becomes positive near the surfaces at $\alpha = 0$. On the other hand, $\mathcal{F}(\boldsymbol{r})$ at $\alpha = \pi/4$ is almost flat and is always negative along the trajectory because odd-frequency pairs are absent in this direction. The results for $\alpha = \pi/2$ are identical to those for $\alpha = 0$ due to the four-fold symmetry. The free-energy density varies gradually from the line with $\alpha = 0$ to that with $\alpha = \pi/4$ as increasing α from $\alpha = 0$. The free-energy of whole disk $\int d\boldsymbol{r}\mathcal{F}(\boldsymbol{r})$ can be negative even though the disk is in the paramagnetic phase. In a p-wave disk, the increasing of $\mathcal{F}(\boldsymbol{r})$ occur only in two surfaces due to its p-wave symmetry. Therefore, we can conclude that both d- and p-wave superconducting states are more stable than a normal state even in their paramagnetic phase.

To analyse the details of the free-energy density further, we decompose the free-energy density at $\alpha = 0$ into $\mathcal{F}_H$ and $\mathcal{F}_\Delta$ as shown in Fig. 4.2(a). When a superconductor shows perfect Meissner effect, the energy of a magnetic field becomes $\mathcal{F}_H = (H^{\rm ext})^2/8\pi$. In a small superconductor (i.e., $R \sim \lambda_L$), an external magnetic field penetrates into whole the disk. This suppresses $\mathcal{F}_H$ from $(H^{\rm ext})^2/8\pi$ at the center of the disk. Near the surface, on the other hand, paramagnetic odd-frequency Cooper pairs attract a magnetic field, which increases $\mathcal{F}_H$ locally. The appearance of odd-frequency pairs also increases $\mathcal{F}_\Delta$ as discussed in Appendix. As a result, $\mathcal{F}(\boldsymbol{r})$ becomes positive at the disk surface in both Fig. 4.2(a) and (b). The condensation energy $\mathcal{F}_\Delta$ is negative at the disk center. While, near the surface, $\mathcal{F}_\Delta$ increases due to the suppression of the pair potential there in both Fig. 4.2(a) and (b). In appendix, we analytically calculate the Green functions and the free-energy density near the surface of a semi-infinite p_x-wave superconductor. The numerical results in Fig. 4.2(a) and (b) show that the free-energy of whole disk $\int d\boldsymbol{r}\mathcal{F}(\boldsymbol{r})$ remains negative because odd-frequency pairs are confined only near the surface. Therefore the paramagnetic superconducting state on d- and p-wave disks is more stable than the normal state.

Next, we study energetic properties of odd-frequency pairs. In our simulation, it is possible to obtain two superconducting states: a superconducting state in the absence of a magnetic field $H^{\rm ext} = 0$ and that in the presence of a magnetic field $H^{\rm ext} \neq 0$. At $H^{\rm ext} = 0$, there is no electric current everywhere. Superconducting states at $H^{\rm ext} \neq 0$, on the other hand, carry electric currents as shown in Fig. 5(a)-(d). Here we compare condensation energies of such two different superconducting states as shown in Fig. 4.3, where we plot $\mathcal{F}_\Delta$ on a p-wave disk for $\alpha = 0$. The solid line and the broken line indicate results for $H^{\rm ext} \neq 0$ and those for $H^{\rm ext} = 0$, respectively. As shown in Fig. 4.3, $\mathcal{F}_\Delta$ near surfaces for $H^{\rm ext} \neq 0$ is lower than that for $H^{\rm ext} = 0$. Odd-frequency pairing state in the presence of electric currents is more stable than that in the absence of electric currents. This energetic property explains the paramagnetic property of odd-frequency Cooper pairs. The argument above is valid also for a d-wave disk. In Appendix, we present analytical expression of difference between free-energy at $H^{\rm ext} = 0$ and that at $H^{\rm ext} \neq 0$. The results show that a magnetic field decreases the free-energy at low temperature because odd-frequency Cooper pairs have the paramagnetic property.

We have confirmed that the paramagnetic superconducting phase are more stable than the normal state by calculating the free-energy.

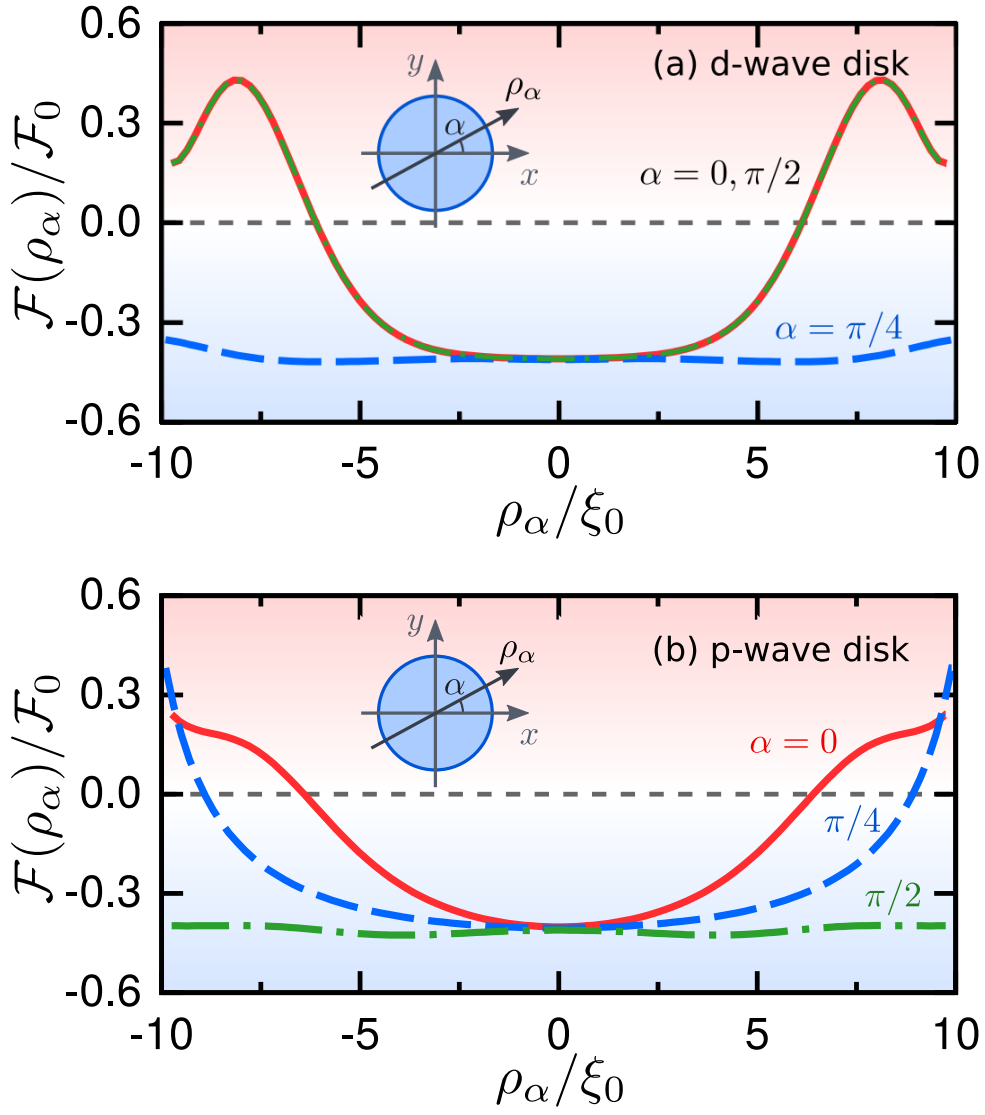

Figure 4.1: Free-energy densities on a trajectory ρ_α of a d-wave disk (a) and a p-wave disk (b), where $\mathcal{F}(\boldsymbol{r})$ is normalized to $\mathcal{F}_0 = N_0\Delta_0^2/2$. The angle α is measured from the x axis as shown in schematics in the figures. The temperature is set to $T = 0.1T_c$ so that the superconducting disks show the paramagnetic response. The second energy cut-off is set to $\omega_{c_2} = 400\Delta_0$. The other parameters are fixed as $R = 10\xi_0$, $\lambda_L = 5\xi_0$, $\omega_c = 10\Delta_0$, $H^{\rm ext} = 0.01H_{c_1}$.

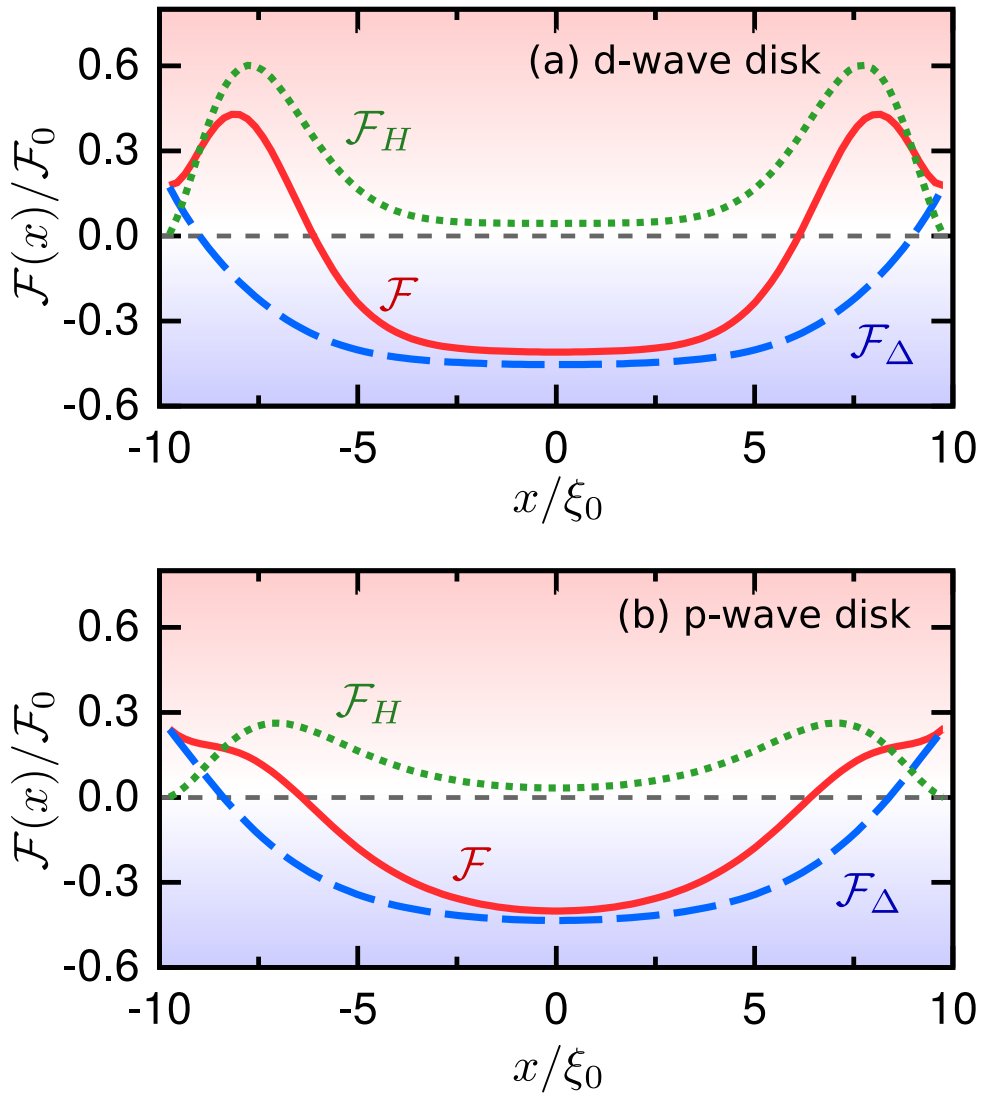

Figure 4.2: Condensation energy density and energy density of a magnetic field for $\alpha = 0$. The results of a d-wave disk and those of a p-wave disk are plotted in (a) and (b), respectively. $\mathcal{F}$, $\mathcal{F}_\Delta$, and $\mathcal{F}_H$ are indicated in solid lines, broken lines, and dotted lines, respectively. All of the energy densities are normalized to $\mathcal{F}_0 = N_0\Delta_0^2/2$, which is the condensation energy density of a homogeneous s-wave superconductor. The all parameters are set to be the same as those of Fig. 4.1.

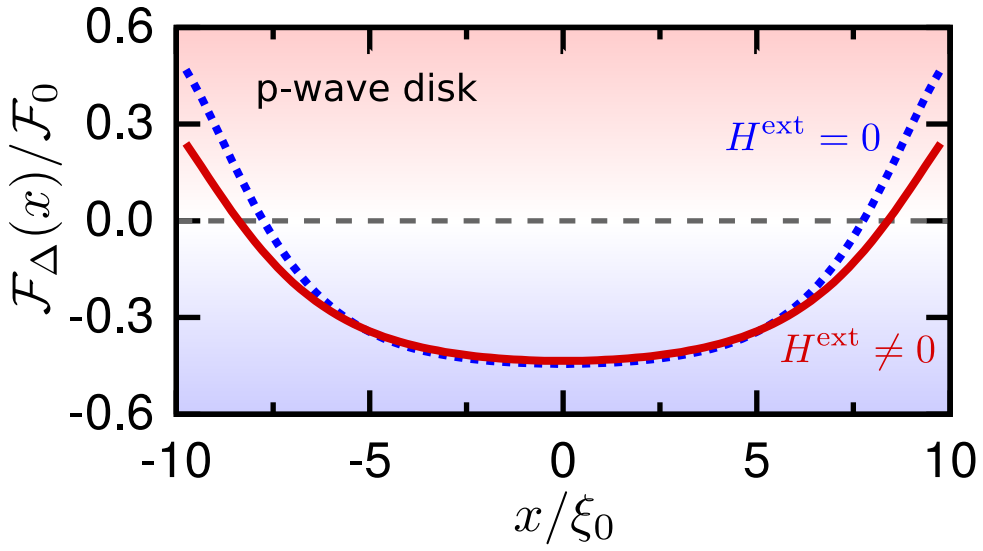

Figure 4.3: Condensation energy density $\mathcal{F}_\Delta$ obtained with a external field (solid line) and without a external field (dotted line). Calculations are carried out for a p-wave superconducting disk. The all parameters are set to be the same as those of Fig. 4.1.

Chapter 5

Effects of surface roughness on the paramagnetic Meissner effect

5.1 Abstract

We theoretically study effects of surface roughness on the magnetic response of small unconventional superconductors by solving the Eilenberger equation for the quassiclassical Green function and the Maxwell equation for the vector potential simultaneously and self-consistently. The paramagnetic phase of spin-singlet d-wave superconducting disks is drastically suppressed by the surface roughness, whereas that of spin-triplet p-wave disks is robust even in the presence of the roughness. Such difference derives from the orbital symmetry of paramagnetic odd-frequency Cooper pairs appearing at the surface of disks. The orbital part of the paramagnetic pairing correlation is p-wave symmetry in the d-wave disks, whereas it is s-wave symmetry in the p-wave ones. Our results are consistent with an experimental finding on high-T_c thin films.

5.2 Introduction

Diamagnetic response to an external magnetic field is a fundamental property of all superconductors [1]. The Meissner current (coherent motion of the Cooper pairs) screens a weak magnetic field at a surface of a superconductor. As a result, the phase coherence of superconducting condensate is well preserved far away from the surface. A number of experiments, however, have reported the paramagnetic response of small superconductors and mesoscopic proximity structures [9, 10, 13–15, 17].

Recent theoretical studies have suggested the existence of paramagnetic Cooper pairs in inhomogeneous superconductors [48–51, 56]. A spatial gradient of the superconducting order parameter induces subdominant pairing correlations. The pairing symmetry of such induced Cooper pairs is different from that of principal Cooper pairs in bulk superconducting state [38, 39, 56]. For example, the principal Cooper pairs in high-T_c superconductors belong to the spin-singlet d-wave (even parity) class. In (110) direction of a high-T_c cuprate, a surface acts as a pair breaker and suppresses the pair potential drastically. Simultaneously, the spin-singlet odd-parity pairs are locally induced at the surface as a subdominant correlation. A surface generates odd-parity pairing correlations from the d-wave even-parity correlation because the surface breaks inversion symmetry locally. Since the pairing correlation function must be antisymmetric under the permutation of two electrons, the induced pairs have the odd-frequency symmetry [31]. To our knowledge, such induced odd-frequency pairs indicate the paramagnetic response to an external magnetic field. Odd-frequency Cooper pairs can be generated also from conventional superconductors in the presence of spin-dependent potentials [36].

In a previous paper [54], we have shown that magnetic susceptibility of small enough unconventional superconducting disks can be paramagnetic at a sufficiently low temperature. Odd-frequency Cooper pairs induced by a surface are responsible for the unusual paramagnetic Meissner effect. The magnetic response of Cooper pair is well characterized by so called "pair density" which is defined by diagonal elements of the response function to a magnetic field. Even-frequency Cooper pairs have a positive pair density, whereas induced odd-frequency pairs have a negative pair density. So far an experiment has reported the decrease of pair density at low temperature in high-T_c superconducting films on which internal surfaces are introduced by the heavy-ion irradiation [6]. Thus our theoretical results are consistent with the experiment at least qualitatively. However, signs of the paramagnetic effect in the experiment [6] is much weaker than our theoretical prediction. The discrepancy may come from sample quality at surfaces. Artificially introduced internal surfaces can be very rough in the experiment, whereas surfaces are specular in the theory. Actually, several theories have pointed out that the surface roughness affects properties of the surface Andreev bound states of a high-T_c superconductor [78–82].

The purpose of this paper is to clarify effects of surface roughness on the paramagnetic Meissner response of small unconventional superconductors. We consider a two-dimensional superconducting disk with spin-singlet d-wave symmetry or spin-triplet p-wave one. In numerical simulation, we solve the Eilenberger equation and the Maxwell equation simultaneously and self-consistently. Surface roughness is considered through an impurity self-energy within the self-consistent Born approximation. We find that the surface roughness suppresses drastically the paramagnetic response of a spin-singlet d-wave

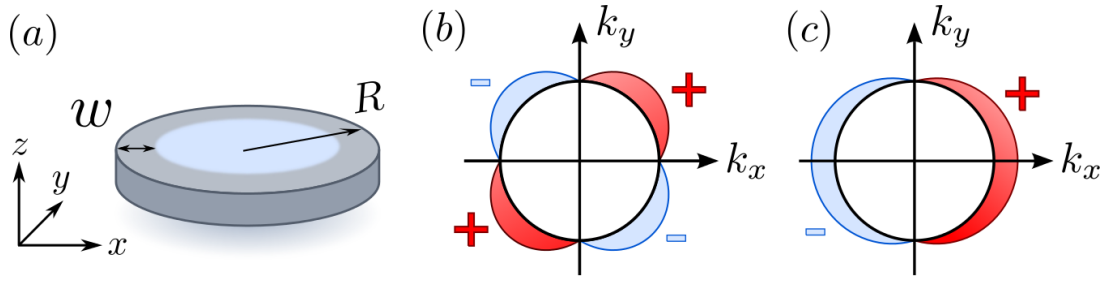

Figure 5.1: (a) Schematic figure of a superconducting disk with rough surface, with R and w are the radius of the disk and the width of the disordered region, respectively. An external magnetic field is applied in the z direction. The origin of a spatial coordinate is located at the center of the disk. The pair potential in momentum space for the d-wave superconductor and that for p-wave one are illustrated in (b) and (c), respectively.

superconducting disk. On the other hand in a spin-triplet p-wave disk, the paramagnetic property is robust even in the presence of surface roughness. The induced odd-frequency pairing correlation has p-wave symmetry in the former, whereas it has s-wave symmetry in the latter. In addition, we also confirm that the paramagnetic superconducting states are more stable than the normal state by calculating free-energies.

This paper is organized as follows. In Sec. II, we explain the theoretical method to analyze the magnetic response of small superconducting disks. In Sec. III, we discuss the magnetic response of small superconducting disks with a rough surface. In Sec. IV, we discuss the stability of a paramagnetic state by calculating the free-energies of a superconducting state. We summarize this paper in Sec. V.

5.3 Formulation

Let us consider a superconducting disk in two-dimension as shown in Fig. 5.1(a), where R is the radius of the disk. To describe rough surfaces, we introduce random impurity potentials near the surface. The width of the disordered region w is measured from the surface as shown in Fig. 5.1(a). An external magnetic field $H^{\rm ext}$ is applied in the z direction. Throughout this paper, we use a unit of $\hbar = c = k_B = 1$ with k_B and c being the Boltzmann constant and the speed of light, respectively.

Superconducting states in equilibrium are described by solutions of the quasiclassical Eilenberger equation [72],

$$iv_F \boldsymbol{k} \cdot \boldsymbol{\nabla}_{\boldsymbol{r}} \check{g} + \left[\check{H} + \check{\Sigma}, \check{g} \right] = 0, \tag{5.1}$$

where v_F is the Fermi velocity, $\boldsymbol{k}$ is the unit vector on the Fermi surface. $\check{g}$ and $\check{H}$ are

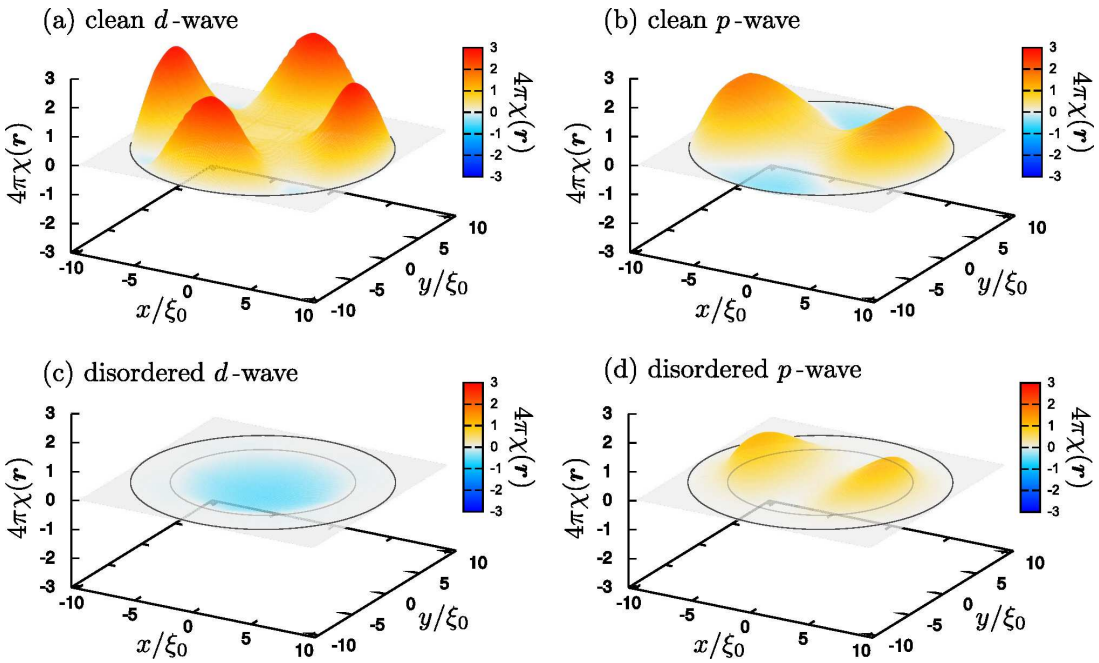

Figure 5.2: Local susceptibilities of the small superconducting disks. The results of a d-wave and those of a p-wave superconductor with a clean surface (i.e., $w = 0$, $\xi/\ell = 0$) are presented in (a) and (b), respectively. The results of a d-wave and those of a p-wave superconductor with rough surface ($w = 3\xi_0$, $\xi_0/\ell = 1.0$) are demonstrated in (c) and (d), respectively. The parameters used in the simulation are $R = 10\xi_0$, $\lambda_L = 5\xi_0$, $\omega_c = 10\Delta_0$, $H^{\rm ext} = 0.01H_{c_1}$ and $T = 0.1T_c$.

defined as follows,

$$\check{g}(\boldsymbol{r},\boldsymbol{k},i\omega_n) = \begin{bmatrix} \hat{g}(\boldsymbol{r},\boldsymbol{k},i\omega_n) & \hat{f}(\boldsymbol{r},\boldsymbol{k},i\omega_n) \\ -\underset{\sim}{\hat{f}}(\boldsymbol{r},\boldsymbol{k},i\omega_n) & -\underset{\sim}{\hat{g}}(\boldsymbol{r},\boldsymbol{k},i\omega_n) \end{bmatrix}, \tag{5.2}$$

$$\check{H}(\boldsymbol{r},\boldsymbol{k},i\omega_n) = \begin{bmatrix} \hat{\xi}(\boldsymbol{r},\boldsymbol{k},i\omega_n) & \hat{\Delta}(\boldsymbol{r},\boldsymbol{k}) \\ \underset{\sim}{\hat{\Delta}}(\boldsymbol{r},\boldsymbol{k}) & \underset{\sim}{\hat{\xi}}(\boldsymbol{r},\boldsymbol{k},i\omega_n) \end{bmatrix}, \tag{5.3}$$

$$\hat{\xi}(\boldsymbol{r},\boldsymbol{k},i\omega_n) = (i\omega_n + ev_F\boldsymbol{k}\cdot\boldsymbol{A}(\boldsymbol{r}))\,\hat{\sigma}_0, \tag{5.4}$$

where $\omega_n = (2n+1)\pi T$ is the fermionic Matsubara frequency, n is an integer number, and T is a temperature. In this paper, the symbol $\cdot\check{\cdot}\cdot$ represents a 4×4 matrix structure, $\cdot\hat{\cdot}\cdot$ represents a 2×2 matrix structure in spin space and $\hat{\sigma}_0$ is the identity matrix in spin space. A vector potential is denoted by $\boldsymbol{A}(\boldsymbol{r})$. We introduced a definition $\underset{\sim}{K}(\boldsymbol{r},\boldsymbol{k},i\omega_n) \equiv K^*(\boldsymbol{r},-\boldsymbol{k},i\omega_n)$ for all functions $K(\boldsymbol{r},\boldsymbol{k},i\omega_n)$. Effects of rough surfaces are taken into account through an impurity self-energy of a quasiparticle defined by,

$$\check{\Sigma}(\boldsymbol{r},i\omega_n) = \Theta\left(|\boldsymbol{r}| - R + w\right)\ \frac{i}{2\tau_0}\int\frac{d\boldsymbol{k}}{2\pi}\ \check{g}(\boldsymbol{r},\boldsymbol{k},i\omega_n), \tag{5.5}$$

where τ_0 is the life time of a quasiparticle and $\Theta(x)$ is the Heviside step function. The mean free path of a quasiparticle is defined by $\ell = v_F\tau_0$ in the disordered region. The anomalous Green function $\hat{f}(\boldsymbol{r},\boldsymbol{k},i\omega_n)$ is originally defined by an average of two annihilation operators of an electron. The relation

$$\hat{f}(\boldsymbol{r},\boldsymbol{k},i\omega_n) = -\hat{f}^{\,\mathrm{T}}(\boldsymbol{r},-\boldsymbol{k},-i\omega_n), \tag{5.6}$$

represents the antisymmetric property of the anomalous Green function under the permutation of two electrons, where T represents the transpose of a matrix.

The direction of $\boldsymbol{k}$ in two-dimensional momentum space is represented by an angle θ measured from the x axis, (i.e., $k_x = \cos\theta$ and $k_y = \sin\theta$). In what follows, we consider two unconventional superconductors with different pairing symmetries. One is spin-singlet d-wave symmetry $\hat{\Delta}(\boldsymbol{r},\theta) = \Delta(\boldsymbol{r})\sin(2\theta)\,i\hat{\sigma}_2$. The other is spin-triplet p-wave symmetry $\hat{\Delta}(\boldsymbol{r},\theta) = \Delta(\boldsymbol{r})\cos(\theta)\,\hat{\sigma}_1$, where $\hat{\sigma}_j$ for j = 1-3 are the Pauli matrices in spin space. A d-wave and a p-wave pair potentials in momentum space are shown schematically in Fig. 5.1(b) and (c), respectively. We do not consider any spin-dependent potentials in

this paper. The matrix structure of Green function is represented by

$$\hat{g}(\boldsymbol{r},\theta,i\omega_n) = g(\boldsymbol{r},\theta,i\omega_n)\hat{\sigma}_0, \tag{5.7}$$

$$\hat{f}(\boldsymbol{r},\theta,i\omega_n) = f(\boldsymbol{r},\theta,i\omega_n) \times \begin{cases} \hat{\sigma}_2 & \text{for spin-singlet} \\ -i\hat{\sigma}_1 & \text{for spin-triplet} \end{cases}, \tag{5.8}$$

with scalar Green functions $g(\boldsymbol{r},\theta,i\omega_n)$ and $f(\boldsymbol{r},\theta,i\omega_n)$. Spatial dependence of $\Delta(\boldsymbol{r})$ is determined self-consistently from the gap equation

$$\Delta(\boldsymbol{r}) = \pi N_0 g_0 T \sum_{\omega_n} \int \frac{d\theta}{2\pi} f(\boldsymbol{r},\theta,i\omega_n) V_x(\theta), \tag{5.9}$$

where N_0 is the density of states per spin of normal metal at the Fermi level, g_0 is the coupling constant, and V_x represents attractive electron-electron interactions with $x = p$-wave or d-wave indicating pairing symmetries. The interaction kernel V_x depends upon pairing symmetries as

$$V_x(\theta) = \begin{cases} 2\cos\theta & \text{for } x = p\text{-wave} \\ 2\sin(2\theta) & \text{for } x = d\text{-wave} \end{cases}. \tag{5.10}$$

The constant $N_0 g_0$ is determined by

$$(N_0 g)^{-1} = \ln\left(\frac{T}{T_c}\right) + \sum_{0 \le n < \omega_c/2\pi T} \frac{1}{n + 1/2}, \tag{5.11}$$

with T_c and ω_c being the transition temperature and the cut-off energy, respectively.

In a type-II superconductor, an electric current is represented by

$$\boldsymbol{j}(\boldsymbol{r}) = \frac{\pi e v_F N_0}{2i} T \sum_{\omega_n} \int \frac{d\theta}{2\pi} \mathrm{Tr}\left[\check{T}_3 \boldsymbol{k}\, \check{g}(\boldsymbol{r},\theta,\omega_n)\right], \tag{5.12}$$

with $\check{T}_3 = \mathrm{diag}[\hat{\sigma}_0, -\hat{\sigma}_0]$. From Eq. (6.13) and the Maxwell equation $\boldsymbol{\nabla} \times \boldsymbol{H}(\boldsymbol{r}) = 4\pi \boldsymbol{j}(\boldsymbol{r})$, we obtain spatial profiles of a vector potential $\boldsymbol{A}(\boldsymbol{r})$ and a local magnetic field $\boldsymbol{H}(\boldsymbol{r})$. A local magnetic susceptibility is defined by

$$\chi(\boldsymbol{r}) = \frac{1}{4\pi} \frac{H(\boldsymbol{r}) - H^{\mathrm{ext}}}{H^{\mathrm{ext}}}, \tag{5.13}$$

where H^{ext} is an amplitude of external magnetic field applied in the z direction. By

integrating the local susceptibility, we obtain a susceptibility of a whole disk X as

$$X = \frac{1}{\pi R^2} \int_{|\boldsymbol{r}|\leq R} d\boldsymbol{r}\, \chi(\boldsymbol{r}). \tag{5.14}$$

To solve the Eilenberger equation Eq. (6.1) in a disk geometry, we use a Riccati parametrization [74–76] and a numerical method discussed in Ref. [77]. Using the parametrization, the Eilenberger equation can be separated into two Riccati type differential equations. When we solve the Riccati type equation along a long enough quasiclassical trajectory, solutions of the equation do not depend on initial conditions [77]. In this paper, the length of classical trajectories is more than 30 times of the coherence length. Solving the Eilenberger equation and the Maxwell equation, we determine the pair potential, the vector potential, and the self-energy self-consistently with one another. At surfaces, we consider specular classical trajectories for calculating the Green functions [77]. The vector potential out side of the superconducting disk is $\boldsymbol{A}(\boldsymbol{r}) = (H^{\rm ext}/2)(-y\hat{\boldsymbol{x}} + x\hat{\boldsymbol{y}})$ which gives a uniform magnetic field in the z direction, where $\boldsymbol{x}$ and $\boldsymbol{y}$ are the unit vector in the x and y direction, respectively.

5.4 Results

Throughout this paper, we fix several parameters as $R = 10\xi_0$ and $\omega_c = 10\Delta_0$, where Δ_0 is the amplitude of the pair potential at the zero temperature, and $\xi_0 = \hbar v_F/2\pi T_c$ is the coherence length. Strength of the disorder is tuned by changing a parameter ξ_0/ℓ. Width of disordered region is $w = 3\xi_0$ because odd-frequency pairs induced by a surface localize within this range. All lengths are measured in units of ξ_0. The current density is normalized to $J_0 = \hbar c^2/4\pi|e|\xi_0^3$. Here we express $\hbar$ and c explicitly to avoid misunderstandings. The characteristic length scale of the Maxwell equation is the penetration depth defined as $\lambda_L = (4\pi n e^2/mc^2)^{-1/2}$ and is a parameter in numerical simulations. In this paper, we choose $\lambda_L = 5\xi_0$ to realize type-II superconductors and fix $H^{\rm ext} = 0.01H_{c_2}$. Here $H_{c_2} = \hbar c/|e|\xi_0^2$ is the second critical magnetic field. The first critical magnetic field at low temperature is estimated as $H_{c1} = H_{c_2}(\xi_0/\lambda_L)^2 \log(\lambda_L/\xi_0) \approx 0.03H_{c2} > H^{\rm ext}$ at $\lambda_L = 5\xi_0$. Thus vortices are not expected at low temperature. We start numerical simulations with initial conditions of a spatially uniform pair potential $\Delta(\boldsymbol{r}) = |\Delta_{\rm Bulk}(T)|$ and a homogeneous magnetic field $\boldsymbol{A}(\boldsymbol{r}) = (H^{\rm ext}/2)(-y\hat{\boldsymbol{x}} + x\hat{\boldsymbol{y}})$, where $\Delta_{\rm Bulk}(T)$ is the pair potential obtained in a homogeneous superconductor at a temperature T. If we choose an alternative initial condition hosting a vortex in a superconductor, a vortex state might be realized in numerical simulations [84] even for $H^{\rm ext} < H_{c1}$. Such vortex issue, however, goes beyond the scope of this paper.

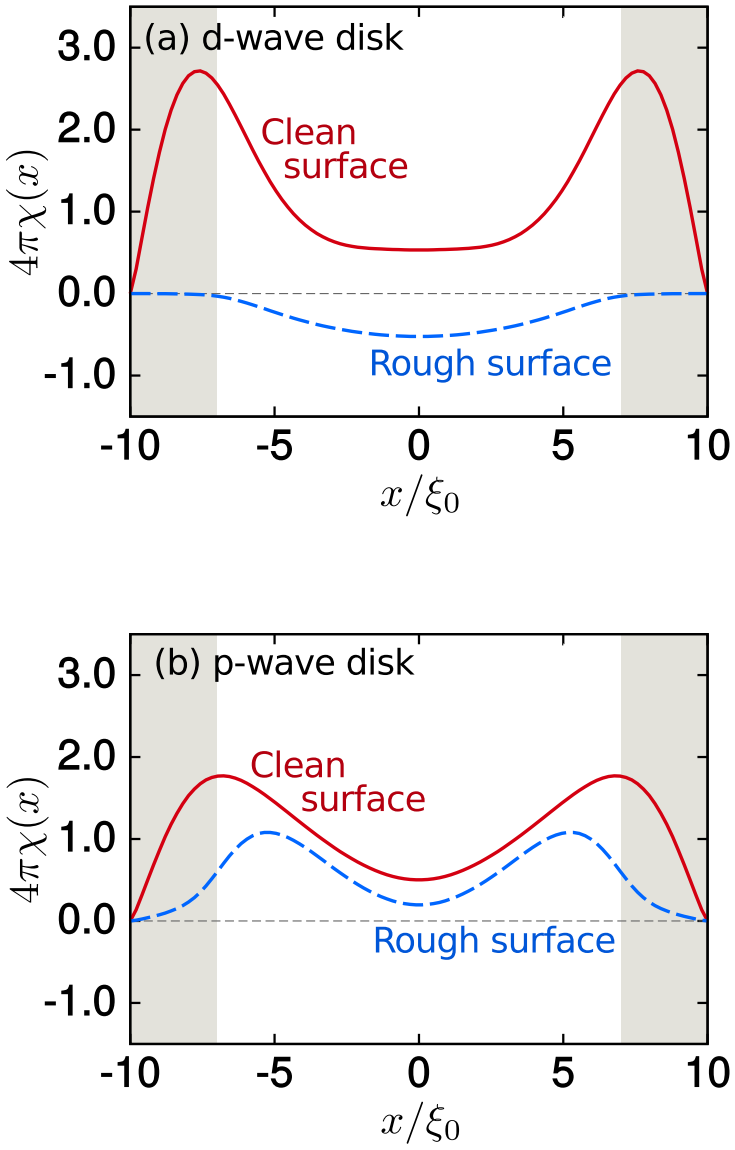

Figure 5.3: Local susceptibilities on the x axis (i.e., $y = 0$). The results for a d-wave disk and for a p-wave disk are plotted in (a) and (b), respectively. The all parameters are set to be the same as those of Fig. 5.2. The solid and the broken lines indicate the result for the disk with clean surface and those with the rough surface, respectively. The shadowed areas indicate the disordered regions.

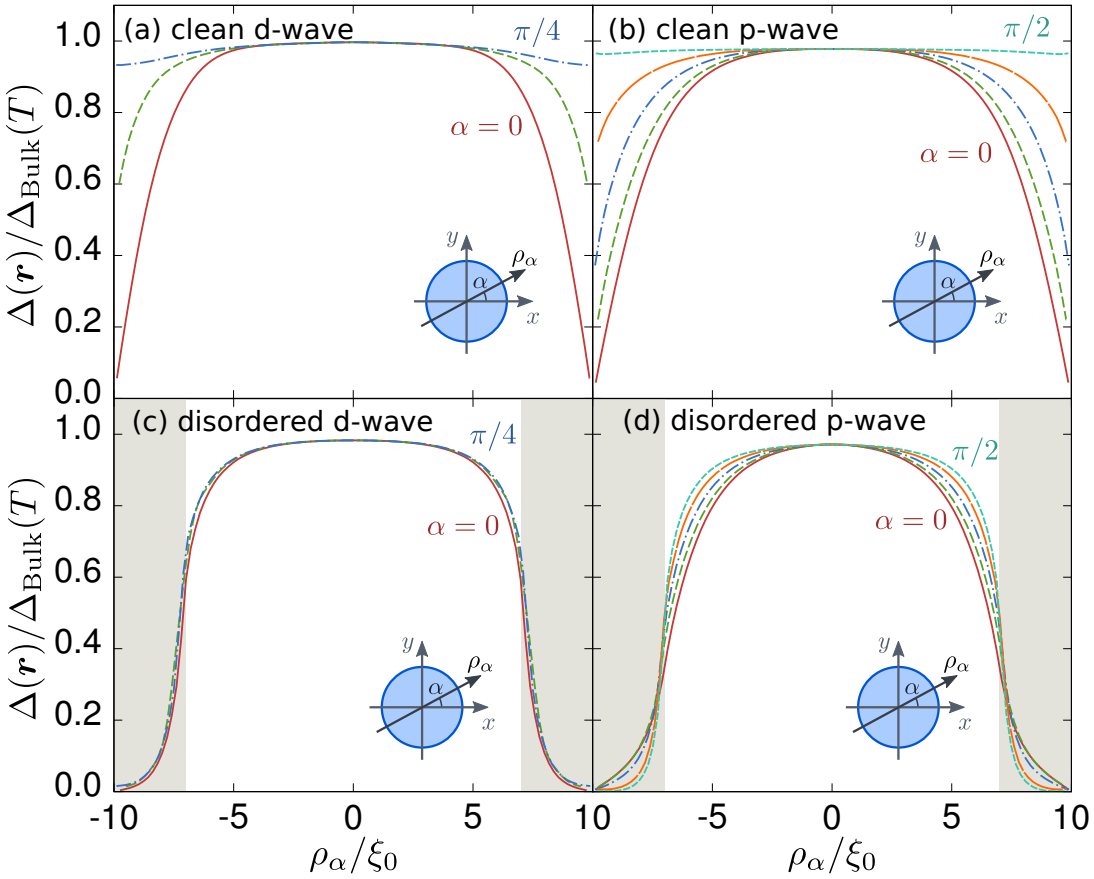

Figure 5.4: Amplitudes of pair potentials in real space for several azimuthal angle α measured from the x axis. The results of a d-wave disk with $\ell/\xi_0 = 0.0$ and $\ell/\xi_0 = 1.0$ are shown in (a) and (c), respectively. Since the pair potential is four-fold symmetric, we plot its spatial profile for $\alpha = 0, \pi/8$, and $\pi/4$. The results of a p-wave disk with $\ell/\xi_0 = 0.0$ and $\ell/\xi_0 = 1.0$ are shown in (b) and (d), respectively. The pair potential for $\alpha = 0, \pi/8, \pi/4, 3\pi/8, \pi/2$ (from bottom to top) are shown under the two-fold symmetry of results. The pair potentials are normalized to $\Delta_{\rm Bulk}(T)$. The all parameters are set to be the same as those of Fig. 5.2. The shadowed areas in (c) and (d) indicate the disordered regions.

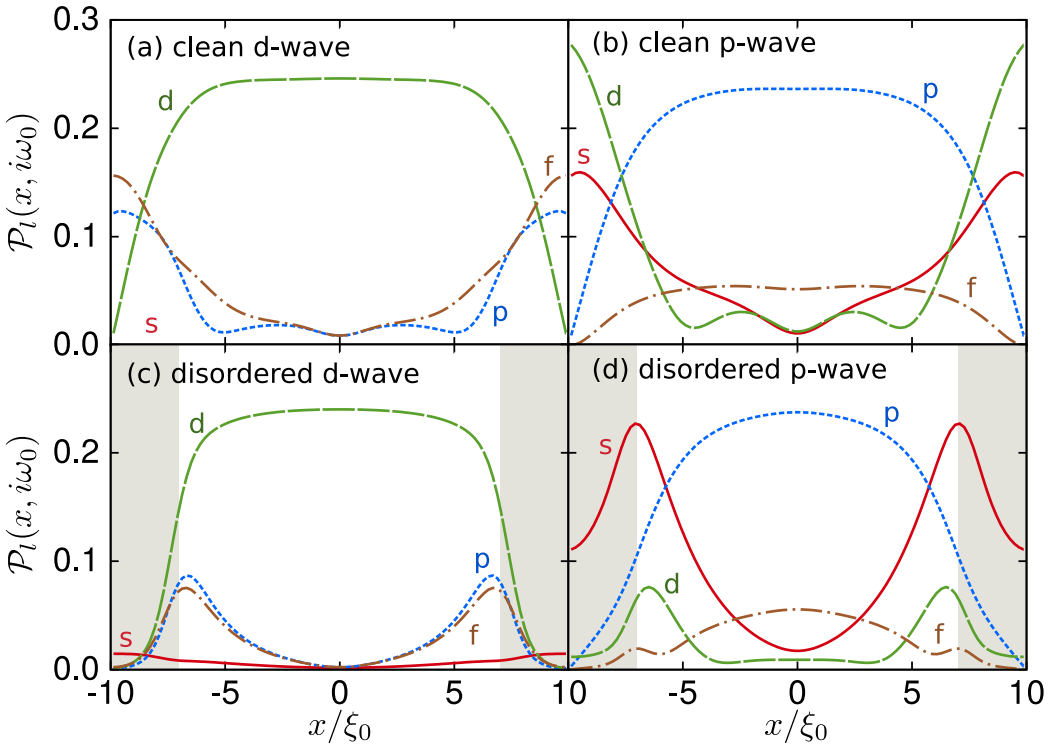

Figure 5.5: Spatial dependencies of the decomposed pairing functions at the lowest Matsubara frequency on the x-axis for (a) a clean d-wave, (b) a clean p-wave, (c) a disordered d-wave, and (d) a disordered p-wave disk. The parameters are set to be the same values as those in Fig. 5.2. The shadowed areas indicate the disordered regions.

First we discuss calculated results for a small superconducting disk with a *specular* surface (i.e., $w = 0$, $\xi_0/\ell = 0$). Then we discuss effects of surface roughness by comparing numerical results in a disk with a rough surface with those with a specular one.

5.4.1 Disks with a specular surface

We briefly explain the paramagnetic Meissner effect in a superconducting disk with a specular surface. Figure 5.2(a) shows the local susceptibility in a d-wave superconductor. The result are four-fold symmetric reflecting the d-wave pair potential. The magnetic susceptibility is positive (paramagnetic) near four surfaces in the x and the y directions. In Fig. 5.3(a), we show a spatial profile of the local susceptibility of Fig. 5.2(a) along the x axis at $y = 0$. We also show the amplitudes of pair potential in real space $|\Delta(\boldsymbol{r})|$ in Fig. 5.4(a). The pair potential is calculated along a trajectory ρ_α oriented by an angle α measured from the x axis as shown in Fig. 5.4. In a d-wave disk, the pair potential is four-fold symmetric. The pair potential is strongly suppressed at the four surfaces in x and y directions as a result of appearing surface Andreev bound states [83], whereas it is

totally constant in the directions in which the surface Andreev bound states are absent. In contrast to the pair potential around a vortex core [84], the results in Fig. 5.4(a) are anisotropic in real space. As shown in Ref. [56], the spatial gradient of pair potential generates paramagnetic pairing correlations with odd-frequency symmetry. Thus odd-frequency pairs are expected at four surfaces in the x and y directions, which explains inhomogeneous and angular anisotropic paramagnetic response in Fig. 5.2(a). In this paper, we analyze the frequency symmetries of Cooper pairs by decomposing pairing functions into a series of Fourier components. In a d-wave disk, the anomalous Green function are described by two components

$$\hat{f}(\boldsymbol{r}, \theta, i\omega_n) = [f_{\rm ep}(\boldsymbol{r}, \theta, i\omega_n) + f_{\rm op}(\boldsymbol{r}, \theta, i\omega_n)]\, \hat{\sigma}_2, \tag{5.15}$$

where $f_{\rm ep}$ is an even-parity (d-wave) function representing the principal pairing correlation and $f_{\rm op}$ is an odd-parity function representing the induced pairing component at a surface. To satisfy Eq. (5.6), $f_{\rm op}$ must be an odd function of ω_n. We decompose pair functions $f(\boldsymbol{r}, \theta, i\omega_n)$ as

$$\mathcal{P}_l(\boldsymbol{r}, i\omega_n) = 2\sqrt{C_l^2 + S_l^2}, \tag{5.16}$$

$$S_l = \int \frac{d\theta}{2\pi}\, {\rm Re}\left[f(\boldsymbol{r}, \theta, i\omega_n)\right] \sin\left(l\theta\right), \tag{5.17}$$

$$C_l = \int \frac{d\theta}{2\pi}\, {\rm Re}\left[f(\boldsymbol{r}, \theta, i\omega_n)\right] \cos\left(l\theta\right), \tag{5.18}$$

where $l = 0, 1, 2$ and 3 correspond to s-, p-, d- and f-wave orbital functions, respectively. In the presence of a magnetic field, the imaginary part of $f(\boldsymbol{r}, \theta, i\omega_n)$ is induced by the vector potential as analytically shown in Appendix. We focus only on the real part of f to analyze pairing symmetries. Figure 5.5(a) indicate the spatial profile of $\mathcal{P}_l(x, i\omega_0)$ at the lowest Matsubara frequency as a function of x at $y = 0$. The pairing functions of induced Cooper pairs have p- and f-wave symmetries and their amplitudes localize near the surface. Such odd-frequency Cooper pairs shows the paramagnetic response to a magnetic field. The surface also generates spin-singlet s-wave correlation. Its amplitude, however, is too small to confirm at a scale of plot in Fig. 5.5(a). Figure 5.6(a) shows the spatial distribution of electric current on a d-wave disk. The diamagnetic current flows at the central region because of the usual Meissner effect. Near the surfaces in the x and y directions, however, the current flows the opposite direction to the Meissner current. Therefore a small d-wave superconductor can be paramagnetic due to the induced odd-frequency Cooper pairs at its surface.

A spin-triplet p-wave disk also indicates the similar paramagnetic effect as shown the

results of magnetic susceptibility in Figs. 5.2(b), its spatial profile on the x axis in 5.3(b), pair potential in 5.4(b) and electric current in 5.6(b). The results are two-fold symmetric reflecting the p-wave superconducting pair potential. The paramagnetic effect can be seen near the surface in the x direction because of induced odd-frequency Cooper pairs. The anomalous Green function is represented by Eq. (5.15) with replacing $\hat{\sigma}_2$ by $-i\hat{\sigma}_1$. In the p-wave case, $f_{\rm ep}$ represents induced pairing correlations and is an odd function of ω_n. As shown in Fig. 5.5(b), $f_{\rm ep}$ mainly consists of s- and d-wave pairing correlations.

In the end of this subsection, we summarize an important difference between the paramagnetic effect of a d-wave superconductor and that of a p-wave one. In a d-wave disk, surface odd-frequency Cooper pairs have a p- or f-wave symmetry [39, 54]. In a p-wave disk, on the other hand, s- or d-wave odd-frequency Cooper pairs are responsible for the paramagnetic effect [39, 54]. In the next subsection, we will show that the paramagnetic response of a disk with rough surface depends sensitively on the orbital symmetry of induced odd-frequency pairs at the surface.

5.4.2 Disks with a rough surface

Next, we discuss effects of the surface roughness on the magnetic response of a small superconductor. The calculated results of the local susceptibility for a d-wave superconducting disk with rough surface are shown in Fig. 5.2(c), where we choose $\xi_0/\ell = 1.0$. Comparing Fig. 5.2(a) with (c), we can find that the surface roughness completely suppresses the paramagnetic response at the four surfaces in a d-wave disk. The central region of the disk with the rough surface recovers the usual diamagnetic response. Such effect is demonstrated more clearly in a spatial profile of local susceptibilities at $y = 0$ in Fig. 5.3(a), where the shadowed area indicates the disordered region. The amplitude of pair potential in real space is shown in Fig. 5.4(c). The pair potential in the disordered region is totally suppressed because the random impurity potential acts as a pair breaker for d-wave Cooper pairs. Spatial profiles of decomposed pairing functions are shown in Fig. 5.5(c). In the disordered region, a d-wave pairing function $\mathcal{P}_d$ is drastically suppressed due to impurity scatterings. The disordered region can be considered as a diffusive normal metal because the spatial profile of order parameter is proportional to $\mathcal{P}_d$. Odd-frequency Cooper pairs are also fragile in the presence of surface roughness because they have p- or f-wave pairing symmetry. Therefore, both the paramagnetic current and the diamagnetic one disappear in the disordered region as shown in Fig. 5.6(c). The magnetic property of a disk is determined by that at the clean central region where even-frequency d-wave Cooper pairs stay and contribute to the diamagnetic response. We conclude that the paramagnetic effect in a d-wave disk is fragile in the presence of surface

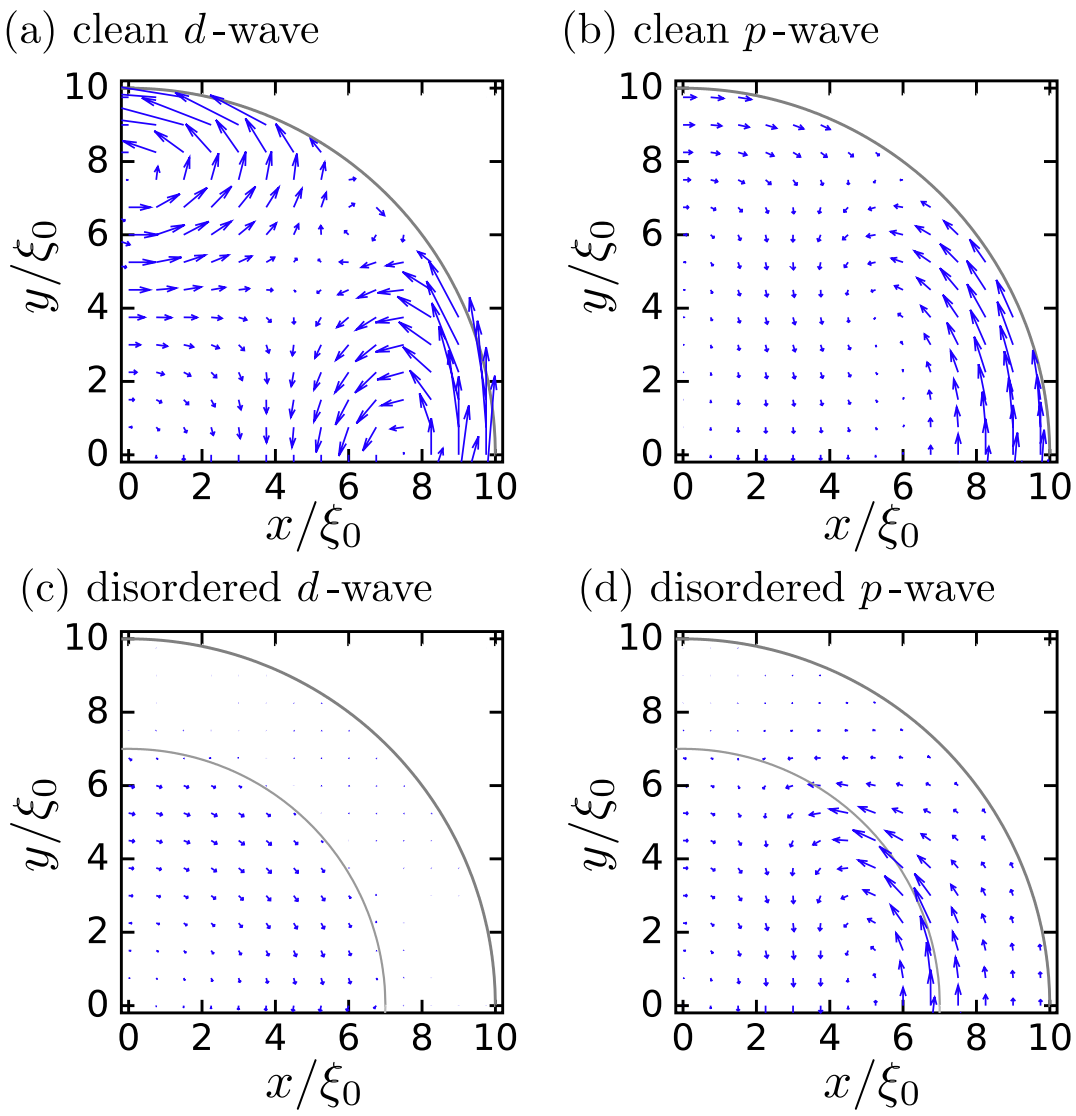

Figure 5.6: Spatial distribution of current density on a superconducting disk. The results of a d-wave and a p-wave superconductor with clean surface ($w = 0$, $\xi/\ell = 0.0$) are shown in (a) and (b), respectively. The results with rough surface are shown in (c) and (d). The outer circles indicate the edge of the disk and the inner circles in (c) and (d) indicate the effective interface between the clean region and the disordered region. The parameters are set to be the same values as those in Fig. 5.2.

roughness because odd-frequency pairs have a p-wave or a f-wave orbital symmetry.

A p-wave disk indicates qualitatively different magnetic response from a d-wave one. The local susceptibility of a p-wave disk with rough surface is shown in Fig. 5.2(d) and Fig. 5.3(b) with a broken line. Although the surface is rough enough, a p-wave superconducting disk still show the strong paramagnetic response. The peak of the χ in Fig. 5.3(b) shifts to inside of the disk in the presence of surface roughness. This suggests that the

Andreev bound states appear at a boundary between the clean central region and the disordered surface region. Such Andreev bound states always accompany the paramagnetic odd-frequency Cooper pairs. In addition to this, the paramagnetic response in Fig. 5.3(b) suggests the penetration of odd-frequency Cooper pairs into the surface disordered region. The spatial profiles of the electric current in Fig. 5.6(d) shows that the paramagnetic current flows not only in the clean region but also in the disordered one. Odd-frequency pairs in a p-wave disk survive even in the presence of surface roughness because they have s-wave orbital symmetry. Therefore, the paramagnetic effect in a p-wave disk is robust against the surface roughness.

5.4.3 Temperature dependence

Here we discuss the magnetic susceptibility of a whole disk which is a measurable value in experiments. The disk susceptibility in a d-wave superconductor and that in a p-wave one are plotted as a function of temperature in Fig. 5.7(a) and (b), respectively. We present the results for several choices of the disorder ξ_0/ℓ. In simulation, we first calculate the pair potential and the vector potential self-consistently at a temperature just below T_c under an external magnetic field $H^{\rm ext} = 0.01H_{c_2}$. Then the temperature is decreased with keeping $H^{\rm ext}$ unchanged. In the clean limit ($\xi_0/\ell = 0.0$), both a d-wave disk and a p-wave one show the usual diamagnetic response just below T_c. With decreasing the temperature, however, the sign of susceptibility changes around $T = T_p \sim 0.3T_c$ for both cases. Here, we define T_p as a diamagnetic-paramagnetic crossover temperature. Blow T_p, superconducting disks show the anomalous paramagnetic response. The paramagnetic effect is stronger in lower temperature because odd-frequency Cooper pairs energetically localize at the Fermi level.

In a d-wave disk, the reentrance is slightly suppressed in the presence of the moderate surface roughness with $\xi_0/\ell = 0.1$ as shown in Fig. 5.7(a). When we increase the degree of the roughness further, the paramagnetic response gradually becomes weaker. At $\xi_0/\ell = 0.5$, the response is diamagnetic and the susceptibility recovers the monotonic temperature dependence which is usually observed in large enough superconductors in experiments. In the d-wave superconductors, the specular Andreev reflection is necessary for forming the surface bound states at the zero-energy [86] and for appearing odd-frequency pairs. In other wards, odd-frequency pairs have p- or f-wave orbital symmetry. Therefore the rough surface brakes odd-frequency pairs and suppresses the paramagnetic response. This conclusion is totally consistent with the experiment [6], where temperature dependences of the pair density on a high-T_c superconducting film show a small reentrant behavior at low temperature. But the total pair density remains positive. Actually, the experimental

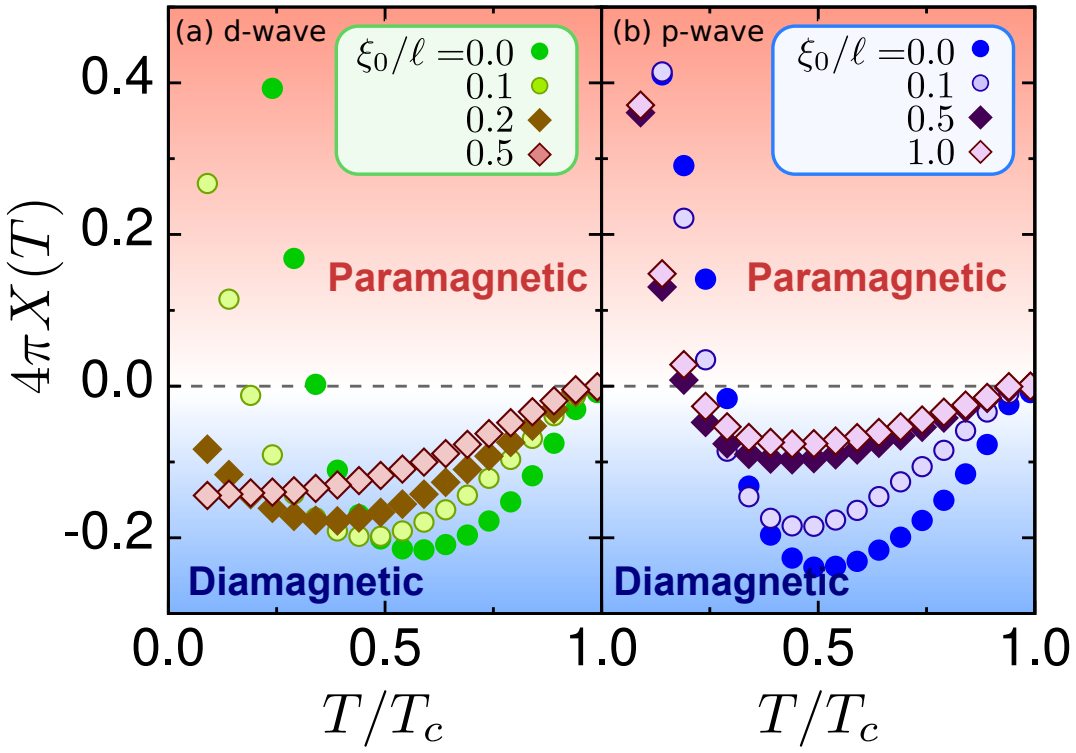

Figure 5.7: Temperature dependencies of the whole disk susceptibility $X(T)$ for the d-wave disk (a) and the p-wave disk (b).

data are very similar to the results for $\xi_0/\ell = 0.2$ in Fig. 5.7(a). The experimental results can be interpreted as an appearance of a small amount of odd-frequency pairs. In the experiment, the surface roughness may partially breaks odd-frequency pairs because a number of the internal surfaces are introduced by the heavy ion irradiation.

On the contrary to a d-wave disks, the susceptibility of a p-wave disk $X(T)$ shows the reentrance and the crossover to the paramagnetic phase at low temperature for all ξ_0/ℓ as shown in Fig. 5.7(b). It has been pointed out that the surface Andreev bound states of a p-wave superconductor are robust under potential disorder because of the pure chiral property of surface bound states [85]. In other wards, odd-frequency pairs accompanied by the Andreev bound states have s-wave orbital symmetry [39, 54]. Since s-wave pairs is robust under the disordered potential, the paramagnetic effect of the p-wave superconductors persists even in the presence of surface roughness. We conclude that the robust paramagnetic response in a small size sample is a unique property of spin-triplet p-wave superconductors. Such property would enable us to identify the spin-triplet p-wave superconductivity in experiments.

5.5 Conclusion

We have theoretically studied effects of surface roughness on the anomalous paramagnetic response of small unconventional superconducting disks by using the quasiclassical Green function method. We conclude that the paramagnetic property of p-wave superconductors is robust under the surface roughness because the p-wave superconductors host the s-wave odd-frequency Cooper pairs at their surface. On the other hand, the paramagnetic property in d-wave superconductor is fragile in the presence of the surface roughness. In this case, the odd-frequency pairs at the surface have p-wave orbital symmetry.

Chapter 6

Spontaneous edge current in small chiral superconductors with rough surfaces

6.1 Abstract

We study theoretically the spontaneous edge current in a small chiral superconductor with surface roughness. We obtained self-consistent solutions of the pair potential and the vector potential by solving the quasiclassical Eilenberger equation and the Maxwell equation simultaneously. We then employed them to calculate numerically the spatial distribution of the chiral edge current in a small superconductor. The characteristic behavior of the spontaneous edge current depends strongly on the symmetries of the order parameters such as chiral p-, chiral d- and chiral f-wave pairing. The edge current is robust under the surface roughness in the chiral p- and chiral d-wave superconductors. In the chiral d-wave case, the surface roughness tends to flip the direction of the chiral current. On the other hand, the edge current in a chiral f-wave superconductor is fragile when there is surface roughness. We also discuss the temperature dependence of a spontaneous magnetization, which is a measurable value in standard experiments.

6.2 Introduction

The experimental detection of a spontaneous edge current could be direct evidence of chiral superconductivity. A number of Cooper pairs sharing a specific angular momen-

tum carry the spontaneous edge current in chiral superconductors [87, 88] which can be experimentally measured as spontaneous magnetization. Strontium ruthenate Sr_2RuO_4 is a leading candidate for a chiral p-wave superconductor [89–91] whose pair potential is described by $\Delta(k_x \pm ik_y) = \Delta e^{i\chi\theta}$ in momentum space. Here $k_x = \cos\theta$ ($k_y = \sin\theta$) is the normalized wavenumber in the x (y) direction, and Δ is the amplitude of the pair potential. The topological Chern number $\chi = 1$ or -1 corresponds to the angular momentum of a Cooper pair. In addition to chiral p-wave superconductivity, the possibilities of chiral d-wave ($\chi = \pm 2$) and chiral f-wave ($\chi = \pm 3$) superconductivity have been discussed in recent experiments. [92–102] Several theories have suggested that the amount of edge current become smaller in a chiral superconductor with a larger $|\chi|$. [107, 108] However, unfortunately, no spontaneous chiral current has yet been experimentally observed. [109, 110]

The absence of spontaneous magnetization in experiments has mainly been attributed to three effects: (i) the Meissner screening of the edge current by the bulk superconducting condensate, (ii) the reduction of the chiral current by the potential disorder near the surface of a superconductor, and (iii) the complicated electronic structures of superconductors. The first effect was partially studied by Matsumoto and Sigrist. [87] They theoretically confirmed a reduction in the edge current caused by the Meissner effect in a chiral p-wave superconductor. However, the resulting spontaneous magnetization is large enough to be measured in experiments. The second effect is linked to the issue of the intrinsic angular momentum in the ^{3}He-A phase. [119, 120] Experimentally it is difficult to make a superconducting sample with a specular surface. For instance, a small ruthenate superconductor cluster can be fabricated by using the focused ion beam technique, [111, 112] which would seriously damage the sample quality near the surface. Several theoretical papers have already suggested the presence of edge states in a chiral p-wave superconductor when there is surface roughness. [113, 114] On the other hand, when a chiral p-wave superconductor is covered by a clean normal metal, the chiral current is dramatically reduced. [115] The third effect has been discussed specifically in Sr_2RuO_4. It has been known that the gap anisotropy [116, 117] and the multiband structures [118] suppress the chiral edge current. Even today, we do not know how the Meissner screening and the surface roughness reduce the edge current in chiral d- and f-wave superconductors. In previous papers, [54, 58] we studied the Andreev bound states [63–67, 69] (ABSs) in time-reversal non-chiral superconductors characterized by $d_{x^2-y^2}$-wave or p_x-wave pair potentials. We found that the ABSs in a p_x-wave superconductor are robust even in the presence of surface roughness, whereas those in a d-wave superconductor are fragile against surface roughness. This conclusion is well explained by the symmetry of the Cooper pairs induced near the surface. However, it is unclear if it is possible to generalize

our conclusions straightforwardly to chiral superconductors. We will address these issues in the present paper.

In this paper, we theoretically study the spontaneous edge currents and the spontaneous magnetization in a small chiral superconducting disk based on the quasiclassical Eilenberger formalism. To discuss the relation between the pairing symmetry and the sensitivity of the chiral edge current to the surface roughness, we consider the simple chiral order parameters on a circular shaped Fermi surface. By solving the Eilenberger and Maxwell equations self-consistently and simultaneously, we obtain the spatial profiles of the chiral edge currents and the temperature dependence of a spontaneous magnetization. The surface roughness is considered in terms of the impurity self-energy of a quasiparticle. To define the magnetization of a sample, we need to consider a finite-size superconductor such as disks. Moreover, setting the radius of a disk to be comparable to the coherence length allows us to justify the assumption that there is no chiral-domain wall in a disk. We conclude that the robustness of the spontaneous edge current depends strongly on the paring symmetry. In a chiral p-wave superconductor, the amplitude of the chiral current in a disk with a rough surface is comparable to that in a disk with a specular surface. In a chiral d-wave superconductor, there are two edge channels in a disk with a specular surface. They carry the chiral currents in opposite directions. In the presence of surface roughness, one channel near the surface disappears and the other channel far from the surface carries the robust chiral current. We show that the surface roughness changes the net-current direction in a chiral d-wave disk. The edge current in a chiral f-wave superconductor is fragile in the presence of surface roughness. The effects of Meissner screening on the chiral edge current depend on the spatial current distribution near the surface. When the current decreases monotonically with increases in the distance from the surface, the Meissner effect always reduces the chiral current. On the other hand, when the chiral current changes its direction as a function of distance from the surface, the Meissner screening effect becomes weaker. Such a complicated current distribution causes the self-screening effect among edge currents flowing in opposite directions.

This paper is organized as follows. In Sec. II, we explain the quasiclassical Eilenberger formalism and define the spontaneous magnetization of a small superconducting disk. In Sec. III, we present results obtained using non-self-consistent simulations (i.e., with a homogeneous pair potential and without a vector potential). In Sec. IV, we discuss the spontaneous edge current in a superconducting disk with a *specular* surface. In Sec. V, we study the effects of surface roughness on the spontaneous edge current. In Sec. VI, we demonstrate the temperature dependence of a spontaneous magnetization, which is a measurable value in experiments. In Sec. VII, we summarize this paper.

6.3 Quasiclassical Eilenberger theory

Let us consider a small chiral superconducting disk as shown in Fig. 6.1. We assume that there is no chiral domains by choosing the radius of the disk R to be comparable to the coherence length $\xi_0 = \hbar v_F/2\pi T_c$, where v_F is the Fermi velocity and T_c is the superconducting transition temperature. We apply the quasiclassical Green function theory of superconductivity [72] to calculate the edge current of a chiral superconductor. In an equilibrium superconductor, the Eilenberger equation takes the form

$$iv_F \boldsymbol{k}\cdot\boldsymbol{\nabla}_{\boldsymbol{r}}\,\check{g} + \left[\check{H}+\check{\Sigma}\,,\check{g}\,\right]_- = 0, \tag{6.1}$$

where v_F is the Fermi velocity, $\boldsymbol{k}$ is the unit wave vector on the Fermi surface, and $[\alpha,\beta]_- = \alpha\beta - \beta\alpha$. We employ the isotropic cylindrical Fermi surface (i.e., no k_z dependence) as studied in Ref. [87] because most chiral superconductors are layered materials. Throughout this paper, we use the set of units $\hbar = k_B = c = 1$, where $2\pi\hbar$ is the Planck constant, k_B is the Boltzmann constant, and c is the speed of light. The matrices $\check{g}$ and $\check{H}$ are defined as follows,

$$\check{g}(\boldsymbol{r},\boldsymbol{k},i\omega_n) = \begin{bmatrix} \hat{g}(\boldsymbol{r},\boldsymbol{k},i\omega_n) & \hat{f}(\boldsymbol{r},\boldsymbol{k},i\omega_n) \\ -\underset{\sim}{\hat{f}}(\boldsymbol{r},\boldsymbol{k},i\omega_n) & -\underset{\sim}{\hat{g}}(\boldsymbol{r},\boldsymbol{k},i\omega_n) \end{bmatrix}, \tag{6.2}$$

$$\check{H}(\boldsymbol{r},\boldsymbol{k},i\omega_n) = \begin{bmatrix} \hat{\xi}(\boldsymbol{r},\boldsymbol{k},i\omega_n) & \hat{\Delta}(\boldsymbol{r},\boldsymbol{k}) \\ \underset{\sim}{\hat{\Delta}}(\boldsymbol{r},\boldsymbol{k}) & \underset{\sim}{\hat{\xi}}(\boldsymbol{r},\boldsymbol{k},i\omega_n) \end{bmatrix}, \tag{6.3}$$

with $\hat{\xi}(\boldsymbol{r},\boldsymbol{k},i\omega_n) = [i\omega_n + ev_F\boldsymbol{k}\cdot\boldsymbol{A}(\boldsymbol{r})]\,\hat{\sigma}_0$, where $\omega_n = (2n+1)\pi T$ is the Matsubara frequencies with n being an integer, T is the temperature, $\hat{\Delta}$ represents the pair potential, $\hat{\sigma}_0$ is the 2×2 identity matrix in spin space, and $\boldsymbol{A}$ is the vector potential induced by the chiral edge current. We introduce the definition $\underset{\sim}{K}(\boldsymbol{r},\boldsymbol{k},i\omega_n) = K^*(\boldsymbol{r},-\boldsymbol{k},i\omega_n)$. The symbol $\check{\cdot}$ represents a 4×4 matrix structure in particle-hole space and the symbol $\hat{\cdot}$ represents a 2×2 matrix structure in spin space.

We consider three chiral superconductors with different pairing symmetries: spin-triplet chiral p-wave, spin-singlet chiral d-wave, and spin-triplet chiral f-wave pairings. In the spin-triplet superconductor, we assume that the pairing interactions work between two electrons with opposite spins. This assumption does not loose any generality of the argument below. The pair potential are described by

$$\hat{\Delta}(\boldsymbol{r},\theta) = \begin{cases} \Delta(\boldsymbol{r},\theta)\hat{\sigma}_1 & \text{for a spin triplet,} \\ \Delta(\boldsymbol{r},\theta)i\hat{\sigma}_2 & \text{for a spin singlet,} \end{cases} \tag{6.4}$$

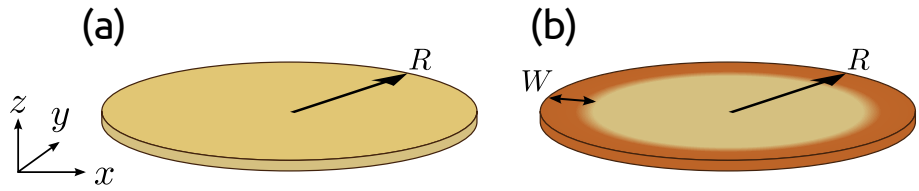

Figure 6.1: Schematics of superconducting disks. The disk with a specular surface and that with a rough surface are shown in (a) and (b), respectively. The radius and thickness of a disk are denoted by R and D, respectively. The width of the disordered region is denoted by W in (b). The small enough radius allows us to assume that there is no chiral domain in the disk.

where $\hat{\sigma}_j$ for j = 1-3 are the Pauli matrices in spin space. The matrix Green functions in Eq. (6.2) can be represented by the scaler Green functions as

$$\hat{g}(\boldsymbol{r},\theta,i\omega_n) = g(\boldsymbol{r},\theta,i\omega_n)\hat{\sigma}_0, \tag{6.5}$$

$$\hat{f}(\boldsymbol{r},\theta,i\omega_n) = \begin{cases} f(\boldsymbol{r},\theta,i\omega_n)(-i\hat{\sigma}_1) & \text{for a triplet} \\ f(\boldsymbol{r},\theta,i\omega_n)\hat{\sigma}_2 & \text{for a singlet.} \end{cases} \tag{6.6}$$

The pair potential in a chiral superconductor is described by

$$\Delta(\boldsymbol{r},\theta) = \Delta_1(\boldsymbol{r})\cos(\chi\theta) + i\Delta_2(\boldsymbol{r})\sin(\chi\theta), \tag{6.7}$$

where θ is the azimuthal angle in the momentum space (i.e., $k_x = \cos\theta$ and $k_y = \sin\theta$), and Δ_1 and Δ_2 are the local amplitudes of two independent components. The topological numbers $\chi = \pm 1$, ± 2, and ± 3 characterize the chiral p-, chiral d-, and chiral f-wave superconductivity, respectively. The doubly degenerate chiral superconducting states are indicated by $\pm\chi$. In this study, we consider superconducting states with a positive χ. Deep inside a superconductor (i.e., bulk region), the relation $\Delta_1 = \Delta_2$ is satisfied. Therefore the pair potentials in the bulk are represented as

$$\Delta(\theta) = \bar{\Delta}(T)e^{i\chi\theta}, \tag{6.8}$$

where $\bar{\Delta}(T)$ is the amplitude of the uniform pair potential at a temperature T. The amplitude of the superconducting gap is isotropic in momentum space. In the simulations, Δ_1 and Δ_2 are self-consistently determined by the gap equation,

$$\begin{bmatrix} \Delta_1(\boldsymbol{r}) \\ \Delta_2(\boldsymbol{r}) \end{bmatrix} = N_0 g_0 \pi T \sum_{\omega_n} \int \frac{d\theta'}{2\pi} f(\boldsymbol{r},\theta',i\omega_n) \begin{bmatrix} V_1(\theta') \\ V_2(\theta') \end{bmatrix} \tag{6.9}$$

where N_0 is the density of states per spin at the Fermi level in three-dimension. The coupling constant g_0 is determined by

$$(N_0 g_0)^{-1} = \ln\left(\frac{T}{T_c}\right) + \sum_{n=0}^{n_c} \frac{1}{n+1/2}, \tag{6.10}$$

where $n_c = (\omega_c/2\pi T)$ with ω_c being the cutoff energy. The functions V_1 and V_2 represent the attractive interactions as

$$V_1(\theta) = 2\cos(\chi\theta), \quad V_2(\theta) = 2\sin(\chi\theta). \tag{6.11}$$

In our model, the Andreev bound states never appear at the surface in the z direction (i.e., the top and bottom surfaces in Fig. 6.1) because the pair potential does not depend on k_z. [69] As a result, the pair potential is less dependent on z. Thus, by setting the disk thin enough $D \lesssim \xi_0 < \lambda_L$, we ignore the z dependence of the quasiclassical Green functions. However the thickness of the disk need to be larger than the Fermi wavelength $1/k_F$, so that the quasiclassical theory can be applied. [121, 122]

The effects of the rough surface are taken into account through the impurity self-energy, which is defined by

$$\check{\Sigma}(\boldsymbol{r}, i\omega_n) = \begin{cases} \dfrac{i}{2\tau_0}\displaystyle\int \frac{d\theta}{2\pi}\check{g}(\boldsymbol{r},\theta,i\omega_n) & \text{for } r > R-W, \\ 0 & \text{for } r < R-W, \end{cases} \tag{6.12}$$

where $r = (x^2+y^2)^{1/2}$ and τ_0 is the mean free time due to the impurity scatterings. The self-energy has finite values only near the surface as shown in Fig. 6.1(b), where W is the width of the disordered region.

The electric current $\boldsymbol{j}(\boldsymbol{r})$ is calculated from the Green function

$$\boldsymbol{j}(\boldsymbol{r}) = \frac{\pi e v_F N_0}{2i} T \sum_{\omega_n} \int \frac{d\theta}{2\pi} \mathrm{Tr}\left[\check{T}_3 \boldsymbol{k}\, \check{g}(\boldsymbol{r},\theta,i\omega_n)\right], \tag{6.13}$$

where $\check{T}_3 = \mathrm{diag}[\hat{\sigma}_0, -\hat{\sigma}_0]$. The vector potential is determined by solving the Maxwell equation,

$$\nabla \times \boldsymbol{A}(\boldsymbol{r}) = \boldsymbol{H}(\boldsymbol{r}), \tag{6.14}$$

$$\nabla \times \boldsymbol{H}(\boldsymbol{r}) = 4\pi \boldsymbol{j}(\boldsymbol{r}). \tag{6.15}$$

In a finite size superconductor, we define the amplitude of a spontaneous magnetization

M in terms of the spontaneous magnetic field $\boldsymbol{H}(\boldsymbol{r})$ as

$$\boldsymbol{M} = \frac{1}{\nu}\int d\boldsymbol{r}\boldsymbol{H}(\boldsymbol{r}). \tag{6.16}$$

where $\nu = \pi R^2 D$ is the volume of a small superconducting disk. In this paper, we did not calculate the magnetic field in the three-dimension. We obtain $\boldsymbol{H}$ by solving the Maxwell equation in the x-y plane with the boundary condition $H(x,y) = 0$ outside of the disk, and assume that the magnetic field is homogeneous in the z direction [i.e., $\boldsymbol{H}(\boldsymbol{r}) = H(x,y)\hat{\boldsymbol{z}}$ with $\hat{\boldsymbol{z}}$ being the unit vector]. We iterate the Eilenberger equation for the Green function and the Maxwell equation for the vector potential to obtain the self-consistent solutions of $\Delta_1(\boldsymbol{r})$, $\Delta_2(\boldsymbol{r})$, $\boldsymbol{A}(\boldsymbol{r})$, and $\check{\Sigma}(\boldsymbol{r}, i\omega_n)$.

We start all of the simulations with the initial condition $\Delta_1(\boldsymbol{r}) = \Delta_2(\boldsymbol{r}) = |\bar{\Delta}(T)|$ and $\boldsymbol{A}(\boldsymbol{r}) = 0$, where $|\bar{\Delta}(T)|$ is the amplitude of the pair potential in a homogeneous superconductor at a temperature T. Throughout this paper, we fix several parameters: the radius of a disk $R = 10\xi_0$, the cutoff energy $\omega_c = 6\pi T_c$. The magnetic field and the spontaneous magnetization are measured in units of the second critical magnetic field $H_{c_2} = \hbar c/|e|\xi_0^2$. The current density is normalized to $j_0 = 2|e|v_F N_0 T_c = \hbar c^2/4\pi^2|e|\lambda_L^2\xi_0$. In the quasiclassical theory, the London length $\lambda_L = (mc^2/4\pi n_e e^2)^{1/2}$ with n_e being the electron density is a parameter characterizing the spatial variation of magnetic fields, and is fixed at $\lambda_L = 5\xi_0$. In this paragraph, we explicitly denoted $\hbar$ and c to avoid misunderstandings.

To solve the Eilenberger equation in a disk geometry, we apply the Riccati parametrization to the Green function [74–76] and the technique discussed in Ref. [77]. By using the Riccati parametrization, we can separate the Eilenberger equation into the two Riccati-type differential equations. Solving the Riccati equations along a long enough quasiclassical trajectory (typically 30 times of the coherence length), we can obtain the solutions of the Eilenberger equation.

As we will demonstrate in the following sections, the edge currents show complicated spatial profiles depending on the pairing symmetry. To analyze such behaviors, we decompose the electric current into a series of current components in terms of the symmetry of Cooper pairs. By using the normalization relation $g^2 - s_\nu f\underset{\sim}{f} = 1$ under the assumption $f\underset{\sim}{f} \ll 1$, we represent the normal Green function as $g \approx 1 + s_\nu f\underset{\sim}{f}/2$, where we have used the Eq. (6.6) and $s_\nu = 1$ ($s_\nu = -1$) for the spin-triplet (spin-singlet) pair potential. By substituting the expression into the current formula in Eq. (6.13), the electric current can

be expressed as [123]

$$\boldsymbol{j}(\boldsymbol{r}) = \sum_{\omega_n>0} \boldsymbol{j}_{\omega_n}(\boldsymbol{r}) \tag{6.17}$$

$$\boldsymbol{j}_{\omega_n} = 4\pi e v_F N_0 T \int \frac{d\theta}{2\pi} \frac{1}{2} s_\nu \boldsymbol{k}\, \mathrm{Im}[f\underset{\sim}{f}], \tag{6.18}$$

where we have used the relation $g(\boldsymbol{r},\theta,i\omega_n) = -g^*(\boldsymbol{r},\theta,-i\omega_n)$. Generally speaking, the pairing function $f(\boldsymbol{r},\theta,i\omega_n)$ can be decomposed into the Fourier series

$$\begin{aligned} f(\boldsymbol{r},\theta,i\omega_n) = &\sum_{a=0} f_a^{\mathrm{c}}(\boldsymbol{r},i\omega_n)\cos(a\theta) \\ &+ \sum_{b=1} i f_b^{\mathrm{s}}(\boldsymbol{r},i\omega_n)\sin(b\theta). \end{aligned} \tag{6.19}$$

The surface breaks locally the inversion symmetry and induces subdominant pairing components whose symmetries are different from that of the pair potential. In the absence of the vector potential, f_a^{c} and f_b^{s} are real functions. When we consider the current profile at $y = 0$, the electric current in the y direction becomes

$$j_y(x) = \sum_{\omega_n} \sum_{ab} j_{ab}(i\omega_n) \tag{6.20}$$

$$j_{ab}(i\omega_n) = 4\pi|e| v_F N_0\, T\, f_a^{\mathrm{c}}\, f_b^{\mathrm{s}}\, I_{ab} \tag{6.21}$$

$$I_{ab} = s_\nu (-1)^b (\delta_{b,1-a} + \delta_{b,a+1} - \delta_{b,a-1})/4 \tag{6.22}$$

where we use the relation $\underset{\sim}{f}(\boldsymbol{r},\theta,i\omega_n) = f^*(\boldsymbol{r},\theta+\pi,i\omega_n)$, and $\int d\theta \sin\theta\cos(a\theta)\sin(b\theta) = (\delta_{b,1-a} + \delta_{b,a+1} - \delta_{b,a-1})\pi/2$ for $a \geq 0$ and $b \geq 1$. The Kronecker's δ functions appearing in Eq. (6.22) suggest that only the limited combinations of f_a^{c} and f_b^{s} contribute to the supercurrents, (e.g., $a = b \pm 1$). Moreover, the direction of the decomposed current j_{ab} in Eq. (6.21) depends on the signs of $f_a^{\mathrm{c}} f_b^{\mathrm{s}}$ and I_{ab}. The signs of I_{ab} mainly determine the current directions because $f_a^{\mathrm{c}} f_b^{\mathrm{s}}$ appearing at a certain surface have the same signs in most cases. We show a chart of $\mathrm{sgn}[I_{ab}]$ in Fig. 6.2. The diagonal lines connecting $\cos(a\theta)$ and $\sin(b\theta)$ mean the possible combinations for carrying the currents. The solid (broken) lines indicate that I_{ab} is positive (negative). In a chiral p-wave superconductor, for example, I_{01} and I_{21} have the opposite signs to each other. As a result, the decomposed currents j_{01} and j_{21} flow in opposite directions.

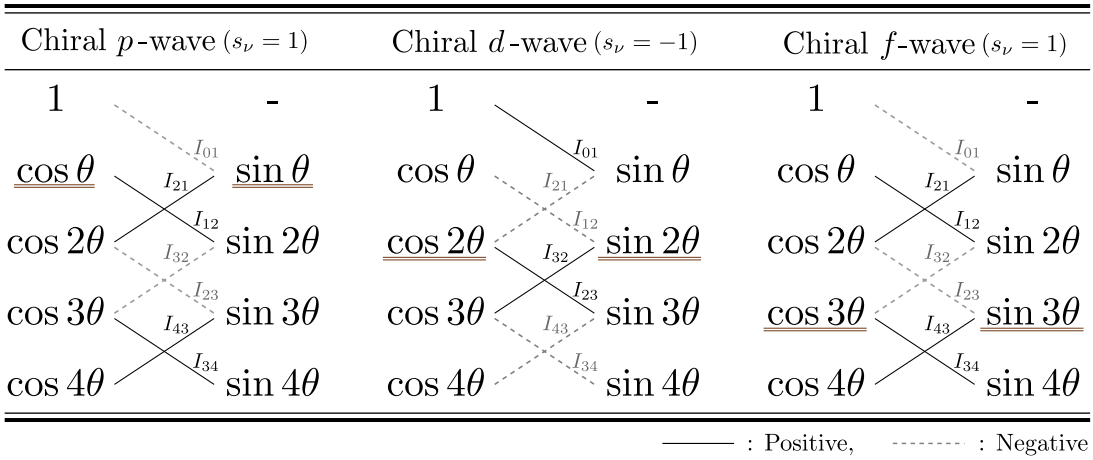

Figure 6.2: Chart of I_{ab} in Eq. (6.22). The diagonal lines connecting $\cos(a\theta)$ and $\sin(b\theta)$ indicate possible combinations of $f_a^{\rm c}$ and $f_b^{\rm s}$ for the chiral currents. The solid (broken) lines means I_{ab} is positive (negative). The sign of I_{ab} in a spin-singlet superconductor is opposite to that in a spin-triplet superconductor due to an extra sign factor s_ν. The double underlines indicate the principal pairing component linking to the pair potential (i.e., $\cos(\chi\theta)$ and $\sin(\chi\theta)$). At the first line, "1" represents s-wave component.

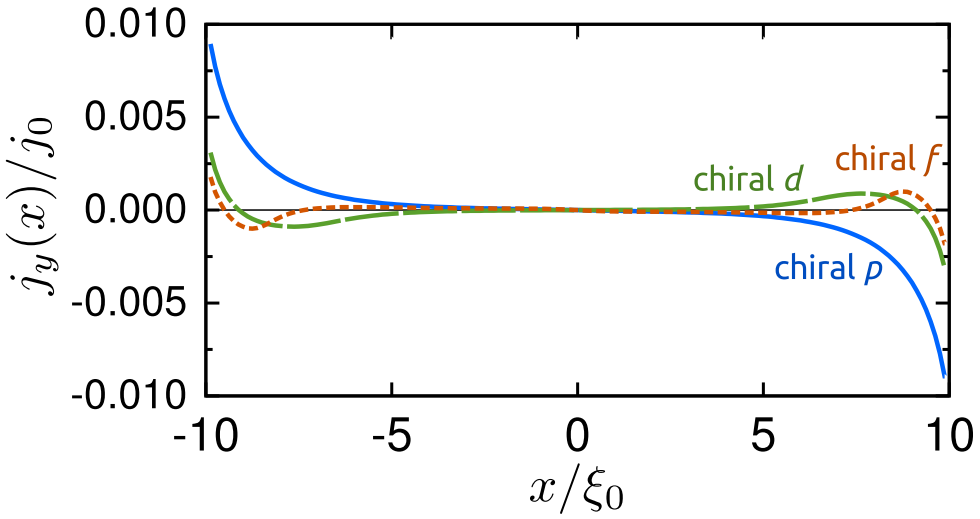

Figure 6.3: Current densities in a disk of a chiral superconductor with a constant pair potential $\Delta_{1(2)}(\boldsymbol{r}) = |\bar{\Delta}(T)|$ at $\boldsymbol{A}(\boldsymbol{r}) = 0$, where $|\bar{\Delta}(T)|$ is the amplitude of the pair potential at a temperature T in a homogeneous superconductor. Here, we show the current distribution at $y = 0$. The radius of a superconducting disk, the temperature, and the cutoff energy are set to $R = 10\xi_0$, $T = 0.2T_c$, and $\omega_c = 6\pi T_c$.

6.4 Non-self-consistent simulation

Before turning into the effects of surface roughness and those of the Meissner screening, the chiral currents in the uniform pair potential at $\boldsymbol{A} = 0$ should be summarized. The results presented in this section are qualitatively the same as those obtained by the Bogoliubov-de Gennes (BdG) formalism in Refs. [107] and [108].

The spatial dependences of the edge current are shown in Fig. 6.3, where we show the spatial distribution of the current in the y direction $j_y(x)$ at $y = 0$, where the temperature is set to $T = 0.2T_c$. The results are circular symmetric on a superconducting disk. In a chiral p-wave superconductor ($\chi = 1$), the amplitude of the edge current takes its maximum at $r = R$ and monotonically decreases with increasing the distance from the surface. When we observe the current from the $+z$ axis, the chiral current flows in the clockwise direction. The current distributions in chiral d-wave ($\chi = 2$) and chiral f-wave ($\chi = 3$) superconductors are rather complicated than that in a chiral p-wave case. The current density is negative (clockwise) around $x/\xi_0 = 10$ and is positive (counterclockwise) for $x/\xi_0 < 9$ in a chiral d-wave superconductor. In a chiral f-wave case, the current density is negative for $9.5 < x/\xi_0 < 10$, positive for $7.8 < x/\xi_0 < 9.5$, and negative again for $x/\xi_0 < 7.8$. The net current density $J = \int_0^R dx\, j_y(x)|_{y=0}$ decreases with increasing the chiral index χ because there are two (three) current channels in a chiral d-wave (f-wave) superconductor and they carry the currents in opposite directions.

6.5 Disk with a specular surface

In this section, we discuss the current distribution of a chiral-superconducting disk with a specular surface under the self-consistent pair potentials and the vector potential. The results are obtained by solving the Eilenberger and Maxwell equations simultaneously and self-consistently. In Sec. IV A, we consider only the self-consistent pair potential at $\boldsymbol{A} = 0$ in Eq. (6.3) to analyze the complicated spatial distribution of the chiral current. The results tell us the symmetry of Cooper pairs that carry the chiral current. The effects of self-induced magnetic fields are briefly discussed in Sec. IV B. The parameters are set to the same values used in Fig. 6.3.

6.5.1 Results under self-consistent pair potential at $\boldsymbol{A} = 0$

In Fig. 6.4, we show the spatial dependence of the pair potentials Δ_1 and Δ_2. In a chiral p-wave superconductor, the pair potential Δ_1 is strongly suppressed, whereas Δ_2 is slightly enhanced near the surface as shown in Fig. 6.4(a). These suppression and enhancement are closely related to the formation of the surface ABSs. Namely, Δ_1 changes its sign while the quasiparticle is reflected by a specular surface. These spatial variations of the pair potentials affect the edge current. The current density $j_y(x)$ at $y = 0$ in Eq. (6.20) is shown in Fig. 6.5(a). In a chiral p-wave disk, the edge current monotonically decreases with increasing the distance from the edge. The edge current under the self-consistent pair potential in Fig. 6.5(a) flows much wider area than that obtained by the uniform pair potential in Fig. 6.3. The range of "edge" is determined by the spatial variation of the pair potential in Fig. 6.4.

The surface breaks locally the inversion symmetry and the spatial variation of the pair potential breaks the translational symmetry. As a result, the subdominant pairing correlations are induced near the surface. [124] In Fig. 6.2, we enumerate the orbital symmetry of such subdominant components. The double underlines indicate the principal pairing component linked to the pair potential. At the first row, "1" represents s-wave symmetry. In a chiral p-wave case, the spatial variation of the principal component $\cos(\theta)$ induces the subdominant component such as s-wave, d-wave $\cos(2\theta)$, f-wave $\cos(3\theta)$, $\cdots$. In the same way, the principal component $\sin(\theta)$ induces the subdominant component of d-wave $\sin(2\theta)$, f-wave $\sin(3\theta)$, $\cdots$. The current is decomposed into the series of j_{ab} in Eq. (6.21). The results for a chiral p-wave disk are shown in Fig. 6.5(b), where j_{01}, j_{21}, j_{23} and j_{43} contribute mainly to the current. Here j_{ab} shown in Fig. 6.5(b) are calculated at the lowest Matsubara frequency ω_0. We have confirmed that $\sum_{ab} j_{ab}(\omega_0)$ is almost identical to the current density obtained from the normal Green function $j(\omega_0)$, and that the

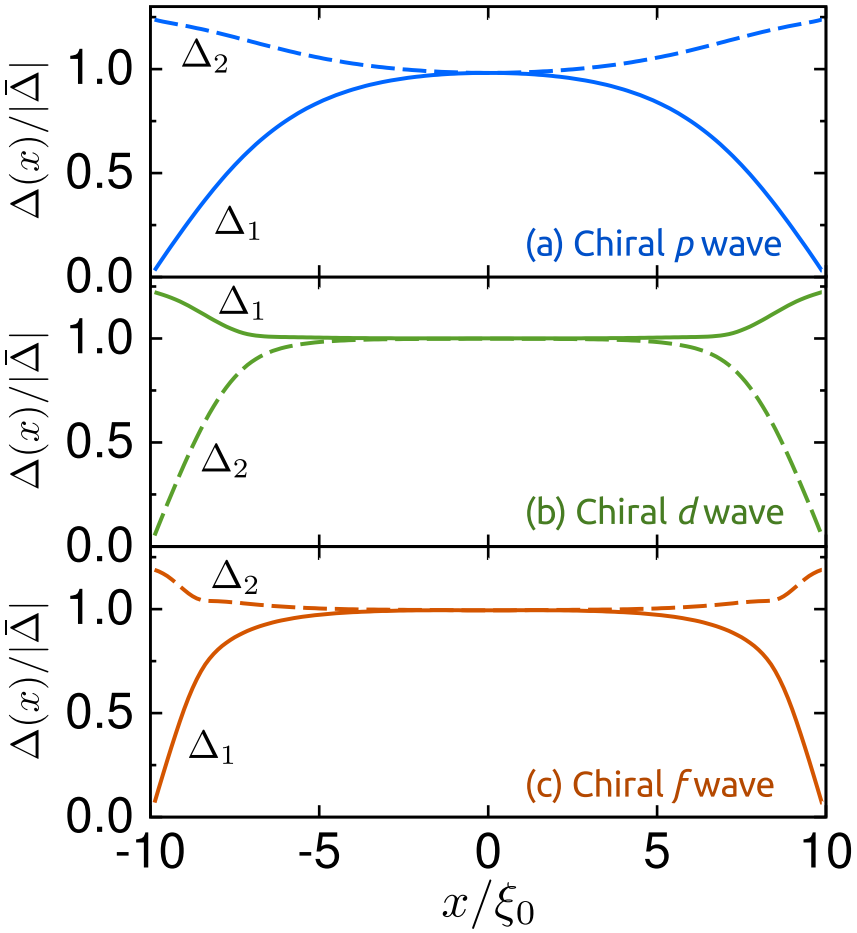

Figure 6.4: Pair potentials in a disk of a chiral superconductor. The results are obtained by solving self-consistently the Eilenberger equation under the condition $\boldsymbol{A}(\boldsymbol{r}) = 0$. The superconducting disk is in the clean limit. The pair potentials are normalized to $|\bar{\Delta}(T)|$, the amplitude of the pair potential in a homogeneous superconductor at a temperature T. The parameters are set to the same values used in Fig. 6.3.

components at higher Matsubara frequencies have almost the similar spatial distribution as j_{ab} at ω_0. Reflecting the signs of I_{ab} in Fig. 6.2, j_{01} and j_{23} flow in the clockwise direction, whereas j_{21} and j_{43} do in the counterclockwise direction. The magnitudes of j_{01} and j_{23} are slightly larger than j_{21} and j_{43}, respectively. As a consequence, the net edge current flows in the clockwise direction. We have confirmed that another possible j_{ab} are negligible. The decomposed currents in Fig. 6.5(b) tell us the symmetry of Cooper pairs that carry the edge current. The partial current j_{01} represents the current carried by the combination of s-wave and p_y-wave Cooper pairs. The current j_{21} are also understood as the current carried by $d_{x^2-y^2}$-wave $\times$ p_y-wave Cooper pairs.

All of the Cooper pairs in a chiral p-wave superconductor belong to the spin-triplet

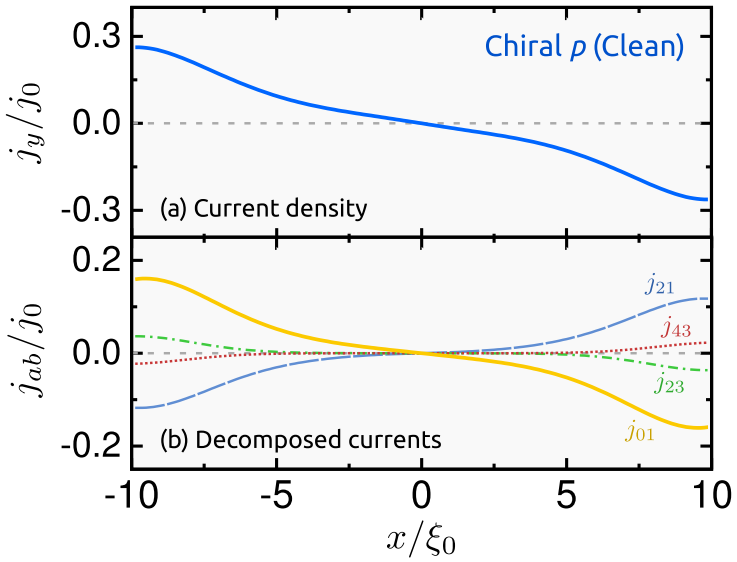

Figure 6.5: Results for a chiral p-wave disk with a *specular* surface obtained by the self-consistent simulation under $\boldsymbol{A}(\boldsymbol{r}) = 0$. The chiral current $j_y(x)$ in Eq. (6.20) at $y = 0$ is shown in (a). The decomposed current j_{ab} at the lowest Matsubara frequency in Eq. (6.21) are shown in (b). All of the currents in (a) and (b) are normalized to $j_0 = 2|e|v_F N_0 T_c$. The parameters are set to the same values used in Fig. 6.3.

symmetry class in the absence of spin-dependent potentials. Therefore, even-parity pairs induced at a surface have the odd-frequency symmetry because of the anti-symmetry relation derived from the Fermi-Dirac statistics of electrons

$$\hat{f}(\boldsymbol{r}, \theta, i\omega_n) = -\hat{f}^{\mathrm{T}}(\boldsymbol{r}, \theta + \pi, -i\omega_n), \tag{6.23}$$

where $\cdot^{\mathrm{T}}$ represents the transpose of a matrix and means the commutation of the two spins of a Cooper pair. The odd-parity symmetry accounts the negative sign on the right-hand side of Eq. (6.23) in a spin-triplet superconductor. On the other hand, the induced spin-triplet even-parity components satisfy Eq. (6.23) by their frequency dependence. They are so-called odd-frequency Cooper pairs. [125, 126] As shown in Fig. 6.5(b) and Eq. (6.21), the spontaneous edge current in a chiral superconductor is carried by the combination of the even- and odd-frequency Cooper pairs staying at a surface.

In a chiral d-wave superconductor, Δ_2 is responsible for the formation of the surface ABSs. Correspondingly, the pair potential Δ_1 is slightly enhanced near the surface as shown in Fig. 6.4(b). The spatial profile of the current is shown in Fig. 6.6(a). As is the case in the non-self-consistent simulation, there are two edge channels in a chiral d-wave disk. The current in the clockwise direction flows along the surface and the current in the counterclockwise flows around $x = \pm 7\xi_0$. In Fig. 6.6(b), we decompose the

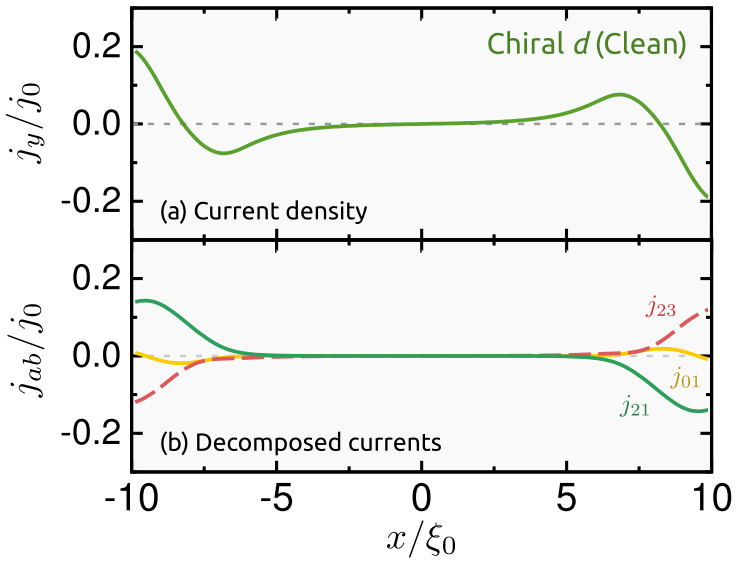

Figure 6.6: Results for a chiral d-wave disk with a specular surface obtained by the self-consistent simulation under $\boldsymbol{A}(\boldsymbol{r}) = 0$: current density j_y (a) and dominant components j_{ab} (b). The results are plotted in the same manner as Fig. 6.5.

current into the series of j_{ab}, where we show only dominant components of j_{21}, j_{23} and j_{01}. We note that j_{12} and j_{32} (not shown) have almost the same profile as j_{01}, and that another components are negligible. The principal pairing components in a chiral d-wave superconductor are $f_2^{\rm c}\cos(2\theta)$ and $f_2^{\rm s}\sin(2\theta)$ as shown in Fig. 6.2. The spatial variation of the pair potential generates the odd-frequency components $f_1^{\rm s}\sin(\theta)$ and $f_3^{\rm s}\sin(3\theta)$. These induced components carry the spontaneous current indicated by j_{21}, j_{23}, j_{12} and j_{32}. As shown in Fig. 6.6(b), j_{21} and j_{23} flow in opposite directions because I_{21} and I_{23} have opposite signs. As a result, the net edge current becomes smaller than that in a chiral p-wave disk.

In a chiral f-wave disk, Δ_1 is suppressed and Δ_2 is slightly enhanced near the surface due to the emergence of the surface ABSs as shown in Fig. 6.4(c). The current profile and the decomposed currents j_{ab} are shown in Fig. 6.7(a) and 6.7(b), respectively. Although the spatial profile of the current is greatly modified by the self-consistent pair potentials, Fig. 6.7(a) suggests that there are three current channels. The current density is negative for $8 < x/\xi_0$, is positive for $6 < x/\xi_0 < 8$, and is negative again for $0 < x/\xi_0 < 6$. Figure. 6.7(b) shows that the spatial dependence of the current components j_{23}, j_{43} and j_{34} are responsible for such a complicated current profile. We note that j_{21} and j_{32} (not shown) have almost the same profile as j_{34}.

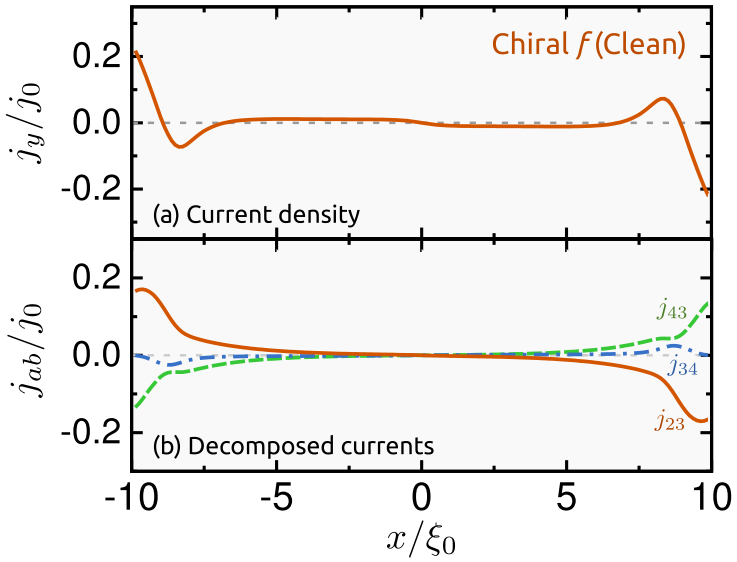

Figure 6.7: Results for a chiral f-wave disk with a specular surface obtained by the self-consistent simulation under $\boldsymbol{A}(\boldsymbol{r}) = 0$: current density j_y (a) and dominant components j_{ab} (b). The results are plotted in the same manner as Fig. 6.5.

6.5.2 Results under self-consistent pair potential and vector potential

We take into account the vector potential $\boldsymbol{A}$ induced by the edge current to investigate the Meissner screening effect. The pair potential and the vector potential are determined in a self-consistent way by solving the Eilenberger and Maxwell equations simultaneously. The spatial profiles of the pair potentials are qualitatively the same as those in Fig. 6.4. The spatial profiles of the chiral edge currents are shown in Fig. 6.8(a). In Figs. 6.8(b)-6.8(d), we compare the local magnetic fields obtained under the self-consistent field (SCF) with that under the non-self-consistent field of the vector potential (non-SCF). The latter is calculated from the current distribution in Figs. 6.5(a), 6.6(a), and 6.7(a) by using the relation in Eq. (6.15).

In a chiral p-wave disk, the Meissner screening by the superconducting condensate suppresses dramatically the spontaneous magnetization as shown in Fig. 6.8(b). As a result, the amplitude of the current at $x = R$ is less than $0.13j_0$ under the SCF in Fig. 6.8(a), whereas it is about $0.27j_0$ under the non-SCF in Fig. 6.5(a). The magnetic field near the center of a disk remains at a finite value in both the SCF and non-SCF simulations. This magnetic-field penetration is a results of the finite-size effects. At the surface of a semi-infinite sample, we have confirmed the current inversion because of the Meissner screening current as seen in Fig. 2 in Ref. [87]. Namely, the bulk condensate

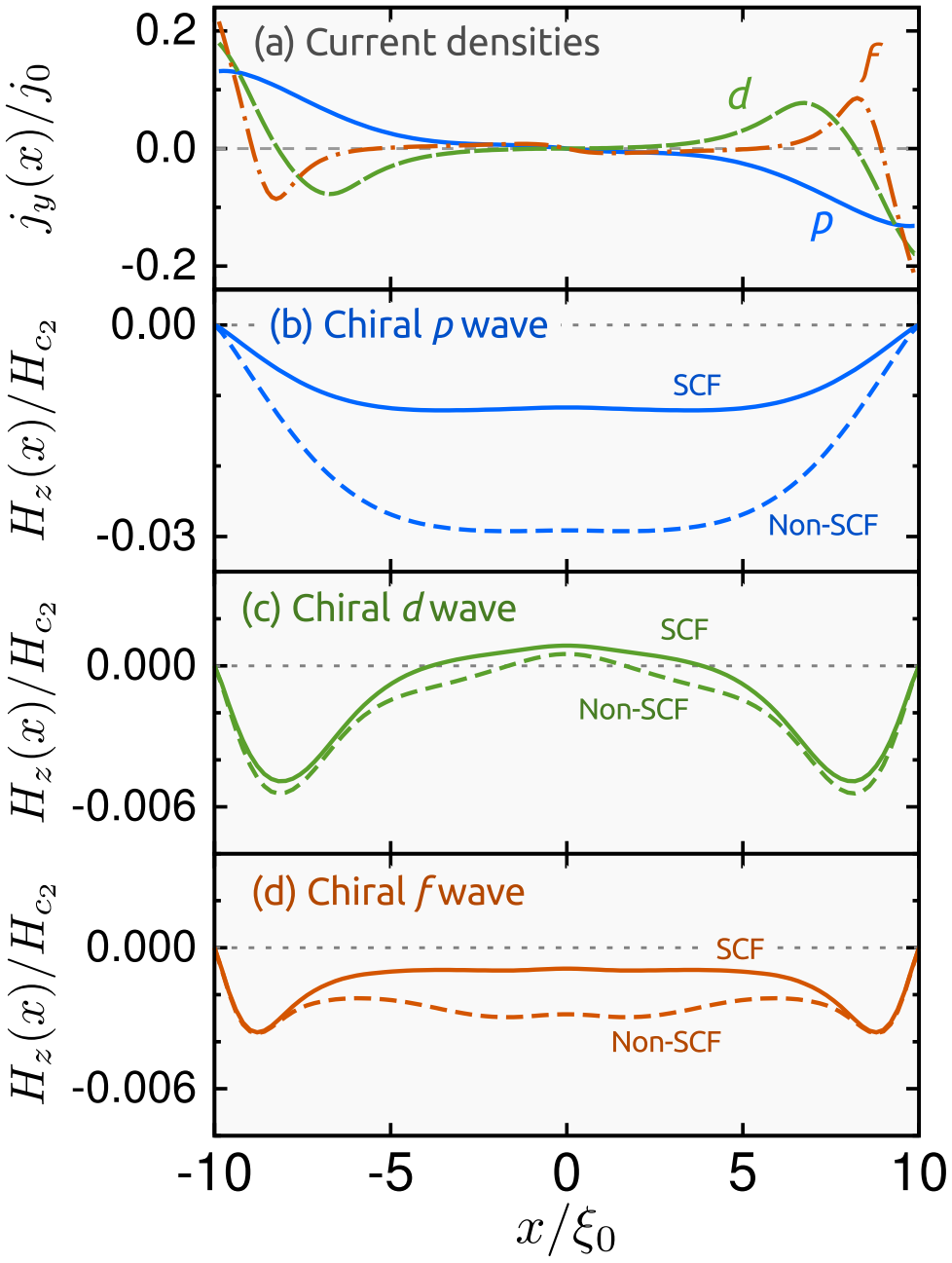

Figure 6.8: (a) Current densities in a disk of a chiral superconductor with a *specular* surface. The results are obtained by solving the Eilenberger and Maxwell equations self-consistently and simultaneously. The penetration depth is fixed at $\lambda_L = 5\xi_0$. The other parameters are set to the same values used in Fig. 6.3. The current densities are normalized to $j_0 = 2|e|v_F N_0 T_c$. In (b)-(d), we compare the spatial distributions of the self-consistent fields (SCF) with those of the non-self-consistent fields (non-SCF). The former is obtained by the current densities in (a) by using the relation in Eq. (6.15). The latter is calculated from the current distributions in Figs. 6.5(a), 6.6(a), and 6.7(a). The magnetic fields are scaled in units of $H_{c_2} = \hbar c/|e|\xi_0^2$.

generates the screening current which flows in the opposite direction to the chiral current at the surface. As a result, the magnetic field in the bulk region vanishes in a semi-infinite superconductor.

In a chiral d-wave superconductor, the magnetic field is mainly localized around $x = \pm 8\xi_0$ as shown in Fig. 6.8(c). The results with the SCF is slightly smaller than those with the non-SCF. Thus the Meissner effect in a chiral d-wave disk is much weaker than that in a chiral p-wave one. The current profile under the non-SCF in Fig. 6.6(a) shows that there are two channels for the edge current. One is the outer channel for the clockwise current and the other is the inner channel for the counterclockwise current. The induced magnetic field by the inner current well screens that by the outer current intrinsically. Such a self-screening effect makes the Meissner screening effect weak in a chiral d-wave disk. Actually such characteristic current profile with the non-SCF in Fig. 6.6(a) are well preserved in the results with the SCF in Fig. 6.8(a). The current amplitude at the surface $x = R$ reaches to about $0.18j_0$ in Fig. 6.8(a) and it is about $0.19j_0$ in Fig. 6.6(a). Thus, in a chiral d-wave disk, the Meissner effect modifies the edge current only slightly as shown in Fig. 6.8(c).

The result of the edge current for a chiral f-wave superconductor in Fig. 6.8(d) can be explained in the same way. There are three channels for the edge current in a chiral f-wave case as discussed in Fig. 6.7(a). The self-screening effect works in this case as well. The characteristic behavior of the edge current with the non-SCF in Fig. 6.7(a) remain almost unchanged even with the SCF as shown in Fig. 6.8(a). However, because the self-screening effect does not sufficiently exclude the local field, the magnetic field around the center of a disk is suppressed by the Meissner effect as shown in Fig. 6.8(d).

6.6 Disk with a rough surface

In this section, we discuss the effects of a rough surface on the chiral edge currents. The width of the disordered region [shadowed in Fig. 6.1(b)] is set to be $W = 3\xi_0$ because the chiral edge current in the clean limit mainly flows in such area as shown in Fig. 6.8(a). The strength of roughness is set to $\xi_0/\ell = 1.0$, where $\ell = v_F\tau_0$ is the elastic mean free path of a quasiparticle. The another parameters are set to the same values used in Fig. 6.5. The rough surface drastically changes the spatial profile of the pair potential and that of induced subdominant pairing components. Thus we first summarize symmetry of Cooper pairs appearing near the rough surface in Sec. V A. Then we discuss briefly the Meissner screening effect by the bulk condensate in Sec. V B.

6.6.1 Results under self-consistent pair potential at $\boldsymbol{A} = 0$

Here we discuss the results obtained by solving *only* the Eilenberger equation under the condition $\boldsymbol{A} = 0$ in Eq. (6.3). We obtain the self-consistent solutions of $\Delta_1(\boldsymbol{r})$, $\Delta_2(\boldsymbol{r})$, and $\hat{\Sigma}(\boldsymbol{r}, i\omega_n)$. The pair potentials are presented in Fig. 6.9. The surface roughness strongly suppresses the pair potentials Δ_1 and Δ_2 in the disordered region of a chiral p-wave disk. At the interface between the disordered and clean regions (we refer to it as the d/c interface in what follows), Δ_1 is suppressed more significantly than Δ_2, which suggests the formation of the ABSs there. [114] We show the current density j_y at $y = 0$ and the dominant current components j_{ab} in Fig. 6.10. Comparing Fig. 6.5(a) with 6.10(a), one can find that the peak of the edge current moves from the surface to the d/c interface, and that its maximum value $0.20 j_0$ is comparable to the maximum value in the clean limit. As shown in Fig. 6.10(b), the edge current in a chiral p-wave disk is mainly carried by three components; j_{01}, j_{21}, and j_{12}. Among them, the combination of s-wave $\times$ p_y-wave pairs (j_{01}) dominates obviously the chiral current in a disk with a rough surface. The spatial variation in Δ_1 generates the s-wave and $d_{x^2-y^2}$-wave odd-frequency pairs. [58] The induced s-wave pairs, in particular, are robust even under the random potential. Such property supports the robustness of the chiral edge current in a chiral p-wave superconductor.

The edge current in a chiral d-wave disk shows a qualitatively different behavior from that in a chiral p-wave case. As shown in Fig. 6.11(a), the chiral current in a disk with surface roughness flows only in the counterclockwise direction. This behavior can be understood by comparing the current profile in Fig. 6.6(a) with that in Fig. 6.11(a). In the clean disk, there are two edge currents: the outer current running flowing in the clockwise direction and the inner current running in the counterclockwise direction as shown in Fig. 6.6(a). The surface roughness eliminates the outer current channel. However, the inner current channel remains even in the presence of the surface roughness and are responsible for the chiral current in the counterclockwise direction. We have confirmed that the inner current can survive in the presence of much stronger roughness such as $\xi_0/\ell \sim 30$. The decomposed components of the current j_{ab} are shown in Fig. 6.11(b). The edge current is mainly carried by five combinations: j_{01}, j_{12}, j_{21}, j_{23}, and j_{32}. The four components j_{12}, j_{21}, j_{23}, and j_{32} almost cancel one another. As shown in Fig. 6.9(b), the surface roughness suppresses both Δ_1 and Δ_2 in the same manner near the shadowed area, which results in

$$f_2^{\rm c}(x) \simeq f_2^{\rm s}(x). \tag{6.24}$$

The spatial variation of Δ_1 generates mainly $f_1^{\rm c}\cos(\theta)$ and $f_3^{\rm c}\cos(2\theta)$ with $f_1^{\rm c}(x) \simeq f_3^{\rm c}(x)$.

In the same way, the spatial variation of Δ_2 induces $f_1^{\rm s}\sin(\theta)$ and $f_3^{\rm s}\sin(3\theta)$ with $f_1^{\rm s}(x) \simeq f_3^{\rm s}(x)$. Therefore, the relation

$$f_1^{\rm c}(x) \simeq f_3^{\rm c}(x) \simeq f_1^{\rm s}(x) \simeq f_3^{\rm s}(x), \tag{6.25}$$

holds among the four coefficients. By applying the relation in Esq. (6.24) and (6.25) into Eq. (6.21) with the I_{ab} in Fig. 6.2, we can conclude that j_{21} cancels j_{32}, and j_{12} cancels j_{23}. The remaining component j_{01}, the contribution from the s-wave $\times$ p_y-wave pairs, dominates the edge current. Because s-wave Cooper pairs are robust against surface roughness, j_{01} can exist even under much stronger disordered potential.

As shown in Fig. 6.12(a), the edge current in a chiral f-wave disk with a rough surface becomes almost zero in this scale of the plot (i.e., $|j_y| \ll j_0$). Within the accuracy of our numerical simulation, the maximum value of the current density is less than $4 \times 10^{-3} j_0$. The dominant components j_{23}, j_{32}, j_{34}, and j_{43} are shown in Fig. 6.12(b). As shown in Fig. 6.9(c), the surface roughness suppresses both Δ_1 and Δ_2 in the same manner near the shadowed area. By applying the same logic used in a chiral d-wave case, it is possible to show the relations

$$f_3^{\rm c}(x) \simeq f_3^{\rm s}(x), \tag{6.26}$$

$$f_2^{\rm c}(x) \simeq f_4^{\rm c}(x) \simeq f_2^{\rm s}(x) \simeq f_4^{\rm s}(x). \tag{6.27}$$

These relations and I_{ab} in Fig. 6.2 explain the cancellation among the current components such as $j_{23} + j_{34} \simeq 0$ and $j_{32} + j_{43} \simeq 0$. As a result, the net edge current totally disappears as shown in Fig. 6.12(a).

The symmetry of Cooper pairs is determined by the pair potential and the random impurity potential at a surface. Thus, even if a superconductor is semi-infinitely large and is realized with a single chiral domain, we can find the similar behavior of the edge currents against surface roughness as they show in a small superconductor.

6.6.2 Results under self-consistent pair potential and vector potential

We discuss the effects of the self-induced vector potential on the chiral current in a disk with surface roughness. By solving simultaneously the Eilenberger and Maxwell equations, we obtain the self-consistent solutions of $\Delta_1(\boldsymbol{r})$, $\Delta_2(\boldsymbol{r})$, $\boldsymbol{A}(\boldsymbol{r})$, and $\hat{\Sigma}(\boldsymbol{r}, i\omega_n)$. Here we do not show the pair potentials because they remain unchanged from those in Fig. 6.9 even quantitatively. The results of the edge currents are shown in Fig. 6.13(a). The spatial

distributions of the magnetic field are presented in Figs. 6.13(b)-(d). For comparison, we show the non-SCF calculated from the current profiles of Figs. 6.10(a), 6.11(a) and 6.12(a) by applying the relation in Eq. (6.15).

As shown in Fig. 6.13(b), the Meissner effect suppresses the magnetic field around the center of a chiral p-wave disk. When we compare the results for a chiral p-wave disk with the SCF in Fig. 6.13(a) and those with the non-SCF in Fig. 6.10(a), the current profile in Fig. 6.13(a) is spatially compressed into a narrower region by the Meissner effect.

The similar features are found also in the results of a chiral d-wave disk as shown in Fig. 6.13(c). In the presence of the surface roughness, the current profile under the non-SCF has a monotonic spatial dependence between the center of the disk and the d/c interface as presented in Fig. 6.11(a). Therefore, the self-screening effect observed in a clean disk does not work at all. In a chiral d-wave disk with a rough surface, the Meissner effect becomes stronger than that in a disk with a specular surface. The Meissner effect suppress the magnetization near the center of the disk as shown in Fig. 6.13(c).

In a chiral f-wave disk, the surface roughness strongly suppresses the chiral current. Thus the magnetic field is much smaller than H_{c_2} everywhere in the disk as shown in Fig. 6.13(d). Within the numerical accuracy, the magnetic field is less than $7 \times 10^{-5} H_{c_2}$ in our simulation.

6.7 Temperature dependence of spontaneous magnetizations

Finally, we discuss the dependences of the spontaneous magnetization on temperature which are measurable values in experiments. All of the simulations ware started at $T \simeq T_c$ with a homogeneous pair potential $\Delta_1(\boldsymbol{r}) = \Delta_2(\boldsymbol{r}) = |\bar{\Delta}(T)|$ and without an external magnetic field. The magnitude of a spontaneous magnetization is defined in Eq. (6.16). In our simulations, the pair potential, the impurity self-energy, and the vector potential are calculated self-consistently. The results in a disk with a *specular* surface are shown in Fig. 6.14. At a low temperature $T = 0.1T_c$, the magnetization of a chiral p-wave disk reaches to about $0.009H_{c_2}$. In chiral d- and f-wave disks, the magnetizations are about $0.002H_{c_2}$. Although the magnetization decreases with increasing the radius of a disk by its definition Eq. (6.16), $0.002H_{c_2}$ at $R = 10\xi_0$ would be detectable value in experiments. The results in a disk with a *rough* surface are shown in Fig. 6.15, we choose $\xi_0/\ell = 1.0$ and $W = 3\xi_0$. In a chiral p-wave superconductor, the amplitude of the magnetization is smaller than the results in the clean limit at every temperatures. As we discussed in Sec. V, however, the amplitude of the current density in a disk with a rough surface is

comparable to that in a disk with a specular surface. In Eq. (6.16), the magnetization is normalized by the area of a whole disk. As shown in Fig. 6.9, however, the effective radius of the superconducting region shrinks down to $R_{\rm eff} = R - W$ in the presence of the surface roughness. When we renormalize the magnetization by the effective superconducting area, the renormalized magnetization $\tilde{M} = MR^2/(R-W)^2 \approx 2M$ is comparable to the magnetization in the clean disk. This fact means the robustness of the chiral current in the presence of the surface roughness.

In a chiral d-wave disk, the sign of the magnetization in Fig. 6.15 changes from that in Fig. 6.14 because only the inner chiral edge channel survives in a disk with a rough surface and flows the current in the counterclockwise direction. We have confirmed that the magnetization of a chiral d-wave disk becomes small but remains finite even in the presence of the much stronger disorder (e.g., $\xi_0/\ell = 30$). As discussed in Sec. V A, the combination of s-wave and p_y-wave Cooper pairs carry the spontaneous current in both chiral p- and chiral d-wave disks. Therefore, the robust spontaneous edge current and the robust spontaneous magnetization are common features in these two superconductors. In the case of a chiral f-wave superconductor, the amplitude of the magnetization is almost zero in the scale of Fig. 6.15. Within the numerical accuracy, we estimate that the magnetization is smaller than $4 \times 10^{-5} H_{c_2}$.

6.8 Conclusion

We have studied the effects of surface roughness on the spontaneous edge current in small chiral superconductors characterized by chiral p-, chiral d- and chiral f-wave pairing symmetries. On the basis of the quasiclassical Eilenberger formalism, we calculated the chiral current and the spontaneous magnetization of the small superconducting disk numerically. By solving the Eilenberger and Maxwell equations simultaneously, we obtained self-consistent solutions of the pair potential, the impurity self-energy, and the vector potential. To understand the physics behind the complicated current distribution in real space, we decomposed the current into a series of components in terms of the symmetry of a Cooper pair. The chiral edge current is carried by a combination of two pairing components: the even-parity component and the odd-parity component. In a spin-singlet (spin-triplet) superconductor, the odd-parity (even-parity) Cooper pairs have odd-frequency symmetry.

The effects of the surface roughness depend on the pairing symmetry of the superconductor. The chiral current is robust in the presence of surface roughness in a chiral p- and chiral d-wave symmetries. With chiral p-wave symmetry, the characteristic features of the chiral current are insensitive to the surface roughness. With chiral d-wave symme-

try, the chiral current changes its direction as a result of the surface roughness. In both the chiral p-wave and chiral d-wave cases, the chiral current is carried by a combination consisting of two pairing correlations. One is the correlation with p-wave symmetry and the other is the correlation with s-wave symmetry. The Meissner screening effect by the bulk condensate reduces a spontaneous magnetization. However, the resulting amplitude of the magnetization is still large enough to be detected in experiments. In a chiral f-wave superconductor, the surface roughness significantly suppresses the spontaneous edge current.

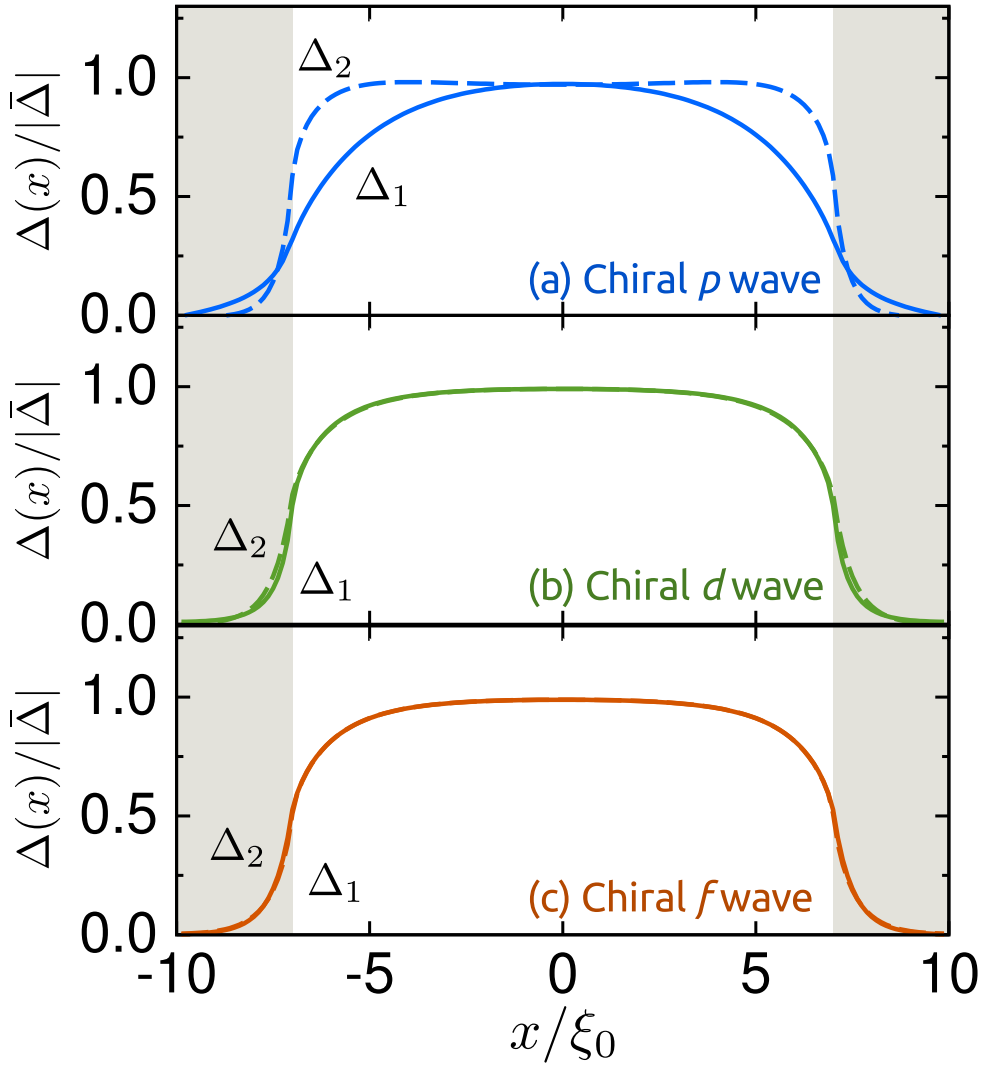

Figure 6.9: Pair potentials in a disk of a chiral superconductor with a rough surface as indicated by the shadowed area. The results are obtained by solving the Eilenberger equation self-consistently at $\boldsymbol{A} = 0$. The parameters are set to the same values used in Fig. 6.3. The magnetic penetration depth is $\lambda_L = 5\xi_0$.

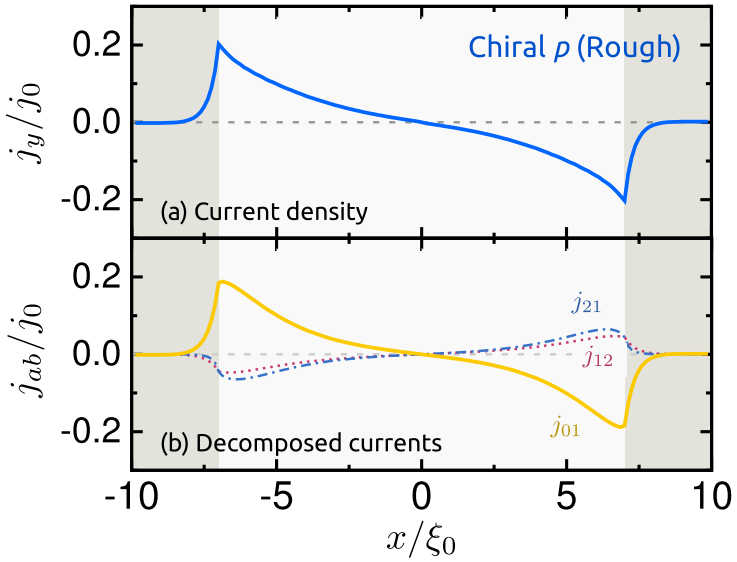

Figure 6.10: Results for a chiral p-wave disk with a rough surface obtained by the self-consistent simulation at $\boldsymbol{A}(\boldsymbol{r}) = 0$. The current density $j_y(x)$ at $y = 0$ in Eq. (6.20) is shown in (a). The dominant components j_{ab} at the lowest Matsubara frequency are shown in (b).

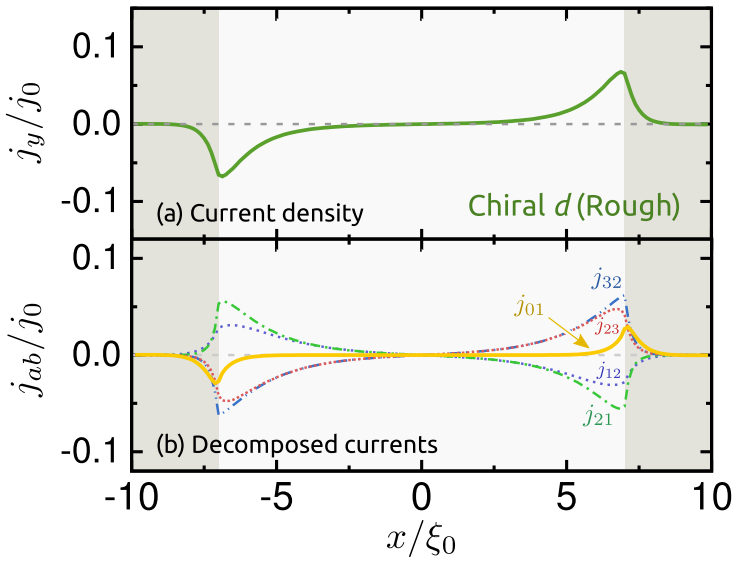

Figure 6.11: Results for a chiral d-wave disk with a rough surface obtained by the self-consistent simulation at $\boldsymbol{A}(\boldsymbol{r}) = 0$: current density j_y (a) and dominant components j_{ab} (b). The results are plotted in the same manner as Fig. 6.10.

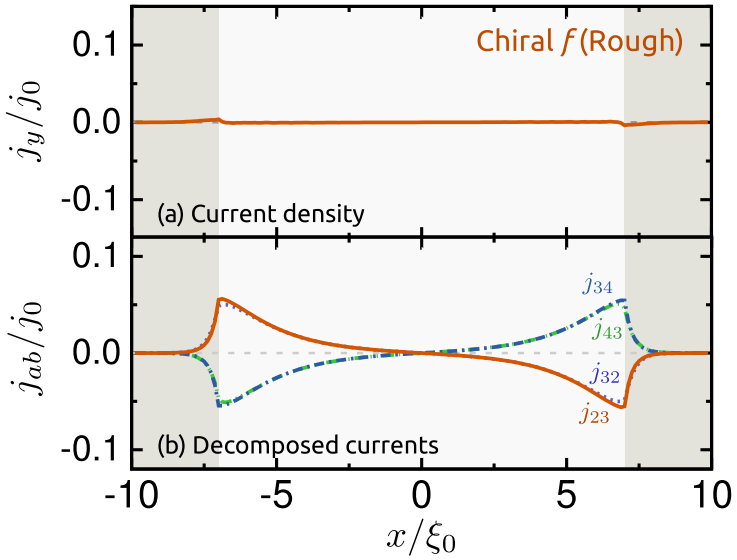

Figure 6.12: Results for a chiral f-wave disk with a rough surface obtained by the self-consistent simulation at $\boldsymbol{A}(\boldsymbol{r}) = 0$: current density j_y (a) and dominant components j_{ab} (b). The results are plotted in the same manner as Fig. 6.10.

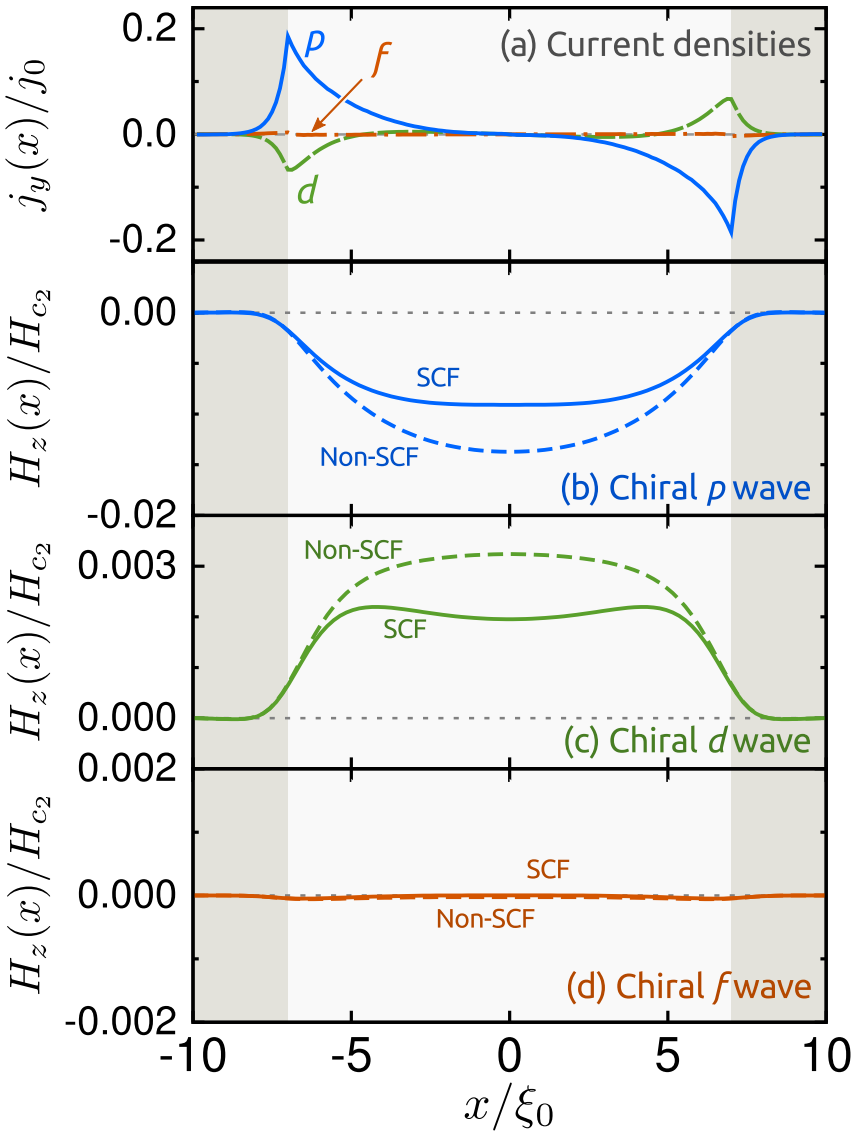

Figure 6.13: (a) Current densities in a disk of a chiral superconductor with a *rough* surface. The results are obtained by solving the Eilenberger and Maxwell equations self-consistently and simultaneously. (b)-(d) Comparisons of the SCF with the non-SCF. The strength of the disorder and the width of the disordered region is set to $\xi_0/\ell = 1$ and $W = 3\xi_0$, respectively. The another parameters are set to the same values used in Fig. 6.8.

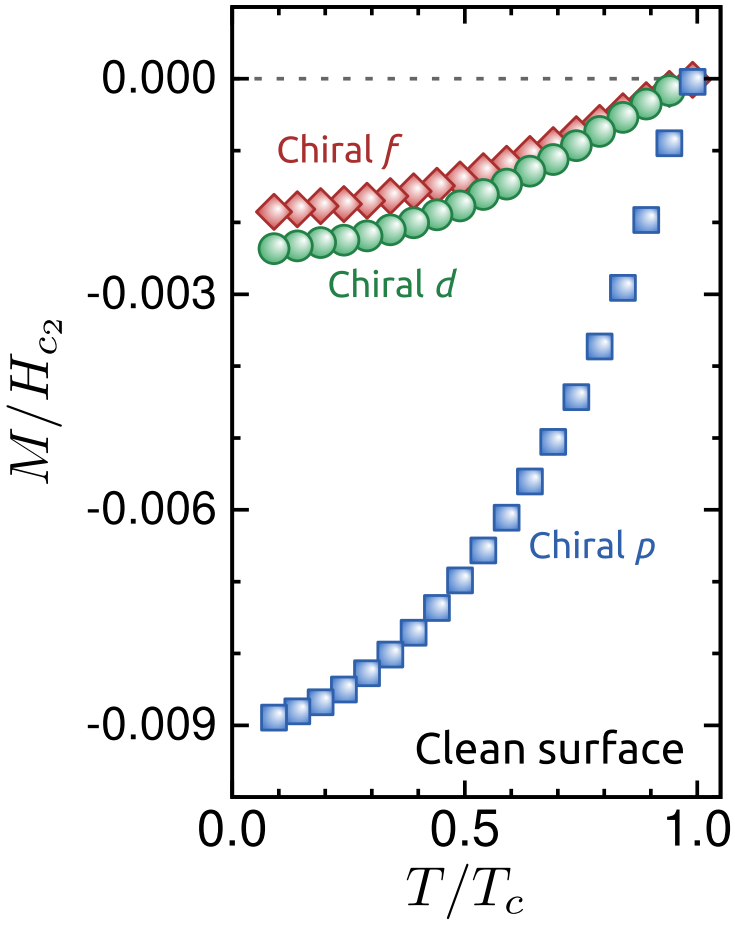

Figure 6.14: Temperature dependences of the spontaneous magnetization of a small chiral superconductor with a *clean* surface. The magnetization is defined by Eq. (6.16) and is normalized to the second critical magnetic field H_{c_2}.

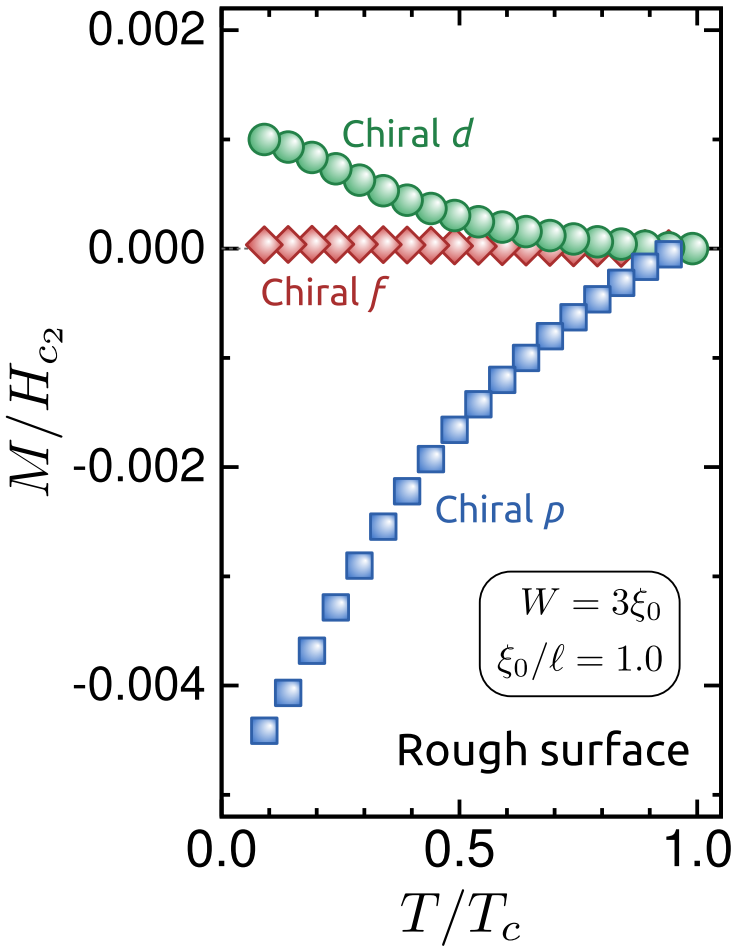

Figure 6.15: Temperature dependences of the spontaneous magnetization of a small chiral superconductor with a *rough* surface. The parameters related to the surface roughness are set to $\xi_0/\ell = 1.0$ and $W = 3\xi_0$.

Chapter 7

Conclusion

We have theoretically studied the magnetic response of small superconductors by using the quasiclassical Green function method. The electric current is calculated from the Green functions that obey the Eilenberger equation and the magnetic field is given by solving the Maxwell equation. In numerical simulations, the superconducting pair potential and the vector potential are determined self-consistently to each other.

We calculate magnetic susceptibility in small superconducting disks with unconventional pairing symmetries such as spin-singlet d wave and spin-triplet p wave. The small unconventional superconductors change their magnetic response depending on temperatures. They indicate the usual diamagnetic response just below the superconducting transition temperature. At low temperature, however, they show unusual paramagnetic response while retaining the stable superconducting phase. Cooper pairs belonging to the odd-frequency symmetry class are responsible for the paramagnetic response. The spatial variation in the pair potential generates odd-frequency Cooper pairs. In an unconventional superconductor, the pair potential is drastically suppressed at a surface which hosts the subgap Andreev bound states. Odd-frequency Cooper pairs always appear at such a surface as local subdominant pairing correlations. The paramagnetic property of odd-frequency pairs explains well the paramagnetic response of a small unconventional superconductor at low temperature. The paramagnetic superconducting phase, however, disappears when the size of the disk is much larger than the superconducting coherence length.

To make clear the observability of the paramagnetic superconducting phase, we have studied the effects of surface roughness on the paramagnetic response of small unconventional superconductors. The surface roughness is considered through the impurity self-energy in the simulations. We conclude that the paramagnetic property of a p-wave superconductor is robust under the surface roughness because the p-wave superconductor hosts s-wave odd-frequency Cooper pairs at its surface. On the other hand, the paramag-

netic property in a d-wave superconductor is fragile in the presence of surface roughness. In this case, odd-frequency pairs at the surface have p-wave symmetry. It is well known that the impurities break such Cooper pairs with anisotropic orbital symmetry. Thus we conclude that the paramagnetic property at low temperature is a robust feature of a small spin-triplet odd-parity superconductor.

Finally we have analyzed the spontaneous edge currents in a small chiral superconductor based on the obtained knowledge of odd-frequency Cooper pairs. So far, the absence of the chiral edge current in experiments have been attributed to the roughness at a surface of a superconductor. We have found that the spontaneous chiral current is robust against surface roughness in a chiral p-wave and a chiral d-wave superconductor. The surface roughness flips the current direction in a chiral d-wave superconductor. In a chiral f-wave case, the chiral edge current is fragile under the surface roughness. These differences come from the symmetry of Cooper pairs that carry the edge current. The obtained current expression indicates that the chiral edge current is carried by a combination of two types of Cooper pairs: an even-parity Cooper pair and an odd-parity one. Since the spin-configuration is common in the two Copper pairs, one of them belongs to odd-frequency symmetry. In a chiral p- and d-wave superconductor, the chiral current is mainly carried by the combination of s-wave and p-wave Cooper pairs. The resulting amplitude of the spontaneous magnetization of a disk with rough surface is still large enough to be detected in experiments. On the other hand, in a chiral f-wave superconductor, the combination of d-wave and f-wave Cooper pairs mainly carries the chiral edge current. Therefore, the surface roughness would wash out the spontaneous magnetization in a realistic superconductor.

Throughout this study, we have been focusing on a paramagnetic property of odd-frequency Cooper pairs. Our results indicate a way of observing odd-frequency Cooper pairs in experiments.

Appendices

Appendix A

Magnetic response of a conventional s-wave disk

We supply the calculated results for conventional spin-singlet s-wave superconductors. Fig. A.1 shows the calculated results of the local susceptibility (a) and the current density (b) for the s wave superconducting disk, where we fix the parameters as $R = 3\,\xi_0$, $\lambda_L = 3\,\xi_0$, and $T = 0.2\,T_c$. Because of the isotropic property in the s wave pair potential, the results are also isotropic in real space. Therefore we plot the results as a function of x at $y = 0$. The results in (a) show that the response is diamagnetic everywhere in the disk. Correspondingly the current profile in (b) suggests the usual Meissner screening current. The amplitude of the s-wave component of the anomalous Green function is almost uniform because s wave superconductors are topologically trivial and do not host any surface states. The amplitude of the p wave component is much smaller than that of s wave one. The susceptibility of disk is plotted as a function of temperature in (d). The susceptibility decreases monotonically with decreasing temperature, which is usually observed in experiments. Since the disk size is not much larger than λ_L, the perfect diamagnetism (i.e., $4\pi\chi = -1$) is not archived.

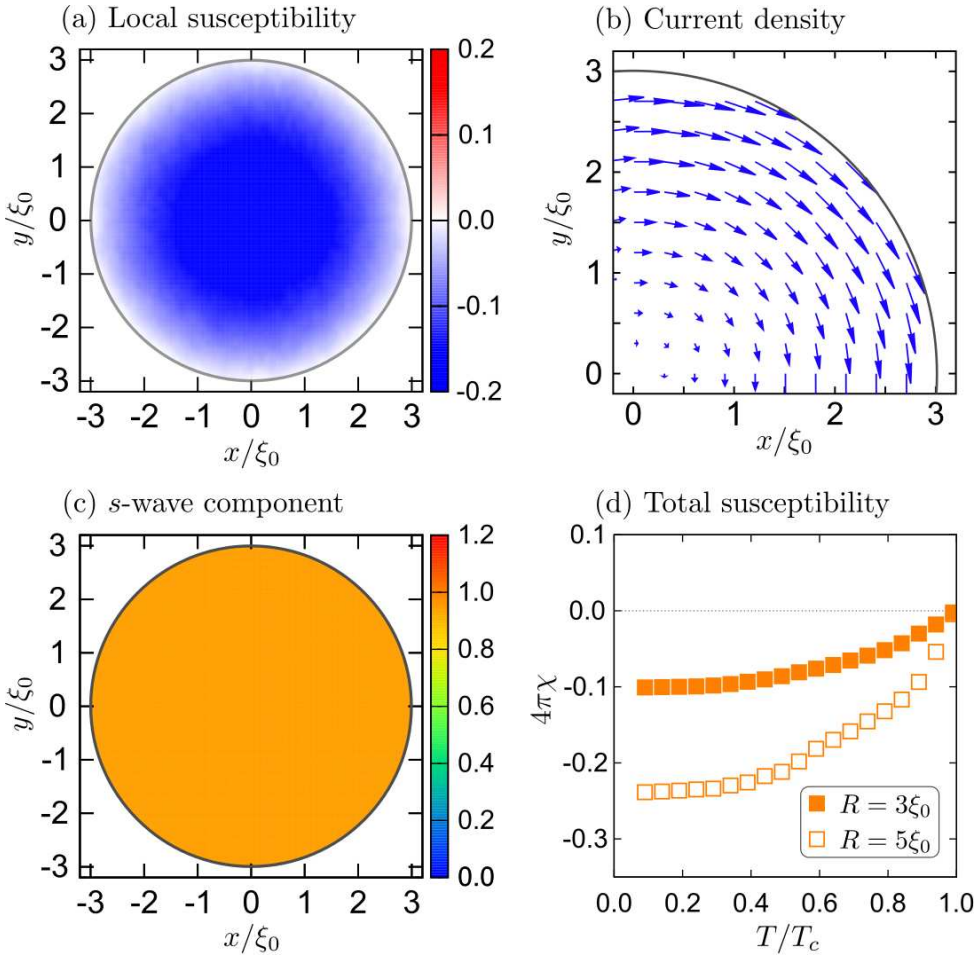

Figure A.1: (a) Local susceptibility and (b) current density of the s-wave superconductor with $R = 3\,\xi_0$, $\lambda_L = 3\,\xi_0$, $\omega_c = 10\,\Delta_0$, $H^{\rm ext} = 0.001 H_{c1}$ and $T = 0.2 T_c$. (c) Spatial profile of the s wave component of the anomalous Green function. (d) Susceptibility vs temperature.

Appendix B

Analysis in a semi-infinite p_x-wave superconductor

In a semi-infinite superconductor in two-dimension, it is possible to obtain analytic expression of Green functions in the clean limit. The evaluation of a electric current and free-energy by using analytical expressions would be helpful to understand numerical results in the text.

We assume that a superconductor occupies $x \geq 0$ and uniform in the y direction. An magnetic field applied in the z direction and its vector potential is given by $\boldsymbol{A} = A(x)\hat{\boldsymbol{y}}$. The Eilenberger equation in 2×2 Nambu space reads,

$$iv_F \boldsymbol{k} \cdot \nabla \hat{g} + [\hat{H}, \hat{g}] = 0, \tag{B.1}$$

$$\hat{g}(x, \boldsymbol{k}, i\omega_n) = \left[\begin{array}{cc} g & f \\ s_p \underset{\sim}{f} & -g \end{array} \right]_{(x, \boldsymbol{k}, i\omega_n)}, \tag{B.2}$$

$$\hat{H} = \left[\begin{array}{cc} i\omega_n + ev_F \boldsymbol{k} \cdot \boldsymbol{A} & i\Delta(x, \boldsymbol{k}) \\ is_p \underset{\sim}{\Delta}(x, \boldsymbol{k}) & -i\omega_n - ev_F \boldsymbol{k} \cdot \boldsymbol{A} \end{array} \right], \tag{B.3}$$

$$s_p = \left\{ \begin{array}{cc} 1 & \text{even-parity} \\ -1 & \text{odd-parity} \end{array} \right. . \tag{B.4}$$

where a factor s_p depends on the parity of order parameter and the Green functions satisfy $g^2 + s_p \underset{\sim}{f} f = 1$. The Green functions can be expanded with respect to the vector potential

as

$$
\begin{aligned}
g =& g^{(0)} + (-iev_F \boldsymbol{k}\cdot\boldsymbol{A})\partial_{\omega_n} g^{(0)} \\
&+ \frac{1}{2}(-iev_F \boldsymbol{k}\cdot\boldsymbol{A})^2 \partial_{\omega_n}^2 g^{(0)} + \cdots , \qquad \text{(B.5)} \\
f =& f^{(0)} + (-iev_F \boldsymbol{k}\cdot\boldsymbol{A})\partial_{\omega_n} f^{(0)} \\
&+ \frac{1}{2}(-iev_F \boldsymbol{k}\cdot\boldsymbol{A})^2 \partial_{\omega_n}^2 f^{(0)} + \cdots , \qquad \text{(B.6)}
\end{aligned}
$$

because a vector potential shifts the Matsubara frequency, where $g^{(0)}$ and $f^{(0)}$ are the Green function in the absence of a vector potential. In what follows, we omit "(0)" from the Green function for simplicity. We note in Eq. (B.6) that parity and frequency symmetry of the second term on the right-hand side are opposite to those of the first term because $\boldsymbol{k}$ is a odd-parity function and $\partial_{\omega_n} f$ changes a frequency symmetry [56]. The imaginary part of an anomalous Green function represents a pairing correlation deformed by a vector potential.

In the case of a p_x-wave superconductor, it is possible to obtain a reasonable solution of the Eilenberger equation at $\boldsymbol{A} = 0$. When we assume the spatial dependence of the pair potential as

$$
\Delta(x,\theta) = \Delta(\theta)\tanh(x/\xi) , \qquad \text{(B.7)}
$$

with $\xi = v_F/\Delta_0$, the Green functions are represented by [75]

$$
\begin{aligned}
g(x,\theta,i\omega_n) &= \frac{\omega_n}{\Omega} + \frac{\Delta^2(\theta)}{2\omega_n\Omega}\cosh^{-2}\left(\frac{x}{\xi}\right) , \qquad \text{(B.8)} \\
f_{\rm P}(x,\theta,i\omega_n) &= \frac{\Delta(\theta)}{\Omega}\tanh\left(\frac{x}{\xi}\right) , \qquad \text{(B.9)} \\
f_{\rm I}(x,\theta,i\omega_n) &= -\frac{\Delta^2(\theta)}{2\omega_n\Omega}\cosh^{-2}\left(\frac{x}{\xi}\right) , \qquad \text{(B.10)}
\end{aligned}
$$

where $\Omega = [\,\omega_n^2 + \Delta^2(\theta)\,]^{1/2}$, and $\Delta(\theta) = \Delta_0\cos(\theta)$. The Green function $f_{\rm P}$ represents the principal pairing correlation in the bulk state, whereas $f_{\rm I}$ represents the pairing correlation induced by a surface at $x = 0$. They are calculated from the anomalous Green function as

$$
\begin{aligned}
f_P(x,\theta,i\omega_n) &= \frac{1}{2}\left(f + s_p\underset{\sim}{f}\right)\Big|_{(x,\theta,i\omega_n)} , \qquad \text{(B.11)} \\
f_I(x,\theta,i\omega_n) &= \frac{1}{2}\left(f - s_p\underset{\sim}{f}\right)\Big|_{(x,\theta,i\omega_n)} . \qquad \text{(B.12)}
\end{aligned}
$$

At the deep inside of the supercondcutor (i.e., $x \gg \xi$), we obtain $f_P = f$ and $f_I = 0$.

Current density

From an expression of electric current in Eq. (6.13), we define a linear response function $\mathcal{R}_{\mu,\nu}$ by

$$j_\mu(\boldsymbol{r}) = -\frac{e^2}{m}\mathcal{R}_{\mu,\nu}A_\nu, \tag{B.13}$$

$$\frac{\mathcal{R}_{\mu,\nu}}{n_e} = 4\pi T\sum_{\omega_n}\int\frac{d\theta}{2\pi}k_\mu k_\nu \partial_{\omega_n} g(\boldsymbol{r},\theta,i\omega_n). \tag{B.14}$$

with $\boldsymbol{k} = (\cos\theta, \sin\theta)$ and $n_e = v_F^2 N_0 m$ being an electron density in two-dimension. The diagonal elements of the response function $\mathcal{R}_{\mu,\mu}$ correspond to so called pair density. In the present situation, by substituting Eq. (B.8) into Eq. (B.14), we obtain

$$\frac{\mathcal{R}_{y,y}}{n_e} = 1 - \kappa_1\frac{\Delta_0}{\omega_0}\cosh^{-2}\left(\frac{x}{\xi}\right), \tag{B.15}$$

$$\kappa_1 = \int\frac{d\theta}{2\pi}\sin^2(\theta)|\cos(\theta)| = \frac{2}{3\pi}, \tag{B.16}$$

where $\omega_0 = \pi T$ is a low energy cut-off in the Matubara summation. Using the normalization condition, the integrand in Eq. (B.14) can be represented in an alternative way,

$$\partial_{\omega_n} g = \left[-f_{\rm P}\partial_{\omega_n} f_{\rm P} + f_{\rm I}\partial_{\omega_n} f_{\rm I}\right]/g. \tag{B.17}$$

It is possible to confirm that $-f_{\rm P}\partial_{\omega_n} f_{\rm P}/g$ corresponds to the first term in Eq. (B.15), whereas $f_{\rm I}\partial_{\omega_n} f_{\rm I}/g$ contribute to the second term. In this way, we can confirm that induced odd-frequency Cooper pairs indicate paramagnetic response to an external magnetic field. Eq. (B.15) suggests that the paramagnetic response is stronger in lower temperature.

Free-energy density

Substituting Eqs. (B.8)-(B.10) into Eqs. (4.4)-(4.6), we find that a free-energy density

at $\boldsymbol{A} = 0$

$$\mathcal{F}_f = N_0\kappa_2\Delta_0^2 \log\left(\frac{2\omega_c}{\Delta_0}\right)\tanh^2\left(\frac{x}{\xi}\right), \tag{B.18}$$

$$\begin{aligned}\mathcal{F}_g =& - N_0\kappa_2\Delta_0^2 \log\left(\frac{2\omega_c}{\Delta_0}\right)\tanh^2\left(\frac{x}{\xi}\right) \\ &+ N_0\Delta_0^2\kappa_2\left[\cosh^{-2}\left(\frac{x}{\xi}\right) - \frac{1}{2}\right],\end{aligned} \tag{B.19}$$

$$\kappa_2 = \int \frac{d\theta}{2\pi}\cos^2(\theta) = \frac{1}{2}. \tag{B.20}$$

As a result, we obtain

$$\mathcal{F}_\Delta = N_0\Delta_0^2\kappa_2\left[\cosh^{-2}\left(\frac{x}{\xi}\right) - \frac{1}{2}\right]. \tag{B.21}$$

The free-energy density becomes positive at $x = 0$ due to appearance of odd-frequency pairs.

Contribution of a magnetic field to the free-energy can be evaluated by applying the expansion in Eqs. (B.5)-(B.6) onto Eqs. (B.8)-(B.10). Within the second order expansion, we find that both the pair potential obtained by Eq. (5.9) and $\mathcal{F}_f$ remain unchanged. The second order correction to $\mathcal{F}_g$ is given by

$$\mathcal{F}_g^{(2)} = \frac{1}{2}N_0\left[ev_F A(x)\right]^2\left[1 - \kappa_1\frac{\Delta_0}{\omega_0}\cosh^{-2}\left(\frac{x}{\xi}\right)\right]. \tag{B.22}$$

The results indicate that $\mathcal{F}_g^{(2)}$ can be locally negative (paramagnetic) at low enough temperature. This explains the decrease of the free-energy in a magnetic field shown in Fig. 4.3. We also obtain the electric current in Eqs. (B.13) and (B.15) by $j_y(x) = -\partial\mathcal{F}/\partial A_y$.

Bibliography

[1] M. Tinkham, *Introduction to Superconductivity*, 2nd ed., (McGraw-Hill, 1996).

[2] J. R. Schrieffer, *Theory of Superconductivity*, (Benjamin-Cummings Pub Co, 1983).

[3] P. G. de Gennes, *Superconductivity of Metals and Alloys*, (Addison Wesley, 1989).

[4] A. A. Abrikosov, L. P. Gor'kov, I. E. Dzyaloshinski, *Methods of Quantum Field Theory in Statistical Physics* (Dover Publications ,1975).

[5] J. Bardeen, L. N. Cooper, and J. R. Schrieffer, Phys. Rev. **108**, 1175 (1957)

[6] H. Walter, W. Prusseit, R. Semerad, H. Kinder, W. Assmann, H. Huber, H. Burkhardt, D. Rainer, and J. A. Sauls, Phys. Rev. Lett. **80**, 3598 (1998).

[7] W Prusseit, H Walter, R Semerad, H Kinder, W Assmann, H Huber, B Kabius, H Burkhardt, D Rainer, and J.A Sauls, Physica C: Superconductivity 317396 (1999).

[8] A. Carrington, F. Manzano, R. Prozorov, R. W. Giannetta, N. Kameda, and T. Tamegai, Phys. Rev. Lett. **86**, 1074 (2001).

[9] P. Visani, A. C. Mota, and A. Pollini, Phys. Rev. Lett. **65**, 1514 (1990).

[10] A. C. Mota, P. Visani, A. Pollini, K. Aupke, Physica B **197**, 95 (1994).

[11] F. Bernd Muller-Allinger, A. C. Mota, Phys. Rev. Lett. **84**. 3161(2000).

[12] F. Bernd Muller-Allinger, A. C. Mota, Physica B, **284**, 683 (2000).

[13] D. J. Thompson, M. S. M. Minhaj, L. E. Wenger, and J. T. Chen, Phys. Rev. Lett. **75**, 529 (1995).

[14] A. K. Geim, S. V. Dubonos, J. G. S. Lok, M. Henini and J. C. Maan, Nature (London) **396**, 144 (1998).

[15] W. Braunisch, N. Knauf, V. Kataev, S. Neuhausen, A. Grutz, A. Kock, B. Roden, D. Khomskii, and D. Wohlleben, Phys. Rev. Lett. **68**, 1908 (1992).

[16] W. Braunisch, N. Knauf, G. Bauer, A. Kock, A. Becker, B. Freitag, A. Grutz, V. Kataev, S. Neuhausen, B. Roden, D. Khomskii, and D. Wohlleben, Phys. Rev. B **48**, 4030 (1993).

[17] B. Schliepe, M. Stindtmann, I. Nikolic, and K. Baberschke, Phys. Rev. B **47**, 8331 (1993).

[18] Ch. Heinzel, Th. Theilig, and P. Ziemann Phys. Rev. B **48**, 3445 (1993).

[19] A. Di Bernardo, Z. Salman, X.L. Wang, M. Amado, M. Egilmez, M.G. Flokstra, A. Suter, S.L. Lee, J.H. Zhao, T. Prokscha, E. Morenzoni, M.G. Blamire, J. Linder, and J.W.A. Robinson Phys. Rev. X **5**, 041021 (2015).

[20] A. E. Koshelev and A. I. Larkin, Phys. Rev. B **52**, 13559 (1995).

[21] V. V. Moshchalkov, X. G. Qiu, and V. Bruyndoncx, Phys. Rev. B **55**, 11793 (1997).

[22] D. Dominguez, E. A. Jagla, and C. A. Balseiro, Phys. Rev. Lett. **72**, 2773 (1994).

[23] W. Belzig, C. Bruder, and A. L. Fauchere, Phys. Rev. B, **58**, 14531 (1998).

[24] F. B. Mller-Allinger, A. C. Mota, and W. Belzig, Phys. Rev. B 59, 8887 (1999).

[25] S. K. Yip and J. A. Sauls, Phys. Rev. Lett. **69**, 2264 (1992).

[26] S. Higashitani, J. Phys. Soc. Jpn. **66**, 2556 (1997).

[27] M. Fogelström, D. Rainer, and J. A. Sauls, Phys. Rev. Lett. **79**, 281 (1997).

[28] Yu. S. Barash, M. S. Kalenkov, and J. Kurkijarvi, Phys. Rev. B **62**, 6665 (2000).

[29] T. Löfwander, V. S. Shumeiko, and G. Wendin, Phys. Rev. B **62**, 14653R (2000).

[30] A. Zare, T. Dahm and N. Schopohl, Phys. Rev. Lett. **104**, 237001 (2010).

[31] V. L. Berezinskii, JETP Lett. **20**, 287 (1974).

[32] A. Balatsky and E. Abrahams, Phys. Rev. B **45**, 13125(R) (1992).

[33] P. Coleman, E. Miranda, and A. Tsvelik, Phys. Rev. B **49**, 8955 (1994).

[34] M. Vojta and E. Dagotto, Phys. Rev. B **59**, R713 (1999).

[35] Y. Fuseya, H. Kohno, and K. Miyake, J. Phys. Soc. Jpn. **72**, 2914 (2003).

[36] F.S. Bergeret, A.F. Volkov, and K.B. Efetov, Phys. Rev. Lett. **86**, 4096 (2001).

[37] F.S. Bergeret, A.F. Volkov, and K.B. Efetov, Rev. Mod. Phys. **77**, 1321 (2005).

[38] Y. Tanaka and A. A. Golubov, Phys. Rev. Lett. **98**, 037003

[39] Y. Tanaka, Y. Tanuma, and A. A. Golubov, Phys. Rev. B **76**, 054522 (2007).

[40] Y. Asano, Y. Tanaka, and A. A. Golubov, Phys. Rev. Lett. **98**, 107002 (2007).

[41] V. Braude and Yu. V. Nazarov, Phys. Rev. Lett. **98**, 077003 (2007).

[42] Y. Tanaka, A. A. Golubov, S. Kashiwaya, and M. Ueda, Phys. Rev. Lett. **99**, 037005 (2007).

[43] M. Eschrig. Löfwander, T. Champel, J. C. Cuevas, J. KopuGerd Schü, J. Low Temp. Phys. **147**, 457 (2007).

[44] M. Eschrig and T. Löfwander, Nature Physics **4**, 138 (2008).

[45] S. Higashitani, Y. Nagato, and K. Nagai, J. Low Temp. Phys. **155**, 83 (2009).

[46] J. Linder, T. Yokoyama, A. Sudb, and M. Eschrig, Phys. Rev. Lett. **102**, 107008 (2009).

[47] J. Linder, A. Sudb, T. Yokoyama, R. Grein, and M. Eschrig, Phys. Rev. B **81**, 214504 (2010).

[48] Y. Asano, A. A. Golubov, Y. V. Fominov, and Y. Tanaka, Phys. Rev. Lett. **107**, 087001 (2011).

[49] Y. Asano, M. Ozaki, T. Habe, A. A. Golubov, and Y. Tanaka, Phys. Rev. B **86**, 024510 (2012).

[50] T. Yokoyama, Y. Tanaka, N. Nagaosa, Phys. Rev. Lett. **106**, 246601 (2011).

[51] S. Mironov, A. Mel'nikov, and A. Buzdin, Phys. Rev. Lett. **109**, 237002 (2012).

[52] Y. Asano and Y. Tanaka, Phys. Rev. B **87**, 104513 (2013).

[53] S. Higashitani, H. Takeuchi, S. Matsuo, Y. Nagato, and K. Nagai, Phys. Rev. Lett. **110**, 175301 (2013).

[54] S.-I. Suzuki and Y. Asano, Phys. Rev. B **89**, 184508 (2014).

[55] S. Higashitani, Phys. Rev. B **89**, 184505 (2014).

[56] Y. Asano, Ya. V. Fominov, and Y. Tanaka, Phys. Rev. B **90**, 094512 (2014).

[57] T. Mizushima, Phys. Rev. B **90**, 184506 (2014).

[58] S.-I. Suzuki and Y. Asano, Phys. Rev. B **91**, 214510 (2015).

[59] A. M. Black-Schaffer and A. V. Balatsky, Phys. Rev. B **87**, 220506(R) (2013).

[60] A. M. Black-Schaffer and A. V. Balatsky, Phys. Rev. B **88**, 104514 (2013).

[61] Y. Asano and A. Sasaki, Phys. Rev. B **92**, 224508 (2015).

[62] N. B. Kopnin, *Theory of Nonequilibrium Superconductivity* (Oxford University Press ,2009).

[63] L. J. Buchholtz and G. Zwicknagl, Phys. Rev. B **23**, 5788 (1981).

[64] J. Hara and K. Nagai, Prog. Theor. Phys. **74**, 1237 (1986).

[65] C. R. Hu, Phys. Rev. Lett. **72**, 1526 (1994).

[66] Y. Tanaka and S. Kashiwaya, Phys. Rev. Lett. **74**, 3451 (1995).

[67] S. Kashiwaya, Y. Tanaka, N. Terada, M. Koyanagi, S. Ueno, L. Alff, H. Takashima, Y. Tanuma, K. Kajimura, Journal of Physics and Chemistry of Solids **59** 2034 (1998).

[68] M. Sato, Y. Tanaka, K. Yada, T. Yokoyama, Phys. Rev. B **83**, 224511 (2011). The topological number for two-dimensional d- and p-wave superconductors is defined in terms of the subgap wave functions at partial Brillouin zone in one-dimension. Such characterization explain the dispersionless zero-energy bound states at their surface in the clean limit.

[69] Y. Asano, Y. Tanaka, and S. Kashiwaya, Phys. Rev. B **69**, 134501 (2004).

[70] R. M. Lutchyn, J. D. Sau, and S. Das Sarma, Phys. Rev. Lett. **105**, 077001 (2010).

[71] Y. Oreg, G. Refael, and F. von Oppen, Phys. Rev. Lett. **105**, 177002 (2010).

[72] G. Eilenberger, Z. Phys. **214**, 195 (1968).

[73] G. Eilenberger, Z. Phys. **190**, 142 (1966).

[74] N. Schopohl and K. Maki, Phys. Rev. B **52**, 490 (1995).

[75] N. Schopohl, arXiv:cond-mat/9804064.

[76] M. Eschrig, Phys. Rev. B **80**, 134511 (2009).

[77] Y. Nagai, K. Tanaka, and N. Hayashi, Phys. Rev. B **86**, 094526 (2012).

[78] A. Poenicke, Yu. S. Barash, C. Bruder, and V. Istyukov, Phys. Rev. B **59**, 7102 (1999).

[79] A. Zare, A. Markowsky, T. Dahm, and N. Schopohl, Phys. Rev. B **78**, 104524 (2008).

[80] Yu. S. Barash, M. S. Kalenkov, J. Kurkijarvi, Phys. Rev. B **62**, 6665 (2000).

[81] Y. Tanaka, Y. Tanuma, and S. Kashiwaya, Phys. Rev. B **64**, 054510 (2001).

[82] A. M. Black-Schaffer, D. S. Golubev, T. Bauch, F. Lombardi, M. Fogelström, Phys. Rev. Lett. **110**, 197001, (2013).

[83] The sign change in the pair potential in the normal reflection process by a surface plays an essential role in for forming surface Andreev bound states. Let us assume that k_x (k_y) is a wave number in the perpendicular (parallel) direction to the surface. The pair potential on the way to the surface (on the way back from the surface) is $\Delta(k_x, k_y)$ ($\Delta(-k_x, k_y)$) because a wave number in the perpendicular direction to the surface changes its sign in the normal reflection. The Andreev bound states appears when $\Delta(k_x, k_y)\Delta(-k_x, k_y) < 0$ is satisfied as shown in Y. Asano, Y. Tanaka, and S. Kashiwaya, Phys. Rev. B **69**, 134501 (2004). In a d_{xy}-wave superconductor with a pair potential $\Delta k_x k_y$, the Andreev bound states appears four surfaces in x and y directions (nodal directions). In a p_x-wave superconductor with Δk_x, two surfaces in the x direction (anti-nodal directions) host the Andreev bound states.

[84] M. Ichioka, N. Hayashi, N. Enomoto, and K. Machida, Phys. Rev. B, **53**, 15316 (1996). The authors considered a d-wave superconductor with a vortex without any surface. When a vortex with a nonzero winding number exists, the pair potential must be zero at the vortex core to remove a singularity from the pair potential. Therefore the amplitude of pair potential around the vortex core is basically isotropic in real space. In our simulation, on the other hand, the formation of ABS at a surface suppressed the pair potential there. The pair potential is suppressed by the different reasons in the two cases.

[85] S. Ikegaya, Y. Asano, and Y. Tanaka, Phys. Rev. B, **91**, 174511 (2015).

[86] Y. Asano and Y. Tanaka, Phys. Rev. B, **65**, 064522 (2002).

[87] M. Matsumoto and M. Sigrist. J. Phys. Soc. Jpn. **68**, 994 (1999).

[88] A. Furusaki, M. Matsumoto, and M. Sigrist. Phys. Rev. B **64**, 054514 (2001).

[89] Y. Maeno, H. Hashimoto, K. Yoshida, S. Nishizaki, T. Fujita, J.G. Bednorz, and F. Lichtenberg, Nature **372**, 532 (1994).

[90] T.M. Rice and M. Sigrist, J. Phys.: Condens. Matter **7**, L643 (1995).

[91] A. P. Mackenzie and Y. Maeno, Rev. Mod. Phys. **75**, 657 (2003).

[92] K. Takeda, H. Sakurai, E. Takayama-Muromachi, F. Izumi, R. A. Dilanian, and T. Sakai, Nature **422** 53 (2003).

[93] G. Baskaran, Phys. Rev. Lett. **91**, 097003 (2003).

[94] M. Ogata, J. Phys. Soc. Jpn. **72**, 1839 (2003).

[95] A. Tanaka and X. Hu, Phys. Rev. Lett. **91**, 257006 (2003).

[96] R. Nandkishore, L. S. Levitov, and A. V. Chubukov, Nature Physics **8**, 158 (2012).

[97] M. L. Kiesel, C. Platt, W. Hanke, D. A. Abanin, and R. Thomale, Phys. Rev. B **86**, 020507(R) (2012).

[98] M. L. Kiesel, C. Platt, W. Hanke, and R. Thomale, Phys. Rev. Lett. **111**, 097001 (2013).

[99] M. H. Fischer, T. Neupert, C. Platt, A. P. Schnyder, W. Hanke, J. Goryo, R. Thomale, and M. Sigrist, Phys. Rev. B **89**, 020509(R)

[100] Y. Kasahara, H. Shishido, T. Shibauchi, Y. Haga, T. D. Matsuda, Y Onuki, and Y. Matsuda, New Journal of Physics, **11**, 055061 (2009).

[101] H. Kusunose, J. Phys. Soc. Jpn. **81**, 023704 (2012).

[102] M. Tsuchiizu, Y. Yamakawa, S. Onari, Y. Ohno, and H. Kontani, Phys. Rev. B **91**, 155103 (2015).

[103] J. A. Sauls, J. Low Temp. Phys. **95**, 153 (1994).

[104] H. Tou, Y. Kitaoka, K. Ishida, K. Asayama, N. Kimura, Y. nuki, E. Yamamoto, Y. Haga, and K. Maezawa, Phys. Rev. Lett. **80**, 3129 (1998).

[105] Matthias J. Graf, S.-K. Yip, and J. A. Sauls, Phys. Rev. B **62**, 14393 (2000).

[106] Y. Machida, A. Itoh, Y. So, K. Izawa, Y. Haga, E. Yamamoto, N. Kimura, Y. Onuki, Y. Tsutsumi, and K. Machida, Phys. Rev. Lett. **108**, 157002 (2012).

[107] Y. Tada, W. Nie, and M. Oshikawa, Phys. Rev. Lett. **114**, 195301 (2015).

[108] W. Huang, E. Taylor, and C. Kallin, Phys. Rev. B **90**, 224519 (2014).

[109] P. G. Björnsson, Y. Maeno, M. E. Huber, and K. A. Moler, Phys. Rev. B **72**, 012504 (2005).

[110] J. R. Kirtley, C. Kallin, C. W. Hicks, E.-A. Kim, Y. Liu, K. A. Moler, Y. Maeno, and K. D. Nelson, Phys. Rev. B **76**, 014526 (2007).

[111] K. Saitoh, S. Kashiwaya, H. Kashiwaya, M. Koyanagi, Y. Mawatari, Y. Tanaka, and Y. Maeno, Appl. Phys. Express **5**, 113101 (2012).

[112] K. Saitoh, S. Kashiwaya, H. Kashiwaya, Y. Mawatari, Y. Asano, Y. Tanaka, and Y. Maeno, Phys. Rev. B **92**, 100504(R) (2015).

[113] P. E. C. Ashby and C. Kallin, Phys. Rev. B **79**, 224509 (2009).

[114] S. V. Bakurskiy, A. A. Golubov, M. Yu. Kupriyanov, K. Yada, and Y. Tanaka, Phys. Rev. B **90**, 064513 (2014).

[115] S. Lederer, W. Huang, E. Taylor, S. Raghu, and C. Kallin, Phys. Rev. B **90**, 134521 (2014).

[116] A. Bouhon and M. Sigrist, Phys. Rev. B **90**, 220511(R) (2014).

[117] W. Huang, S. Lederer, E. Taylor, and C. Kallin, Phys. Rev. B **91**, 094507 (2015).

[118] T. Scaffidi and S. H. Simon, Phys. Rev. Lett. **115**, 087003 (2015).

[119] J. A. Sauls. Phys. Rev. B **84**, 214509 (2011).

[120] K. Nagai, J. Low Temp. Phys. **175**, 44 (2014).

[121] A. F. Andreev, Zh. Eksp. Teor. Fiz. **46**, 1823 (1964) [Sov. Phys. JETP **19**, 1228 (1964)].

[122] Y. Nagato and K. Nagai, Phys. Rev. B **51**, 16254 (1995).

[123] S. Higashitani, J. Phys. Soc. Jpn. **83**, 075002 (2014).

[124] In this paper, we assume only the principal pairings (e.g., p_x- and p_y-wave pairs in a chiral p-wave superconductor) are attractive. Nevertheless, subdominant pairing correlations belonging to different symmetry classes from that of the dominant one appear near a surface. The pairing correlations f and the order parameters Δ are directly connected by the gap equation Eq. (6.9). Subdominant order parameters never appear in our formulation because we set the attractive interactions to be zero for subdominant pairing correlations. These subdominant pairing correlations induced by a surface are not related to the stability of a superconductor because they can not become order parameters.

[125] V. L. Berezinskii, Pis'mav Zh. Eksp. Teor. Fiz. **20**, 628 (1974), [JETP Lett. **20**, 287 (1974)].

[126] Y. Tanaka, M. Sato, and N. Nagaosa, J. Phys. Soc. Jpn. **81**, 011013 (2012).